The braincase of *Bissektipelta archibaldi* — new insights into endocranial osteology, vasculature, and paleoneurobiology of ankylosaurian dinosaurs

Ivan Kuzmin[1], Ivan Petrov[2], Alexander Averianov[3], Elizaveta Boitsova[1], Pavel Skutschas[1], and Hans-Dieter Sues[4]

[1]Department of Vertebrate Zoology, Faculty of Biology, Saint Petersburg State University, Universitetskaya nab., 7–9, Saint Petersburg, 199034, Russian Federation;
[2]Saint Petersburg City Palace of Youth Creativity, Nevsky pr., 39A, Saint Petersburg, 191011, Russian Federation;
[3]Zoological Institute, Russian Academy of Sciences, Universitetskaya nab., 1, Saint Petersburg, 199034, Russian Federation;
[4]Department of Paleobiology, National Museum of Natural History, Smithsonian Institution, MRC 121, P. O. Box 37012, Washington, DC 20013–7012, USA

Address correspondence and requests for materials to Ivan Kuzmin, kuzminit@mail.ru

Abstract

We describe in detail three braincases of the ankylosaur *Bissektipelta archibaldi* from the Late Cretaceous (Turonian) of Uzbekistan with the aid of computed tomography, segmentation, and 3D modeling. *Bissektipelta archibaldi* is confirmed as a valid taxon and attributed to Ankylosaurinae based on the results of a phylogenetic analysis. The topographic relationships between the elements forming the braincase are determined using a newly referred specimen with preserved sutures, which is an exceedingly rare condition for ankylosaurs. The mesethmoid appears to be a separate ossification in the newly referred specimen ZIN PH 281/16. We revise and discuss features of the neurocranial osteology in Ankylosauria and propose new diagnostic characters for a number of its subclades. We present a 3D model of the braincase vasculature of *Bissektipelta* and comment on vascular patterns of armored dinosaurs. A complex vascular network piercing the skull roof and the wall of the braincase is reported for ankylosaurs for the first time. We imply the presence of a lepidosaur-like dorsal head vein and the venous parietal sinus in the adductor cavity of *Bissektipelta*. We suggest that the presence of the dorsal head vein in dinosaurs is a plesiomorphic diapsid trait, and extant archosaur groups independently lost the vessel. A study of two complete endocranial casts of *Bissektipelta* allowed us to compare endocranial anatomy within Ankylosauria and infer an extremely developed sense of smell, a keen sense of hearing at lower frequencies (100–3000 Hz), and the presence of physiological mechanisms for precise temperature control of neurosensory tissues at least in derived ankylosaurids.

Keywords: Dinosauria, Ankylosauria, endocast, blood vessels, paleobiology, Late Cretaceous, Uzbekistan.

Introduction

Ankylosaurs constitute a clade of quadrupedal heavily armored ornithischian dinosaurs. Their remains are known from the Jurassic to the Late Cretaceous from every continent except Africa (Tumanova, 1987; Vickaryous et al., 2004). Aspects of ankylosaurian anatomy, phylogeny, and paleobiogeography have been thoroughly studied in the last few decades (e.g., Maryańska, 1977; Tumanova, 1987, 2012; Coombs and Maryańska, 1990; Carpenter, 2001; Vickaryous et al., 2004; Thompson et al., 2012; Arbour and Currie, 2016). Despite this progress, our knowledge of the neurocranial osteology and endocranial morphology within

Table 1. Measurements of the studied braincases of *Bissektipelta archibaldi*. All linear measurements in millimeters

Parameter	ZIN PH 1/16	ZIN PH 281/16	ZIN PH 2329/16
Length from the anterior margin of the sphenethmoidal complex to the posterior tip of occipital condyle	89.2	82.7	84
Depth from the dorsal tip of the laterosphenoid capitate process to the ventral margin of the parabasisphenoid	60.4	58.5	–
Dorsoventral depth of the cranial nerve II foramen	8	6.8	–
Paroccipital process, dorsoventral depth at the mid-section	23.5	22.5	–
Occipital condyle, dorsoventral depth	23.8	21.5	21
Occipital condyle, transversal breadth	36	31.4	42.6
Basioccipital, transversal breadth at the basioccipital-parabasisphenoid contact	52	42	46
Basioccipital, length from the posterior tip of the condyle to the basioccipital-parabasisphenoid contact, in sagittal plane	36	30	35
Foramen magnum, transversal breadth	22	18	18
Foramen magnum, dorsoventral height	19	20	19
Parabasisphenoid, transversal breadth between basipterygoid processes	33	23.8	34

the clade is comparatively poor (see the recent review by Paulina-Carabajal et al. [2018]).

A number of isolated specimens belonging to Ankylosauria are known from the Late Cretaceous of Central Asia (Averianov, 2009). *Bissektipelta archibaldi* is the only valid ankylosaur species from the territory of the former USSR reported to date. It was initially described as "*Amtosaurus*" *archibaldi* based upon a single braincase incorporating the skull roof from the Late Cretaceous Bissekty Formation of Uzbekistan (Averianov, 2002). Later, it was re-assigned to a new genus (*Bissektipelta*) by Parish and Barrett (2004) as these authors concluded the type species of "*Amtosaurus*", "*A. magnus*", is non-diagnostic and should be considered a *nomen dubium*. Since the initial description, the affinities and phylogenetic position of *Bissektipelta* have been debated (Averianov, 2002; Parish and Barrett, 2004; Tumanova, 2012; Arbour and Currie, 2016; see "Phylogenetic analysis" below) but have never been formally assessed. Recently, Alifanov and Saveliev (2019) described a high-quality synthetic endocast made from the holotype of *Bissektipelta archibaldi*. However, many of their anatomical interpretations and biological inferences appear to be controversial and in need of further review.

Here, we redescribe in detail the holotype of *Bissektipelta archibaldi* (ZIN PH 1/16) with the aid of CT scanning. Additionally, two new ankylosaur braincases from the Bissekty Formation are described and assigned to the same species. One of these (ZIN PH 281/16) preserves clear sutures between the elements forming the braincase, which is exceedingly rare for ankylosaurs. Endocasts for two studied specimens have been made, which is the largest sample for a single species of ankylosaurs to date. A thorough review of the literature and comparison between the described taxa allowed us to propose new and revise previously known braincase characters from the most current taxon-character matrices of ankylosaurs (Thompson et al., 2012; Arbour and Currie, 2016; Arbour and Evans, 2017; Zheng et al., 2018) and subsequently test the phylogenetic relationships of *Bissektipelta*. Based on a solid phylogenetic framework and detailed digital endocranial casts, we discuss aspects of cranial vasculature and inferences concerning the paleobiology of ankylosaurs.

Material and methods

Institutional abbreviations. OUVC, Ohio University Vertebrate Collection, USA; ZIN PH, Paleoherpetological Collection, Zoological Institute, Russian Academy of Sciences, Saint Petersburg, Russia.

Material. The studied material comprises three braincases: the holotype of *Bissektipelta archibaldi* (ZIN PH 1/16) and two newly described specimens (ZIN PH 281/16 and ZIN PH 2329/16). The material came from the Late Cretaceous (Turonian) Bissekty Formation at the Dzharakuduk locality in the Central Kyzylkum Desert, Uzbekistan. The measurements for the specimens are provided in Table 1.

The holotype of *Bissektipelta archibaldi* ZIN PH 1/16 is a well-preserved, fully ossified braincase with a partial skull roof. This specimen was the only known cranial material of the Bissekty ankylosaur and constituted the basis of the original description of "*Amtosaurus*" *archibaldi* (Averianov, 2002) and subsequent taxonomic reappraisal of this taxon as *Bissektipelta archibaldi* (Parish and Barrett, 2004). The newly described specimens include ZIN PH 281/16, a partial braincase of slightly

smaller size with open sutures between some bones, and ZIN PH 2329/16, which is similar in size to the holotype of *Bissektipelta archibaldi* (Table 1). ZIN PH 2329/16 preserves most of the braincase and part of the skull roof. The sutures cannot be traced in ZIN PH 2329/16 because it is damaged and partially covered with matrix.

Computed tomography. The holotype ZIN PH 1/16 and the referred specimen ZIN PH 281/16 were X-ray CT scanned using a Toshiba Aquilon 64 medical tomographer at 0.5 mm slice thickness, 120 kV, and 300 mA. The resulting stacks compile 334 images (512×512×334 resolution) in DICOM format for ZIN PH 1/16 and 149 images (512×512×149 resolution) for ZIN PH 281/16. Data acquired from CT scans were imported into the visualization software Amira 6.3.0 (FEI-VSG Company) and manually segmented. The resulting 3D models have the voxel size of 0.313×0.313×0.3 for ZIN PH 1/16 and 0.625×0.625×0.8 for ZIN PH 281/16. Measurements on the 3D models were performed using Amira 6.3.0 and MeshLab (Cignoni et al., 2008). The CT scan data and 3D models are available upon request from the first author.

Description of the holotype of *Bissektipelta archibaldi* ZIN PH 1/16 (Figs. 1–9)

General comments. The braincase of *Bissektipelta* is highly ossified, and the bones of the skull roof are completely fused to it. Most sutures were obliterated. We do not support previous assumptions about incompletely ossified portions of some elements in the holotype (e.g., basal tubera, right basipterygoid process, occipital condyle, and the distal tip of the paroccipital process; Averianov, 2002) and regard those as preservational artifacts. These structures are variably preserved in the three studied braincases (notably, also in the smaller specimen ZIN PH 281/16) and are frequently broken off. The braincase is non-pneumatic. CT scans show that no internal pneumatic structures are present. Externally, there is neither the medial pharyngeal recess on the ventral surface of the basicranium nor a well-defined anterior/lateral pneumatic recess on the lateral surface of the parabasisphenoid.

Skull roof. The preserved skull roof has a relatively flat dorsal surface (Fig. 1A, B). Sutures are completely obliterated and are not evident either on the specimen's surface or in the CT images. General observations suggest that ZIN PH 1/16 preserves the posterior portion of the skull roof that corresponds to the frontoparietal region of taxa with known sutural relationships (e.g., *Pinacosaurus*, Maryańska, 1977; Godefroit et al., 1999; Hill et al., 2003; *Kunbarrasaurus*, Leahey et al., 2015; *Cedarpelta*, Carpenter et al., 2001; "*Zhongyuansaurus*", Xu et al., 2007, = *Gobisaurus* in Arbour and Currie, 2016: Fig. 6D). A truncated Y-shaped groove that separates

three polygonal areas of remodeled bone (= caputegulae; Blows, 2001; Arbour and Currie, 2013a) is present. The resulting areas are identified here as the paired posterolateral nuchal caputegulae (nuca, Fig. 1B) and central parietal caputegulum (paca, Fig. 1B) using the terminology of Arbour and Currie (2013a). Each groove terminates in a pronounced pit; a small offshoot of the left groove is present and is directed anteromedially from the corresponding pit. The CT data for ZIN PH 1/16 shows that these grooves, paired pits, and the skull roof surface are pierced by numerous vascular foramina that connect through canals with the endocranial cavity and the lateral braincase wall. The left branch of the Y-shaped groove interrupts its course for one millimeter, and there is a short contact between the left nuchal and the central parietal caputegulae. The skull roof surface of ZIN PH 1/16 was remodeled, but it is uncertain if osteodermal ossifications were involved in that process. According to the hypothesis of Vickaryous et al. (2001a), "the superficial furrows that divide the cranium…represent the areas of coossification between adjacent cephalic osteoderms". The presence of the Y-shaped groove thus implies that the osteoderms are preserved and co-ossified with the skull roof in ZIN PH 1/16. There is no frontoparietal depression. The posterior edge of the skull roof is broken off. The broken lateral edges of the skull roof overhang the adductor cavities, and there are no traces of the supratemporal fenestrae.

The boundaries between the skull roof and braincase are partly recognized on the preserved right paroccipital process in the occipital view (Fig. 1E), and are inferred on the lateral surface of the specimen based on the position of small vascular foramina that frequently lie near the border between the skull roof and braincase (Galton, 1988; Galton and Knoll, 2006; Fig. 2A). The pattern of facets on the skull roof in the referred specimen ZIN PH 281/16 supports this reconstruction of the boundaries in the holotype. The parietal has two posterolateral processes that are sutured ventrolaterally to the dorsal surface of the paroccipital processes and medially to the supraoccipital (the latter contact is hard to trace; Fig. 1E). The posterolateral processes are anteroposteriorly thin and oriented almost perpendicular to the sagittal plane of the skull. The posterior surface of the posterolateral processes is slightly posteroventrally-anterodorsally inclined. On the lateral aspect of ZIN PH 1/16, the skull roof appears to form an almost horizontal, slightly posteroventrally inclined contact with the braincase posterior to the capitate process of the laterosphenoid and a gently anteroventrally inclined contact anteriorly (Fig. 2A). Posteriorly in lateral view, the parietal roofs a small vascular recess (nvr, Fig. 2A, B) and forms the dorsomedial wall of the adductor cavity. Here the skull roof reaches its greatest dorsoventral thickness of 21 millimeters.
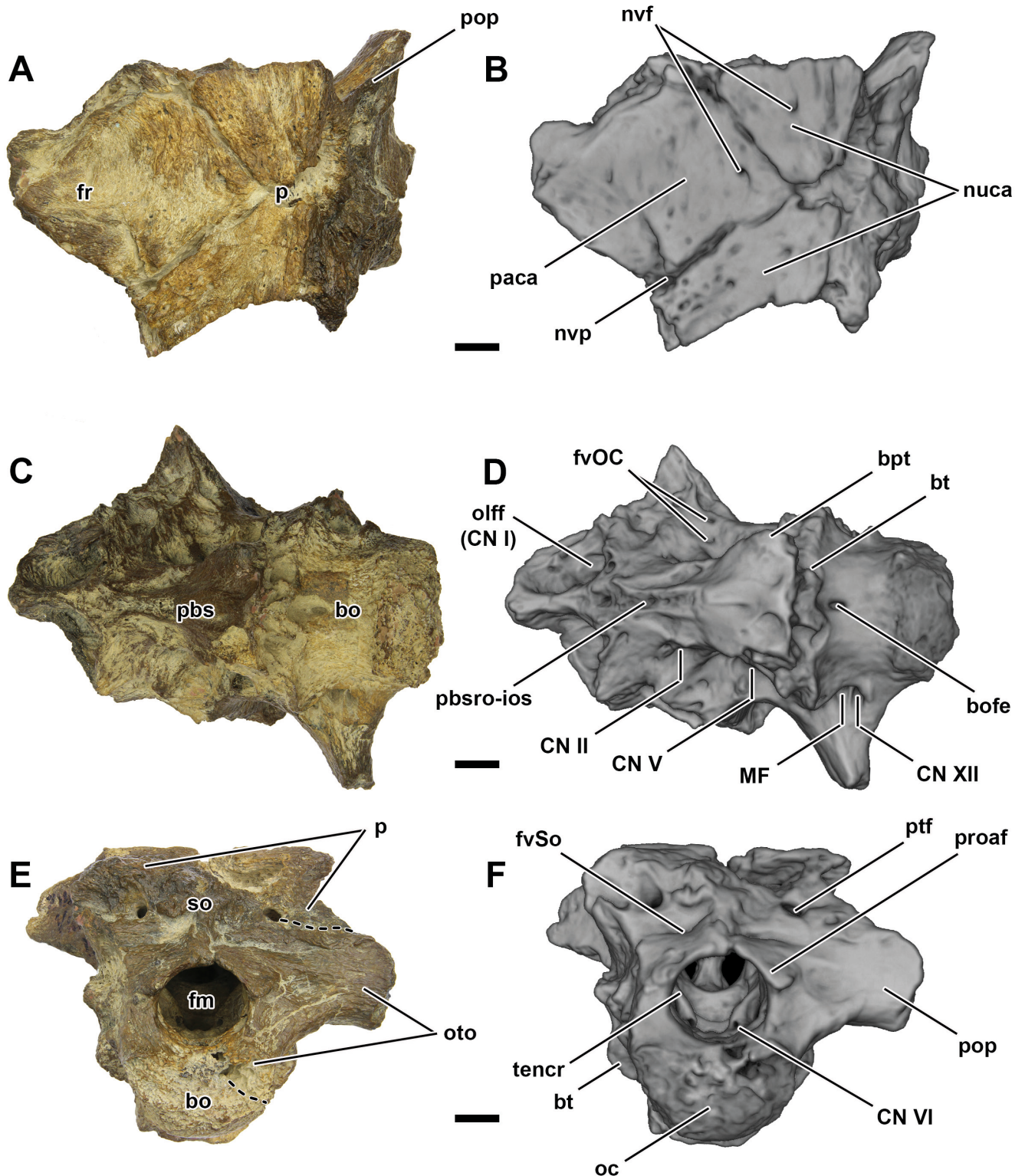
Fig. 1. ZIN PH 1/16, holotype of *Bissektipelta archibaldi* from the Bissekty Formation (Turonian), Uzbekistan. Photographs and corresponding CT-based models in dorsal (A, B), ventral (C, D), and occipital (E, F) views. Scale bars each equal 1 cm. Abbreviations: **bo**, basioccipital; **bofe**, basioccipital fenestra; **bpt**, basipterygoid process; **bt**, basal tuber; **CN II — XII**, cranial nerve foramina; **fm**, foramen magnum; **fr**, frontal; **fvOC**, foramen for orbitocerebral vein; **fvSo**, foramen for supraoccipital vein; **MF**, metotic foramen; **nuca**, nuchal caputegulum; **nvf**, neurovascular foramen; **nvp**, neurovascular pit; **oc**, occipital condyle; **olff (CN I)**, olfactory fenestra; **oto**, otoccipital; **p**, parietal; **paca**, parietal caputegulum; **pbsro-ios**, fused parabasisphenoid rostrum and interorbital septum; **pop**, paroccipital process; **proaf**, proatlas facet; **ptf**, posttemporal fenestra; **so**, supraoccipital; **tencr**, tentorial crest.

Ventral surface of the basicranium. The basioccipital and the parabasisphenoid meet at an angle of approximately 90º in ZIN PH 1/16; the suture between these bones is evident in lateral and ventral views (Figs. 1D, 2). Overall the basioccipital is massive and robust. The neck of the occipital condyle is barely defined. The ventral surface of the basioccipital is posteroventrally oriented, concave, and broad; it is slightly wider lateromedially than the corresponding surface of the parabasisphenoid. The basal tubera (= sphenoccipital tubera in Kurzanov and Tumanova [1978] and Tumanova [1987]) are rounded, anteroposteriorly thin, and project laterally (bt, Fig. 1D, F). The basioccipital fenestra (bofe, Fig. 1D) is present as a distinct blind fissure on the ventral surface between the basal tubera. CT data show that two small, presumably vascular canals extend from it anteriorly and posteriorly inside the bone and gradually disappear in the trabeculae. The basioccipital fenestra is present in the same location ventral to the occipital condyle in present-day crocodylians; a small vein traverses this foramen (Owen, 1850).

The parabasisphenoid has a triangular, anteroventrally oriented ventral surface (Fig. 1C, D). The surface between the basipterygoid processes is mediolaterally wider and gradually tapers anteriorly. The left basipterygoid process is slightly incomplete (bpt, Fig. 1D). The basipterygoid process is a knob that projects ventrolaterally. It is oval in cross-section, with the longer axis directed anteriorly. Its anteroposterior length is nearly twice the mediolateral width at its base. The surface between the basipterygoid processes is relatively flat; there is a shallow depression on each side close to the base of the process. Only the base of the fused parabasisphenoid rostrum (= cultriform process) and the ossified/calcified interorbital septum is preserved. It is situated anterior to the basipterygoid processes (pbsro-ios, Fig. 1D). The base of the fused parabasisphenoid rostrum-interorbital septum extends obliquely anteriorly to the sphenethmoidal complex, where it merges with the septum that separated the olfactory bulbs (= mesethmoid in Miyashita et al. [2011]; Figs. 1D, 2E). Regarding the preserved part, the base of these elements is slightly transversally constricted at its mid-length and then expands anteriorly. On each side of the fused parabasisphenoid rostrum-interorbital septum are longitudinal depressions (possibly for the sphenopalatine artery; gaSP, Fig. 2D). A pronounced ridge ventral to the foramen for the optic cranial nerve (CN II) delimits the course of the longitudinal depression dorsally. No sutures in the region of the sphenethmoidal complex are discernable.

Occipital surface. The occipital surface is inclined at the angle of about 125º to the dorsal surface of the skull (Fig. 2A). When the specimen is held such that its skull roof surface is oriented horizontally, the occipital condyle is directed posteroventrally and barely projects beyond the occipital plane. The articular surface of the condyle is crescent-shaped and transversely elongated (lateromedial length nearly 1.5 times larger its dorsoventral depth; Fig. 1E, F). The articular surface of the condyle is slightly eroded. The suture with the otoccipital is visible on the right lateral and posterior surfaces of the condyle (Figs. 1E; 2A); it indicates that the otoccipitals formed the dorsolateral corners of the occipital condyle. The posterior surface of the basioccipital ventral to the condyle is notably arched dorsally and overall faces posteroventrally (Fig. 2).

The foramen magnum is nearly circular. Its lateral and dorsal margins are formed by the otoccipitals; the supraoccipital appears to be excluded from the dorsal margin. Paired triangular surfaces (proatlas facets) project from dorsolateral corners of the foramen magnum (proaf, Fig. 1F). They merge medially and form a dorsal shelf over the foramen magnum. The proatlas facets overhang rounded notches that are sometimes interpreted as the path of the first spinal nerve (Kurzanov and Tumanova, 1978; Parish and Barrett, 2004). In addition, or as an alternative hypothesis, these sulci can correspond to the route of a venous vessel that branches off from the longitudinal venous sinus or its posterior expansion (occipital sinus) at the foramen magnum and courses ventrolaterally (Porter, 2015). Just dorsal to the proatlas facets, there are paired small foramina with associated grooves. These foramina pierce the occipital surface of the braincase directly to the endocranial cavity and likely transmitted small supraoccipital veins (fvSo, Fig. 1F). A venous foramen in a similar position above the foramen magnum was noted for "*Amtosaurus magnus*" (Kurzanov and Tumanova, 1978). Medial to these vascular foramina, on the assumed posterior surface of the supraoccipital, there is the base of the sagittal nuchal crest; dorsally, this surface is obscured by damage.

Paired rounded posttemporal fenestrae are present lateral to the sagittal nuchal crest (ptf, Fig. 1E, F). In general, the posttemporal fenestrae appear to lie near the contact of the parietal, supraoccipital, and otoccipital, but the precise sutural pattern is entirely obscured on the left side and is not clear on the right. The presumed parietal-otoccipital suture is situated at the ventrolateral margin of the posttemporal fenestra; thus, the ventral margin of the posttemporal fenestra is likely formed by the paroccipital process of the otoccipital, and its dorsolateral margin by the parietal. It is likely that the supraoccipital contributed to the margin of the fenestra medially; alternatively, the medial margin of the fenestra may have been formed by the otoccipital and the parietal. The posttemporal fenestra pierces anteriorly into a small recess on either side of ZIN PH 1/16. This recess is evident in lateral view (nvr+g, Fig. 2A, B); it lies dorsal to the paroccipital process and medial to the adductor cavity. A notable groove is present at the anterior margin of the
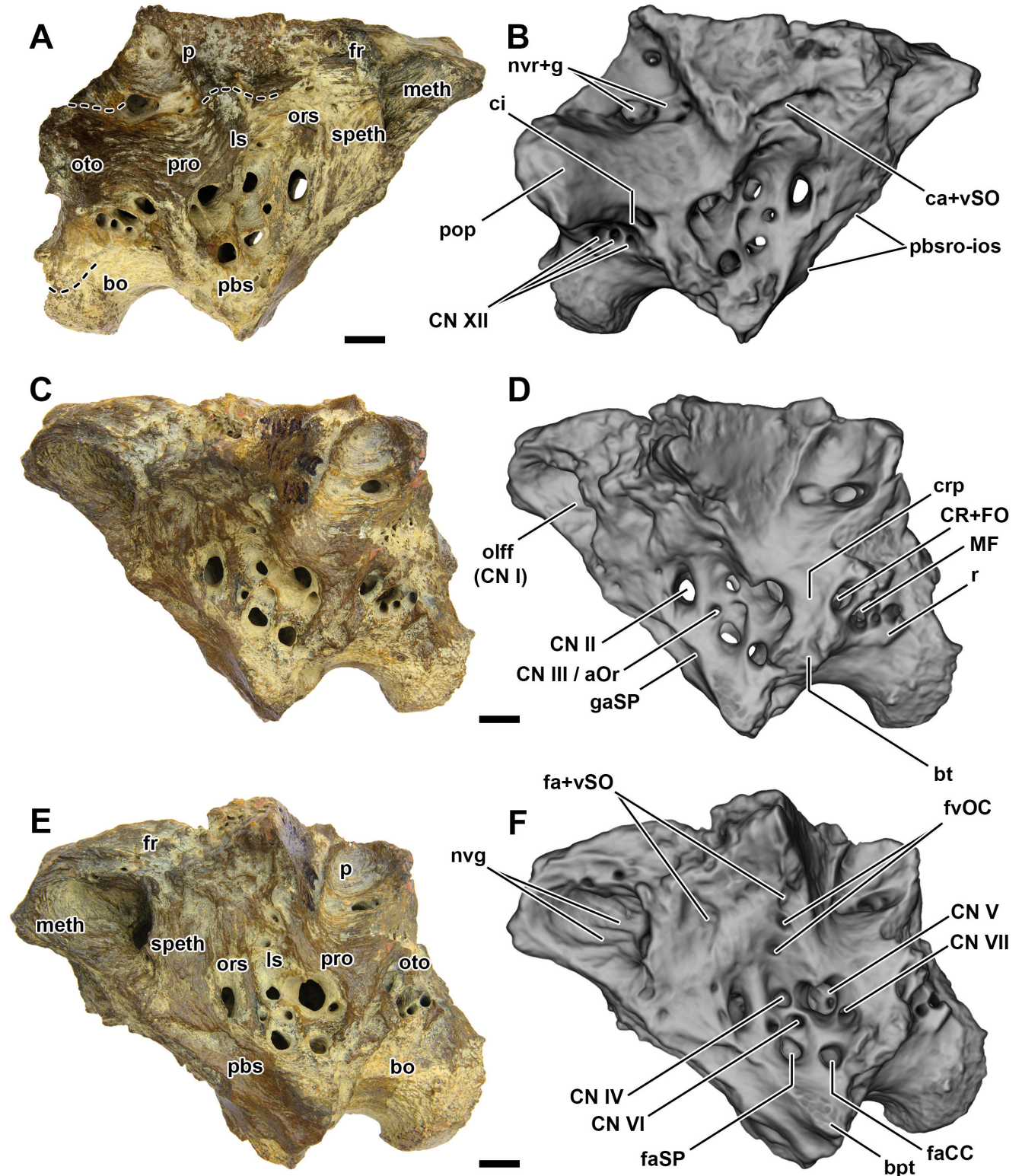
Fig. 2. ZIN PH 1/16, holotype of *Bissektipelta archibaldi* from the Bissekty Formation (Turonian), Uzbekistan. Photographs and corresponding CT-based models in right lateral (A, B), left lateral (C, D), and oblique left lateral (E, F) views. Scale bars each equal 1 cm. Abbreviations: **bo**, basioccipital; **bpt**, basipterygoid process; **bt**, basal tuber; **ca+vSO**, canal for supraorbital artery and vein; **ci**, crista interfenestralis; **CN II — XII**, cranial nerve foramina; **CN III / aOr**, foramen for oculomotor nerve or orbital artery; **CR+FO**, columellar recess and fenestra ovalis; **crp**, crista prootica; **fa+vSO**, foramen for supraorbital artery and vein; **faCC**, foramen for cerebral carotid artery; **faSP**, foramen for sphenopalatine artery; **fr**, frontal; **fvOC**, foramen for orbitocerebral vein; **gaSP**, groove for sphenopalatine artery; **ls**, laterosphenoid; **meth**, mesethmoid; **MF**, metotic foramen; **nvg**, neurovascular groove; **nvr+g**, neurovascular recess and groove; **olff (CN I)**, olfactory fenestra; **ors**, orbitosphenoid; **oto**, otoccipital; **p**, parietal; **pbs**, parabasisphenoid; **pbsro-ios**, fused parabasisphenoid rostrum and interorbital septum; **pop**, paroccipital process; **pro**, prootic; **r**, ridge; **speth**, sphenethmoid.

recess, suggesting the course of a blood vessel along the dorsomedial wall of the adductor cavity. Both the walls of the recess and the anterior groove are pierced by numerous small vascular foramina.

The preserved right paroccipital process extends laterally and slightly posteriorly and is incomplete distally (pop, Fig. 1). It is anteroposteriorly thin at its distal end and thick and robust at its base. The process is relatively narrow dorsoventrally; its depth equals the height of the foramen magnum. Two blunt ridges curve dorsolaterally and converge to form the ventral margin of the paroccipital process. The ventral margin of the paroccipital process is slightly arched dorsally and is nearly at the same level as the ventral border of the foramen magnum. Dorsally, the process is sutured to the skull roof. There is a small but pronounced depression at the posterior surface of the paroccipital process.

Lateral braincase wall. The elements forming the lateral wall of the braincase are fused (e.g., the sphenethmoidal complex, the orbitosphenoid, the laterosphenoid, the parabasisphenoid, the prootic, and the otoccipital). No clear sutures can be observed, with the exception of the basioccipital-otoccipital suture on the condyle on the right side and the suture between the basioccipital and parabasisphenoid. All structures are paired, and the right and left sides of ZIN PH 1/16 have the same general structure and proportions. The lateral wall is penetrated by numerous neurovascular foramina (Fig. 2). These are clustered into two major groups and are relatively closely spaced within the cluster. The anterior group includes the foramina for CN II-VII and two primarily vascular foramina (for the cerebral carotid artery and the sphenopalatine artery and vein). The posterior group is situated ventral to the base of the paroccipital process and comprises the columellar recess/fenestra ovalis, the metotic foramen, and the foramina for CN XII.

The two clusters of foramina are separated by a flattened strip of bone that extends ventrally between the basioccipital and the parabasisphenoid portion of the basal tuber. Dorsally, its posterior margin arches over the fenestra ovalis onto the ventral edge of the paroccipital process (crp, Fig. 2D). This structure corresponds to a poorly developed crista prootica (= otosphenoidal crest in Sampson and Witmer, 2007) that in diapsids separates the more anterior cranial nerve foramina from the posterior depression containing ear-related structures (fenestra ovalis plus metotic foramen). Generally in diapsids, the crista prootica arches posterodorsally from the parabasisphenoid lateral surface, just above the basipterygoid process. The crista prootica in *Bissektipelta* contacts ventrally the basal tubera instead of the basipterygoid proces. This is likely due to the highly divergent braincase structure of *Bissektipelta* (and other ankylosaurs) from the basic diapsid pattern, specifically

the posterior position of the basipterygoid processes close to the basal tubera.

The olfactory fenestrae are the only neurovascular foramina directed anteriorly instead of laterally (olff, Fig. 2D, F). They are paired and separated by a thick bony septum (= mesethmoid in Miyashita et al. [2011]). They are the largest neurovascular foramina and approach the foramen magnum in size. The olfactory fenestrae housed short paired olfactory bulbs and the ethmoid vessels, and they communicated directly with the olfactory region of the nasal cavity (Miyashita et al., 2011). The internal walls of the olfactory fenestrae are covered by numerous anteroposterior grooves, indicating that a large number of neurovascular bundles passed through them (nvg, Fig. 2E, F). The two separate cavities for the olfactory bulbs converge posteriorly into a single chamber that is separated from the rest of the endocranial cavity by a rounded constriction.

Only the base of the broken preorbital septum is preserved. The preorbital septum is a thin transversal bony lamina that separates the nasal and orbital cavities in ankylosaurs; it was first named by Maryańska (1977) (= ectethmoid in Miyashita et al. [2011]; see the description of ZIN PH 2329/16 below). Between the base of the preorbital septum and the anterior cluster of neurovascular foramina, the surface of the braincase wall bears no foramina and has dorsoventral striations. The largest foramen among the anterior cluster is that for CN V; the opening for CN II is the second largest. The foramina for the cerebral carotid artery and for the sphenopalatine vessels are prominent and nearly equal in size (faCC and faSP, Fig. 2F). The large recess of the ganglion of CN V has a triangular projection from its dorsal margin that separates the anteriorly directed groove for CN V_1 (ophthalmic branch of the trigeminal nerve) from posteroventrally directed grooves for CN V_{2+3} (maxillary and mandibular branches of the trigeminal nerve; see Holliday and Witmer [2007]). The small foramen for CN VII lies in the same large recess with that for CN V and is separated by a small ridge from the latter. The foramen for CN II is separated from the more posterior foramina by a thick vertical strut of bone. A small groove on the ventral margin of the foramen for CN II possibly indicates the course of a small vessel (Fig. 2D, E). There is a prominent depression on the lateral braincase wall dorsal to the foramen for CN IV and anterior to the adductor cavity (the postocular shelf is not preserved here in ZIN PH 1/16; see the description of ZIN PH 2329/16 below). The depression is pierced by two foramina for the orbitocerebral vein and a series of smaller vascular openings (fvOC, Fig. 2F).

The columellar recess/fenestra ovalis (CR/FO), the metotic foramen (MF), and three external foramina for CN XII are closely spaced and situated in a single depression ventral to the paroccipital process. This de-

pression is bordered by the crista prootica anteriorly, the basal tuber ventrally, and the prominent blunt ridge posteriorly (r, Fig. 2D). The latter connects with the ventral margin of the paroccipital process so that the foramina for CN XII are not evident in posterior view (Fig. 1E, F). The external openings of the CR/FO and MF are almost equal in size and large. The crista interfenestralis (= ventral ramus of opisthotic in more basal archosaurs; e.g., Gower, 2002; Sobral et al., 2016) separates FO and MF (ci, Fig. 2B). It is a slightly anteroventrally inclined lamina of bone that is barely visible in posterior view. The three foramina for CN XII are almost vertically arranged posterior to MF. The posteriormost foramen is the largest of the three. The anteriormost foramen for CN XII is the smallest and lies below MF.

Endocranial surface. The complex endocranial surface can be anteroposteriorly subdivided into four main concave regions (olfactory and cerebral fossae, and two fossae anterior and posterior to the otic capsule) separated by convex crests (Fig. 3). The anterior part of the endocranial cavity in ZIN PH 1/16 corresponds the posteriormost portion of the olfactory region of the nasal cavity (distinguished by rugose walls with numerous neurovascular grooves) and paired cavities of the olfactory bulbs that merge posteriorly into the cavity for the olfactory tract (olfbc and olftc, Fig. 3). The olfactory tract cavity is constricted laterally by paired blunt crests, which emphasize the division between the olfactory region anteriorly and the cerebral fossa posteriorly.

The cerebral cavity is circumscribed by the blunt olfactory crest anteriorly and by the tentorial crest (sensu Sedlmayr [2002]) posteriorly on each side (olfcr and tencr, Fig. 3A). Several neurovascular structures pierce the surface of the cerebral fossa, including the foramen for CN IV and two conspicuous foramina for the orbitocerebral vein (Fig. 3A). The surface of the cerebral cavity has a gently corrugated texture but lacks prominent vascular valleculae, indicating that the brain was not in close relationship to the endocranial wall and loosely fitted the cerebral cavity (Evans, 2005). The large transverse groove for CN II is offset anteroventrally and opens posteriorly into the cerebral cavity (Fig. 3B). Its dorsal margin forms a blunt crest that arches posterodorsally onto the lateral endocranial surface on each side and merges with the tentorial crest. This oblique crest marks the subdivision of the cerebral fossa into two smaller fossae, roughly corresponding to the cerebral hemispheres anteriorly and the optic lobes posteriorly. The ventral margin of the CN II groove forms a sharp crest that denotes the anterior dorsal limit of the hypophyseal cavity.

The cerebral cavity merges into the hypophyseal cavity ventrally (hypc, Fig. 3). The hypophyseal cavity is comparatively shallow, being half the depth of the cerebral cavity. Foramina for the cerebral carotid and sphenopalatine arteries and for CN III pierce its surface

(Fig. 3). The internal foramen for CN III is unexpectedly situated ventrally, well in the limits of the hypophyseal cavity. A groove connects the internal openings of the sphenopalatine artery and CN III, raising the possibility that the latter may actually be a vascular foramen, perhaps for a branch of the cerebral carotid/sphenopalatine artery (e.g., the orbital artery of extant birds) or for the orbital/hypophyseal vein that drains into the cavernous sinus (Bruner, 1907; Porter and Witmer, 2015; Porter and Witmer, 2016a). In that case, the actual CN III would leave the braincase through the dorsally situated foramen for CN IV, as in *Euoplocephalus* (Miyashita et al., 2011). We tentatively follow the initial description by Averianov (2002) and maintain a conservative interpretation of the foramen in question as for CN III.

The dorsum sellae bulges over the hypophyseal cavity dorsally. It has a short anterior triangular projection surrounded by two grooves medially. This projection is also evident in the referred specimen of *Bissektipelta* ZIN PH 281/16, in "*Amtosaurus magnus*" (Kurzanov and Tumanova, 1978), and is possibly present, though less developed, in several other Mongolian taxa (Averianov, 2002; Parish and Barrett, 2004). We regard these grooves as vascular impressions that indicate the course of posterior venous branches of the cavernous sinus (caudoventral cerebral veins) or, as an alternative hypothesis, the course of the caudal encephalic arteries (Sedlmayr, 2002; Porter, 2015; Porter et al., 2016). Posteriorly to the dorsum sellae, the floor of the endocranial surface is essentially flat.

The tentorial crest is prominent; ventrally, it is confluent with the lateral aspect of the dorsum sellae, arches anterodorsally over the anterior margin of the foramen for CN V, and then curves posterodorsally and extends to the roof of the endocranial cavity (tencr, Fig. 3A). The internal opening for CN VI pierces the base of the tentorial crest; the foramen for CN VII lies dorsolateral to it (Fig. 3B). The tentorial crest circumscribes a fossa dorsal to the foramen for CN V that was likely occupied by the cerebellum and a large venous vessel (middle cerebral vein; vMC, Fig. 3A). The latter opened externally through a series of foramina at the posterodorsal aspect of the fossa. The floccular (= auricular) fossa is very shallow.

The medial wall of the otic capsule is incompletely ossified (sc+ves in Fig. 3A). The amount of the exposure may have been exaggerated by postmortem fracture; however, both the referred specimens have largely medially open vestibules. The recesses for the vestibule, common crus, and lagena are medially open and confluent with the endocranial cavity. Paired unossified fossae with unfinished margins at the floor of the endocranial cavity mark the position of the lagenae (lagf, Fig. 3B). These fossae are comparatively large and probably contained additional structures such as supportive vascular plexus. A bifurcating groove extends posterodorsally
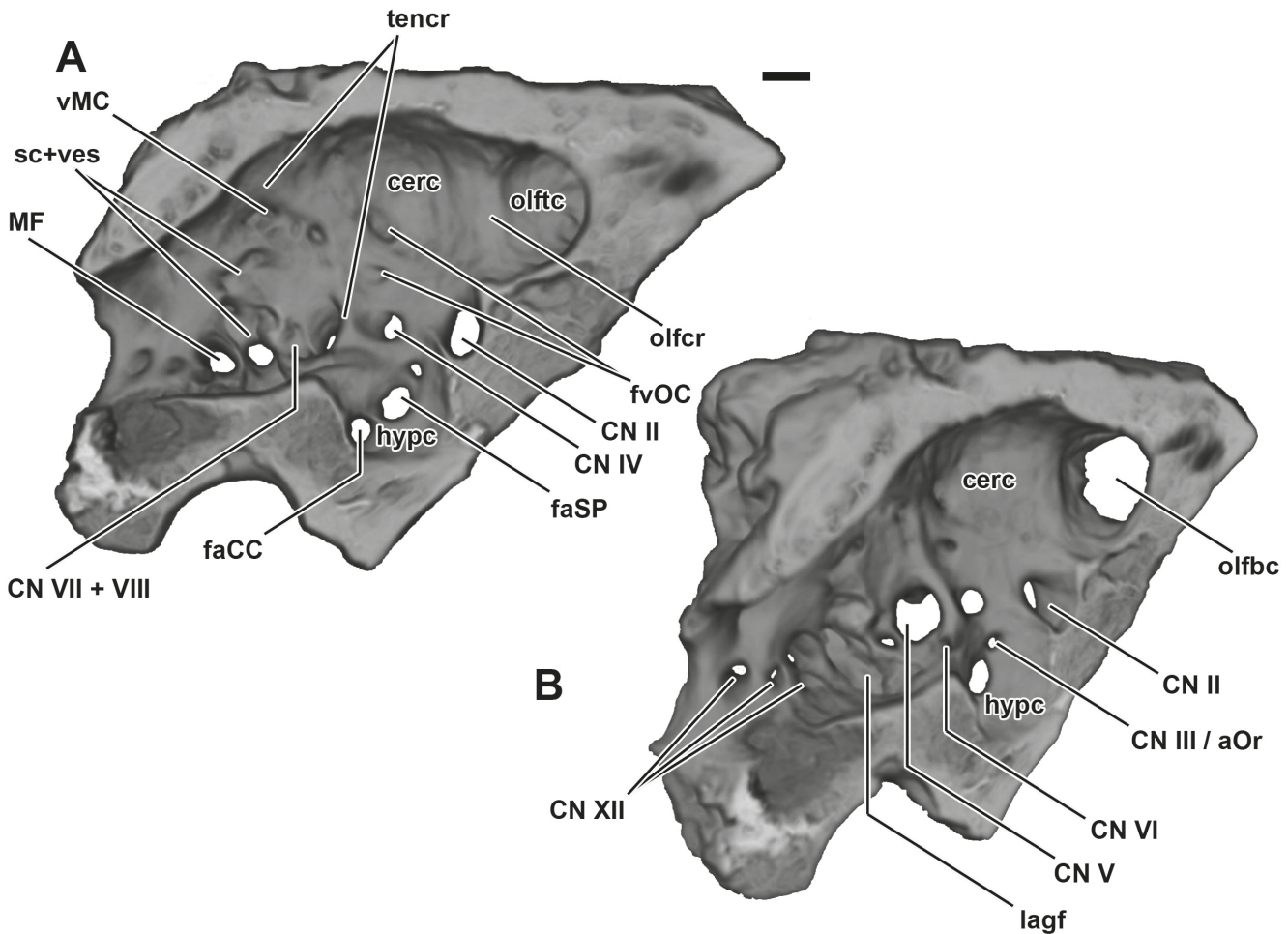
Fig. 3. ZIN PH 1/16, holotype of *Bissektipelta archibaldi* from the Bissekty Formation (Turonian), Uzbekistan. Parasagitally sectioned CT-based models showing left endocranial surface, in medial (A) and posteromedial (B) views. Scale bar equals 1 cm. Abbreviations: **cerc**, cerebral cavity; **CN II — XII**, cranial nerve foramina; **CN III / aOr**, foramen for oculomotor nerve or orbital artery; **faCC**, foramen for cerebral carotid artery; **faSP**, foramen for sphenopalatine artery; **fvOC**, foramen for orbitocerebral vein; **hypc**, hypophyseal cavity; **lagf**, lagenar fossa; **MF**, metotic foramen; **olfbc**, olfactory bulb cavity; **olfcr**, olfactory crest; **olftc**, olfactory tract cavity; **sc+ves**, cavities of semicircular canals and vestibule; **tencr**, tentorial crest; **vMC**, groove for middle cerebral vein.

from the internal foramen for CN VII and indicates the course of CN VIII (Fig. 3A); a similar reconstruction of this region was made for some ornithopods (Hopson, 1979; Sobral et al., 2012). The internal opening of the metotic foramen (MF) is just posterior to the otic capsule. The metotic foramen is undivided (see discussion in Rieppel [1985]; Gower and Weber, 1998; Sobral et al., 2012) and likely transmitted the perilymphatic sac, CN IX–XI, and the posterior cerebral vein (vagal vein in Sedlmayr [2002]). The wall between the vestibular recess and the MF is incised. This notch indicates the position of the incompletely ossified perilymphatic foramen that transmitted the perilymphatic sac from the otic capsule to the MF (Baird, 1960; Gower, 2002; Gower and Walker, 2002). Two larger internal foramina for CN XII pierce the endocranial wall posterior to the MF; a single small opening is just ventral to it. An extensive shallow depression with a deeper pit above these structures indicates the position of the occipital venous sinus (Fig. 3B; Sedlmayr, 2002; Witmer et al., 2008; Porter, 2015).

Endocast. The endocast of ZIN PH 1/16 generated from a CT scan data is complete, undistorted, and relatively detailed (Fig. 4; Table 2). It comprises casts of the endocranial cavity, cranial nerves, both endosseous labyrinths, and vascular canals. The morphology of the inner ear and braincase vasculature of ZIN PH 1/16 are described in separate sections below. The brain of *Bissektipelta* loosely fitted the endocranial cavity as is common for many non-avian dinosaurs and for reptiles in general (Hopson, 1979; Witmer et al., 2008). Thus, the produced endocast is more a cast of the meninges (including endocranial venous sinuses) rather than the brain itself. Nevertheless, it appears to be a faithful inference of gross morphology of the brain as is suggested by recent research on extant archosaurs (Watanabe et al., 2019). Additionally, the endocranial vessels of various extant diapsids have a rather conservative pattern (Porter, 2015; see Vasculature and Fig. 9 below), and their disposition revealed on the endocast of *Bissektipelta* is a reliable proxy for recognition of major brain divisions.
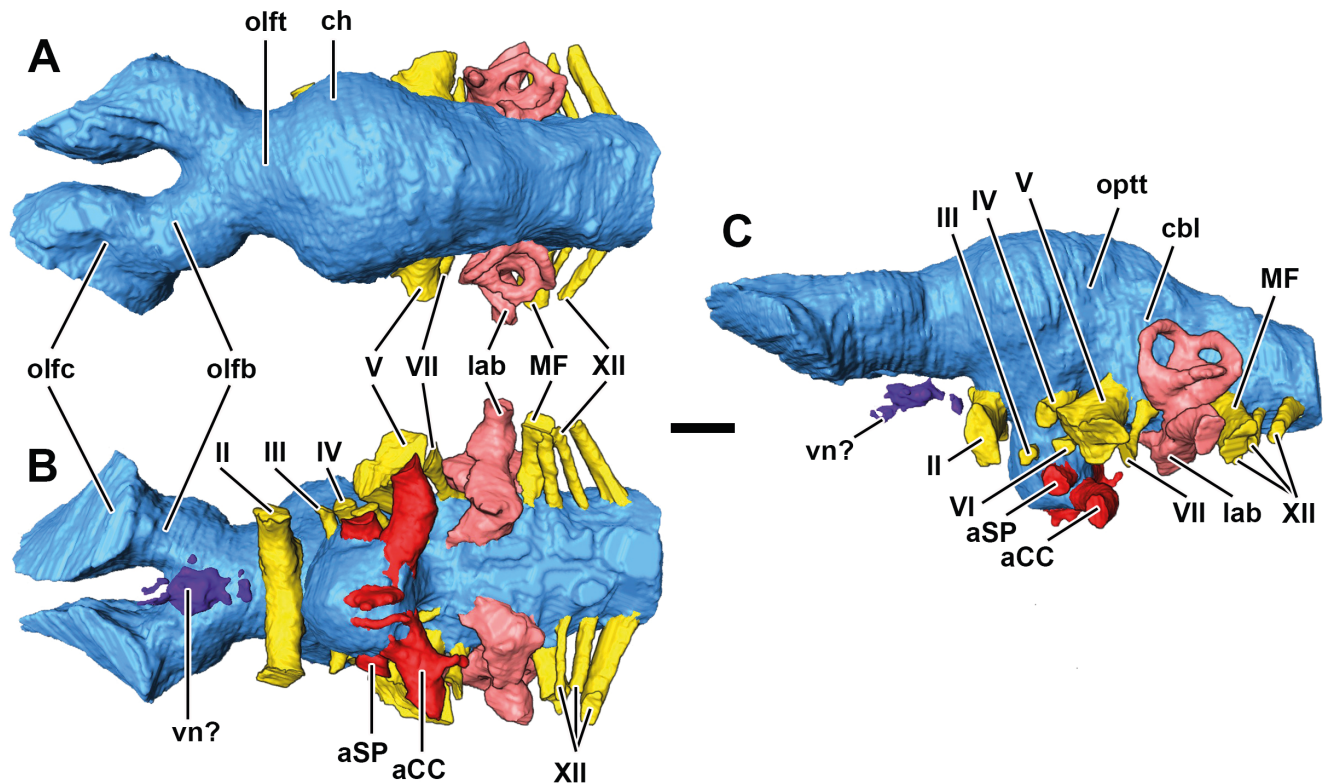
Fig. 4. ZIN PH 1/16, holotype of *Bissektipelta archibaldi* from the Bissekty Formation (Turonian), Uzbekistan. Cranial endocast with endosseous labyrinth of the inner ear in dorsal (A), ventral (B), and left lateral (C) views. Scale bar equals 1 cm. Abbreviations: **aCC**, cerebral carotid artery and vein; **aSP**, sphenopalatine artery and vein; **cbl**, cerebellum; **ch**, cerebral hemisphere; **lab**, endosseous labyrinth; **MF**, metotic foramen passage; **olfb**, olfactory bulb; **olfc**, olfactory cavity cast; **olft**, olfactory tract; **optt**, optic tectum of the midbrain; **vn?**, vomero-nasal bulbs?; **II — XII**, cranial nerves.

The endocranial cast is elongate and relatively straight, with low angles of cerebral and pontine flexures of about 30º; the cranial nerves and the fenestra ovalis of the labyrinth are correspondingly linearly arranged (Fig. 4C). The olfactory bulbs diverge anteriorly at an angle of approximately 80º from a short and broad olfactory tract (CN I; olfb and olft in Fig. 4A). The bulbs and the tract are nearly circular in cross-section. The olfactory ratio (the ratio of the greatest diameter of the olfactory bulb to the greatest diameter of the cerebral hemisphere regardless of their orientation; Zelenitsky et al., 2009) equals nearly 63–69 %. It is comparable to that of other ankylosaurs (see Discussion below) and suggests proportionally large olfactory bulbs in *Bissektipelta* and other ankylosaurs. Anteriorly, the endocast of each olfactory bulb terminates in a rounded expansion with wrinkled walls that corresponds to the olfactory region of the nasal cavity (olfc, Fig. 4A). The wrinkles most likely represent neurovascular bundles passing to and from the endocranial cavity, and part of them was visualized as the vascular olfactory plexus (olfP, Fig. 6; see "Vasculature" section below). Paired cavities within the ossified ethmoidal region, ventral to the olfactory tract, were segmented (vn?, Fig. 4A, B). A similar cavity was also found ventral to the broken mesethmoid in the referred specimen ZIN PH 281/16 (see Figs. 11–14). These struc-tures lie below the olfactory complex of *Bissektipelta* and could correspond to the part of the vomeronasal bulb or vascular sinuses. These structures are reported for the first time in dinosaurs and require additional study to elucidate their nature.

The short olfactory tract posteriorly merges into a rounded cast of the cerebral cavity. The anterior part of the cavity's endocast reaches maximum dorsoventral depth and lateromedial breadth (Table 2) and corresponds to the cerebral hemispheres (ch, Fig. 4A). The cerebral hemispheres are relatively discrete on the endocast. The absence of a dorsal groove between the hemispheres indicates that the dorsal longitudinal venous sinus occupied the space above the latter.

The endocast of *Bissektipelta* lacks the dorsal dural peak present on endocasts of stegosaurs (Galton, 1988; Galton, 2001; Leahey et al., 2015: Fig. 10), most sauropods (Witmer et al., 2008), and some theropods (e.g., Sampson and Witmer, 2007). Dorsal expansions of dinosaur endocasts have been interpreted as an unossified gap plugged with cartilage in life (Hopson, 1979) or as corresponding to extensive dural sinuses that may have surrounded the pineal complex (Sampson and Witmer, 2007; Witmer et al., 2008). In *Bissektipelta*, the only structure of the endocast that may correspond to the pineal complex is a conspicuous median vessel (medVs,

PALAEONTOLOGY

Table 2. Endocast measurements of *Bissektipelta archibaldi*. All linear measurements in millimeters; volume in cm^3

Parameter	ZIN PH 1/16	ZIN PH 281/16
Whole endocast length	103	70
Endocast length without the cast of the olfactory region of the nasal cavity	85	–
Endocast volume (without vessels and nerves)	53	
Endocast width across cerebral hemispheres	33	29
Olfactory bulb maximum cross-sectional diameter	15	–
Olfactory tract width	19.5	12
Pituiatary depth	19	18
Pituitary diameter	16.5	12.5

Fig. 7). Its canal pierces the skull roof all the way through to the endocast and connects to the anterior branching plexuses laterally (see Vasculature below). The median vessel emerges at the surface of the endocast just anterodorsal to the inferred division between the cerebral hemispheres and the optic lobes (assessed by the position of the cerebrotectal venous sinus and the disposition of crests on the endocranial surface), at the level of the optic chiasm and the pituitary. This position broadly corresponds to that of the pineal complex in other diapsids (e.g., *Sphenodon*; Dendy, 1911). Notably, the pineal complex, optic chiasm, and the neurohypophysis are all diencephalic derivates. However, the external pineal (parietal) foramen was lost early in archosauriform evolution (Hopson, 1979; character 63 in Nesbitt, 2011); extant birds have a pineal that lies internally within the braincase, adjacent to the skull roof (Ralph, 1970). Thus, we doubt that the median canal of *Bissektipelta* contained a pineal/parapineal organ that was exposed on the dorsal surface of the skull roof and consider the structure a vascular canal. However, noting its remarkable position, we hypothesize this canal enclosed vessels that may have been connected to pineal vasculature. The point of emergence of the median vessel from the endocast thus marks a possible position of the pineal complex in *Bissektipelta*.

The optic chiasm is located on the ventral surface of the endocast of *Bissektipelta*, below the cerebral hemispheres and just anterior to the hypophysis (Fig. 4). Each CN II leaves the braincase by a separate lateral foramen. The endocasts of the canals for CN II and of the optic chiasm form a single straight trunk that is oriented strictly perpendicular to the longitudinal axis of the braincase (Fig. 4B).

The complete cast of the hypophyseal (pituitary) fossa is present just posterior to the optic chiasm and ventral to the hemispheres (Fig. 4B, C). The pituitary projects vertically from the ventral surface of the endocast. Overall, the pituitary cast is a tubular structure with an even diameter throughout; the stalk itself is not

expressed. It is relatively short dorsoventrally (its dorsoventral depth equals nearly 19 mm and is half the depth of the cerebral cavity above it), broad, and nearly circular in cross-section (Table 2). The hypophyseal fossa apparently contained the infundibulum (hypophyseal stalk) and the hypophysis, which were likely surrounded by the cavernous venous sinus, as it in extant archosaurs (Neumeier and Lametschwandtner, 1994; Sedlmayr, 2002; Porter et al., 2016; Porter and Witmer, 2016a). The hypophyseal fossa of *Bissektipelta* was well vascularized. Large cerebral carotid arteries entered the hypophyseal cavity transversely as in most other ankylosaurs (e.g., Paulina-Carabajal et al., 2018); the sphenopalatine arteries branched off of them and left the hypophyseal cavity slightly anteriorly (a+vCC and a+vSP in Fig. 4B, C). The cerebral carotid and sphenopalatine veins that drained the cavernous sinus and the orbit/palate apparently shared canals with similarly named arteries. The stalk of CN III appears roughly at the mid-height of the endocast of the hypophyseal cavity, which occupies an unusually ventral position compared to those on most other dinosaur endocasts (Fig. 4C). A swelling on the lateral surface of the pituitary endocast connects the CN III trunk with the sphenopalatine artery endocast, which, combined with its low position, possibly indicates that the former represented a vessel (e.g., orbital artery and vein) rather than a nerve.

The optic lobes of the midbrain (optt, Fig. 4C) are not directly discernable on the endocast of ZIN PH 1/16 as they were likely overlain by sizable dural venous sinuses. The approximate position of the midbrain could be determined through the disposition of major encephalic vessels and general topographic cues of the diapsid brain (reviewed by Hopson [1979], Witmer et al. [2008], and others). The optic tectum of the midbrain in *Bissektipelta* apparently laid between the cerebral hemispheres anteriorly and the cerebellum posteriorly (Fig. 4C); thus, the brain had a linear arrangement that is similar to that in extant crocodiles, plesiomorphic for dinosaurs in general, and characteristic of many ornithischians in par-

ticular (Hopson, 1979; Balanoff and Bever, 2017). The endocranial cast of *Bissektipelta* is slightly constricted mediolaterally at the level of the optic tectum; its dorsal outline smoothly arches posteroventrally in lateral view. The short trunk of CN IV projects anterolaterally and slightly ventrally from the endocast above the pituitary (Fig. 4C). If we assume that the canal for CN III housed vascular structures rather than the actual cranial nerve, CN III must have left the braincase through the canal for CN IV.

The cerebellum is not distinctly expressed, and there is no prominent flocculus on the endocast of ZIN PH 1/16 (cbl, Fig. 4A, C). The region of the endocast that corresponds to the cerebellum is posterior to a groove reflecting the position of the tentorial crest. The cerebellum was circumscribed by extensive dural vessels, e.g., the middle cerebral vein anterodorsally and the longitudinal sinus (torcular Herophili part) dorsally (Figs. 6A, 7A, 9A).

Part of the endocast corresponding to the medulla oblongata is nearly as broad mediolaterally as it is anteroposteriorly long. The structure of the medulla oblongata is obscured by extensive occipital venous sinus (sOc, Fig. 7A). The ventral surface of the brainstem is essentially flat and straight in lateral view; it is only slightly notched behind the endocast of the hypophyseal fossa anteriorly (Fig. 4B, C).

The single large trunk of CN V expands shortly after its emergence from the lateroventral surface of the endocast and superficially subdivides into three lobes (Fig. 4C). This expansion of CN V endocast likely corresponds to the Gasserian ganglion, and the three lobes reflect its main branches — the ophthalmic (CN V_I), maxillary (CN V_{II}), and mandibular (CN V_{III}) nerves (see Holliday and Witmer [2007] for a survey of the diapsid condition). The middle cerebral vein exited the braincase together with CN V (vMC, Fig. 9). The endocast of CN VI extends anteroventrally and slightly laterally from the ventral surface of the brainstem. It comes off at the level of CN V, passes by the hypophyseal cavity, and exits the braincase through a separate foramen anterior to CN V (Figs. 2, 3, 4). The trunk of CN VII emerges between the endocasts of CN V and the inner ear and parallels the course of CN V. CN VIII was not digitally rendered; however, a groove at the endocranial surface of ZIN PH 1/16 that extends posterodorsally from the internal foramen of CN VII into the inner ear recess, just below the ampullary spaces, corresponds to the course of CN VIII (Fig. 3A). CN IX and CN X share the same exit via the metotic passage. The endocast of the MF is directly posterior to that of the inner ear and is relatively large (comparable to the endocast of CN II and slightly smaller than that of CN V). Three trunks of CN XII are evenly spaced posterior to the MF endocast; the anteriormost trunk is the smallest and lies adjacent to the MF.

Inner ear. The endosseous labyrinth of the inner ear was digitally reconstructed for both sides of ZIN PH 1/16 (Figs. 4, 5). The endosseous labyrinth is the endocast of inner skull cavities that carried the endolymphatic (otic or membranous) labyrinth surrounded by the perilymphatic (periotic) labyrinth (Baird, 1960; Witmer et al., 2008). Part of the perilymphatic labyrinth associated with semicircular canals is uniform among reptiles and closely matches the semicircular ducts of the endolymphatic labyrinth in shape. The lower part of the perilymphatic labyrinth that surrounds the saccule and the cochlear duct (lagena) of the endolymphatic system has a more complex structure that obscures the form of the endolymphatic labyrinth (Baird, 1960). The endosseous labyrinths of *Bissektipelta*, as well as those of other dinosaurs, reflect the structure of both the endolymphatic and perilymphatic systems as a whole. The perilymphatic labyrinth of *Bissektipelta* has an extracapsular portion (perilymphatic sac) that extends posteromedially into the undivided metotic passage (MF) to participate in a compensatory secondary tympanic membrane (pls, Figs. 4B, 5B). This is a common condition for many diapsids including *Sphenodon*, basal archosaurs, and dinosaurs (Baird, 1960; Gower, 2002; Gower and Walker, 2002; Witmer et al., 2008). The position of extracapsular portion of the perilymphatic sac is marked by a notch between the vestibular recess of the inner ear cavity and the MF and was digitally visualized as part of the endosseous labyrinth (pls, Fig. 5B, C).

The endosseous labyrinths from both sides of ZIN PH 1/16 are undistorted and symmetrical. The medial aspects of both labyrinths are incomplete due to incomplete endocranial ossification of the otic capsules (Fig. 5C). The semicircular canals are robust. The ampullar regions are not discrete and are present as expansions at proximal ends of the canals. Each semicircular canal lies in a single plane and does not curve beyond its limits. The anterior canal is the tallest and the largest of the three; it is roughly circular in shape (asc, Fig. 5B). The angle between the anterior and posterior canals equals approximately 90°. The posterior semicircular canal has a marked elliptical shape and is relatively low (psc, Fig. 5B); the anterior canal is one and a half times taller than the posterior one. The common crus is low (nearly equals the depth of the posterior canal) and broad (nearly twice the average canal breadth) (crc, Fig. 5). The lateral semicircular canal is ovoid in shape and appears to be equal to or only slightly smaller than the posterior canal (lsc, Fig. 5D). The utricular and saccular compartments of the endolymphatic labyrinth are not apparent as they were laterally covered by the periotic cistern of the perilymphatic labyrinth (as in other diapsids; Baird, 1960).

Below the level of semicircular canals, the endosseous labyrinth is markedly constricted anteroposteriorly.
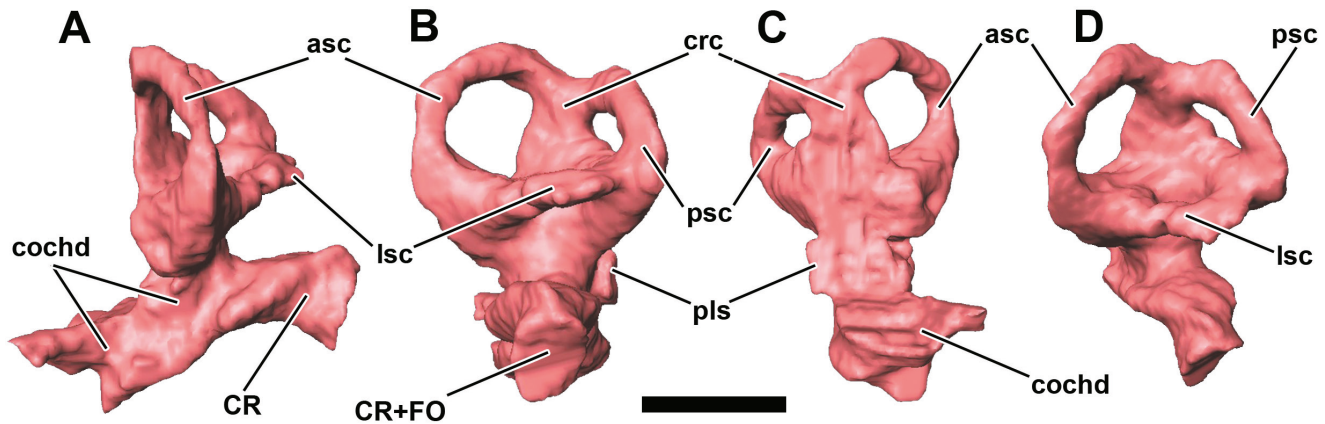
Fig. 5. ZIN PH 1/16, holotype of *Bissektipelta archibaldi* from the Bissekty Formation (Turonian), Uzbekistan. Digital reconstruction of the endosseous labyrinth of the left inner ear in anterior (A), lateral (B), medial (C), and oblique dorsolateral (D) views. Scale bar equals 1 cm. Abbreviations: **asc**, anterior semicircular canal; **cochd**, endosseous cochlear duct; **CR**, columellar recess; **crc**, crus communis; **CR+FO**, external openning of columellar recess leading to fenestra ovalis; **lsc**, lateral semicircular canal; **pls**, perilymphatic sac; **psc**, posterior semicircular canal.

This point is level with the columellar recess and the fenestra ovalis and marks the approximate line of division of the endosseous cochlear duct (lagena). The cochlear duct curves ventromedially below the vestibular portion of the labyrinth (cochd, Fig. 5A). Large unossified spaces below the endocranial cavity on both sides of ZIN PH 1/16 (lagf, Fig. 3B) were segmented as parts of the inner ear labyrinth. Although these structures are natural, symmetric, and observed in all studied specimens, we doubt that the actual cochlea was that elongate in *Bissektipelta* and curved below the endocast as in birds (e.g., Witmer et al., 2008). We suggest that these spaces could have contained either enlarged outgrowths of the perilymphatic sac and/or supportive neurovascular tissues of the inner ear. Overall, they just might have been plugged with cartilage. Accounting for the uncertainty regarding the actual extent of the cochlear duct in ZIN PH 1/16, we perform two sets of measurements of its length (Table 3): a conservative assessment that does not include the medioventral portion of the cochlear endocast and an extended assessment that accounts for a complete model length. The presence of the extracapsular portion of the perilymphatic sac in *Bissektipelta* (which is the continuation of the scala tympani that encircles the lagena medially in archosaurs; see Baird, 1960: Fig. 2) suggests that small portions of the perilymphatic labyrinth bulged out intracranially and, thus, were not visualized in the model. According to our approximate estimates, the length of the endosseous cochlear duct equals nearly 10–11 mm under a conservative measurement and 11–

Table 3. Endosseous labyrinth measurements and hearing properties of *Bissektipelta archibaldi*. The best frequency of hearing and the high-frequency hearing limit are calculated based on the equations from Gleich et al. (2005). We assume that the basilar papilla represents only two thirds of the cochlear duct length as in Gleich et al. (2005). For ZIN PH 1/16, two types of measurements were conducted — a more conservative approach (when a straighter line through the cochlea was measured) and an extended approach (when a strongly ventromedially curved line through the cochlea was measured). A single set of cochlear dimensions was taken from ZIN PH 281/16. All linear measurements in millimeters, hearing frequencies in hertz

Parameter	ZIN PH 1/16	ZIN PH 281/16
Left labyrinth cochlear duct length, conservative	10.8	
Left labyrinth cochlear duct length, extended	13.9	13.1
Right labyrinth cochlear duct length, conservative	10.1	
Right labyrinth cochlear duct length, extended	11.6	14.4
Mean cochlear duct length for both labyrinths, conservative	10.45	
Mean cochlear duct length for both labyrinths, extended	12.75	13.75
Best frequency of hearing, conservative	1002	
Best frequency of hearing, extended	682	576
High-frequency hearing limit, conservative	2889	
High-frequency hearing limit, extended	2299	2105

14 mm under an extended assessment, which amounts to 38–41 % and 41–53 % of the overall height of the endosseous labyrinth (the height of the vestibular part is around 15–16 mm). Thus, the lagena of *Bissektipelta* was moderately elongate.

A long canal extends laterally from the cochlear duct of ZIN PH 1/16 (CR, Fig. 5A). It has two parallel oblique sharp margins along its sides. We hypothesize that this structure represents the stapedial recess partly enclosed in bone due to extensive ossification of the lateral wall of the braincase in ZIN PH 1/16. In dorsal and anterior views, the distal part of the recess delimited by the aforementioned margins resembles the shape of the oblique stapedial footplate (Fig. 5A, D). Thus, the actual fenestra ovalis was likely displaced internally from the lateral surface of the braincase.

Vasculature. The CT data allowed digital reconstruction of a complex pattern of blood vessels in the holotype of *Bissektipelta archibaldi* (Figs. 6–9). Endocranial vasculature and the system of vessels piercing the skull roof and lateral braincase wall has been reconstructed for *Bissektipelta* based on relative osteological correlates such as grooves and canals within bone (Witmer, 1995; Porter, 2015). Major vessels that are external to the braincase and did not leave direct bony features are only briefly mentioned here and are discussed later (see Discussion). As it is often hard to discriminate which component (arterial/venous) is prevalent in a given osteological structure (save for well-known features such as the cerebral carotid canal predominated by the arterial component or grooves for the dural venous sinuses at the endocranial surface; see Porter [2015]), we have not distinguished between the types of blood vessels that pierced the skull roof and the braincase wall in our model. However, many of them are considered mainly or exclusively venous as encephalic arteries form a closed network around the brain under the dura matter and do not communicate with the orbital and temporal vessels (Sedlmayr, 2002; Almeida and Campos, 2010, 2011), with the exception of the ethmoid artery that communicates anteriorly with the supraorbital artery to form the nasal artery (Porter et al., 2016; Porter and Witmer, 2016a).

In extant diapsids, the main artery that supplies the braincase is the internal carotid artery and two of its branches — the cerebral carotid and the stapedial arteries (Porter and Witmer, 2015, 2016; Porter et al., 2016) (aIC, aCC, and aST in Fig. 8). In *Bissektipelta*, each cerebral carotid artery enters almost at the floor of the hypophyseal cavity (a+vCC, Fig. 6A). Small vessels branching off of the cerebral carotid curve anteroventrally along the floor of the hypophyseal cavity (Fig. 4B). These small lobose vessels, though visualized as parts of the cerebral carotid artery endocast, possibly represent ventral parts of the cavernous sinus that drains into the

cerebral carotid vein (compare Fig. 4B with Neumeier and Lametschwandtner, 1994: Fig. 15). The latter vein shares the canal with the cerebral carotid artery; thus, both vessels are represented by a single trunk in the endocast of ZIN PH 1/16. The cerebral carotid arteries were likely connected medially because extant birds and crocodylians show anastomizing vessels/plexuses in the posteroventral region of the hypophyseal cavity (Sedlmayr, 2002; Porter et al., 2016; Porter and Witmer, 2016a). A horizontal swelling at the posterior surface of the pituitary endocast of ZIN PH 1/16, between cerebral carotid arteries, possibly corresponds to the intercarotid anastomosis (Fig. 4B). Just anterior to its entrance into the hypophyseal cavity, the cerebral carotid artery gives off the sphenopalatine artery (a+vSP, Fig. 6A). It is a distinct but smaller-caliber vessel compared to the cerebral carotid. A possible anterior course of the sphenopalatine artery is marked by a notch and depression on each side of the parabasisphenoid (gaSP in Fig. 2D, aSP in Fig. 8). The artery courses anterodorsally into the nasal region. A similar route of the sphenopalatine artery is present in extant birds (Porter and Witmer, 2016a). The dorsal courses of the common encephalic artery (= cerebral carotid after branching off sphenopalatine artery) and its branches that ramify around the brain inside the endocranial cavity are hard to trace. Possible osteological correlates are paired grooves on the dorsum sellae that could correspond to the caudal encephalic artery (Fig. 3A).

Another branch of the internal carotid is the stapedial artery, which continues anteriorly through the temporal region as the temporoorbital artery and then divides into three main orbital vessels (supra-, infraorbital, and ophthalmotemporal arteries; Sedlmayr, 2002; Porter, 2015) (aST, aTO, aSO, aOpt + aIO in Fig. 8). Anterior to the supratemporal fossa, a large curved canal within the lateral wall of the braincase, dorsal to the foramina for CN II–IV, is interpreted as the passage for the supraorbital artery and vein (preserved on the left side of ZIN PH 1/16 and opened by fracture on the right) (ca+v and fa+vSO in Fig. 2B, F; a+vSO in Fig. 6A; aSo in Fig. 8; vSO in Fig. 9). These vessels accompany each other through their course over the anterior surface of the laterosphenoid and ventral surface of the frontal in extant archosaurs (Porter et al., 2016; Porter and Witmer, 2016a). The supraorbital vessels course external to the bone surface in extant taxa; however, some dinosaurs with heavily ossified skulls (e.g., pachycephalosaurids) show evidence for the bony enclosure of their branches into canals (Porter, 2015). The same is likely true for ZIN PH 1/16. The supraorbital artery/vein canal communicates via small-caliber vascular canals with the anterior branching plexus of the cranial roof dorsally and with endocranial vessels medially and posteromedially (Figs. 6, 7, 9). The latter corresponds to numerous

PALAEONTOLOGY
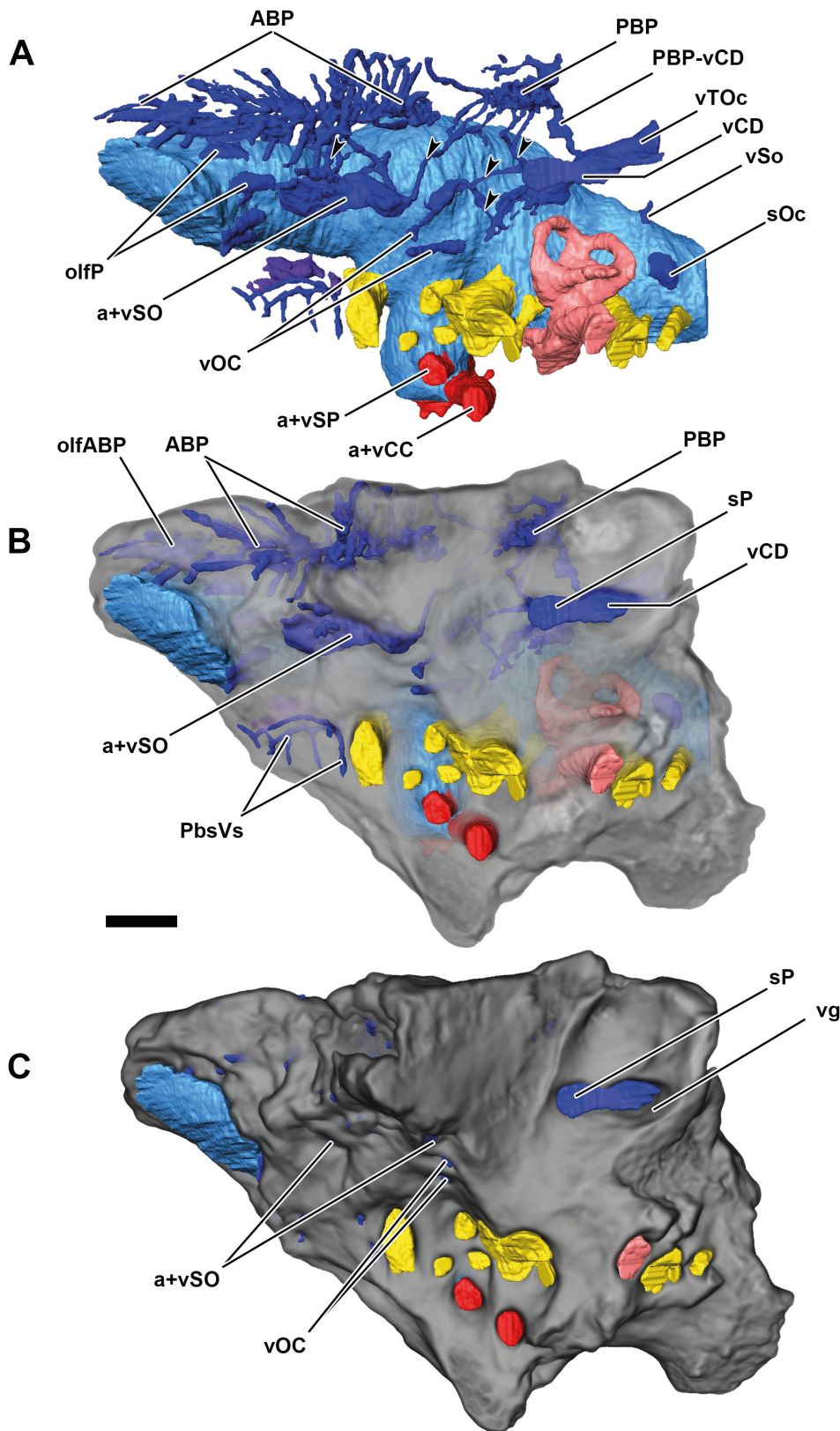
Fig. 6. ZIN PH 1/16, holotype of *Bissektipelta archibaldi* from the Bissekty Formation (Turonian), Uzbekistan. CT-based models showing braincase vasculature in left lateral view; endocast with surrounding vessels (A), semitransparent view of the braincase showing vessels within the skull roof and lateral braincase wall (B), solid braincase (C). Scale bar equals 1 cm. Abbreviations: **a+vCC**, cerebral carotid artery and vein; **a+vSO**, supraorbital artery and vein; **a+vSP**, sphenopalatine artery and vein; **ABP**, anterior branching plexus; **olfABP**, olfactory part of the anterior branching plexus; **olfP**, olfactory plexus; **PBP**, posterior branching plexus; **PBP-vCD**, anastomotic vessel between the posterior branching plexus and the dorsal head vein; **PbsVs**, parabasisphenoid vasculature; **sOc**, occipital venous sinus; **sP**, parietal venous sinus; **vCD**, dorsal head vein; **vg**, venous groove; **vOC**, orbitocerebral vein; **vSo**, supraoccipital vein; **vTOc**, transverso-occipital vein. Black arrow heads mark small anastomotic connections between main vascular elements.
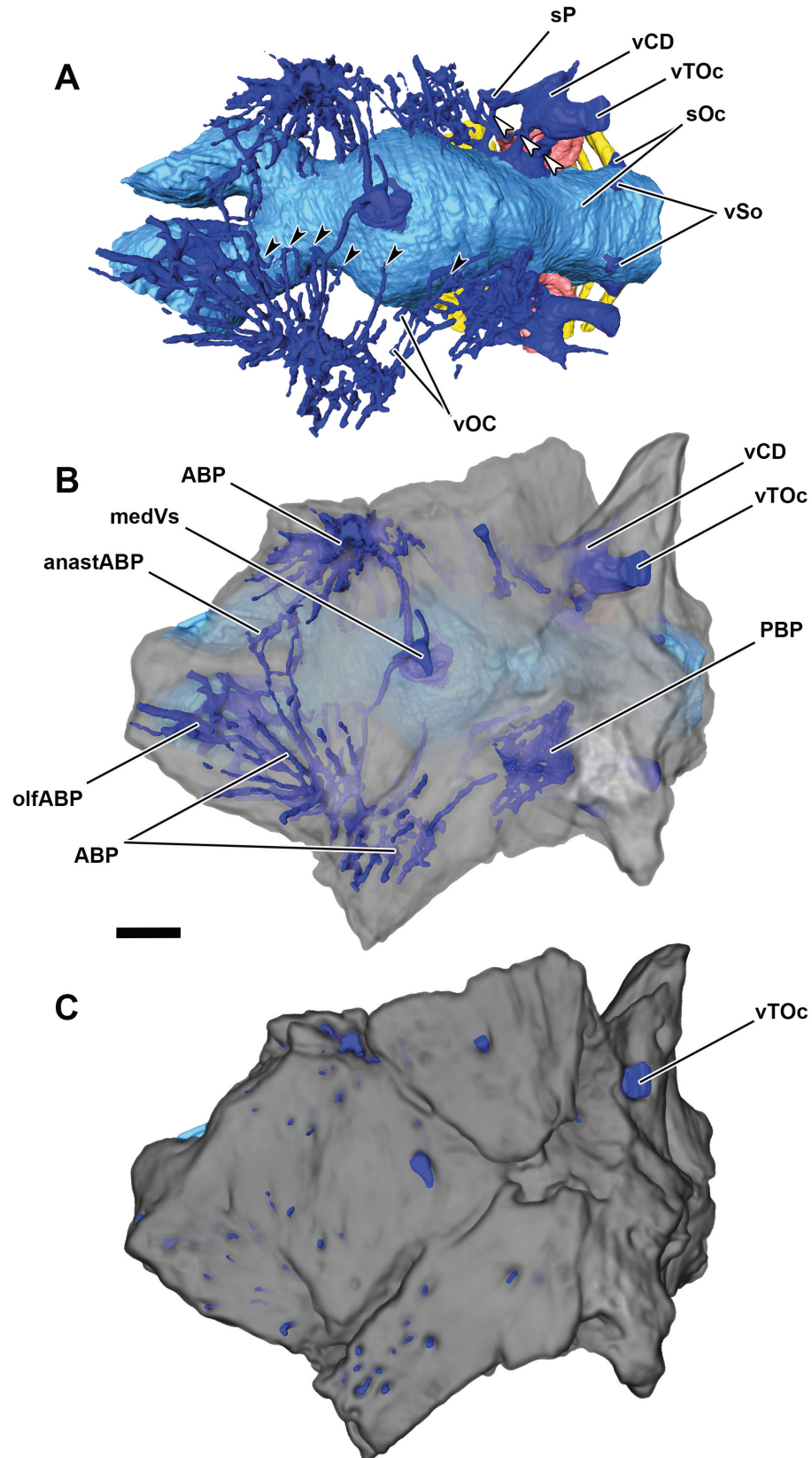
Fig. 7. ZIN PH 1/16, holotype of *Bissektipelta archibaldi* from the Bissekty Formation (Turonian), Uzbekistan. CT-based models showing braincase vasculature in dorsal view; endocast with surrounding vessels (A), semitransparent view of the braincase showing vessels within the skull roof (B), solid braincase and skull roof (C). Scale bar equals 1 cm. Abbreviations: **ABP**, anterior branching plexus; **anastABP**, anastomotic connection between left and right anterior branching plexuses; **medVs**, medial vessel; **olfABP**, olfactory part of the anterior branching plexus; **PBP**, posterior branching plexus; **sOc**, occipital venous sinus; **sP**, parietal venous sinus; **vCD**, dorsal head vein; **vOC**, orbitocerebral vein; **vSo**, supraoccipital vein; **vTOc**, transverso-occipital vein. Black arrow heads mark small anastomotic connections between main vascular elements. White arrow heads mark connections between the dorsal head vein and the middle cerebral vein.
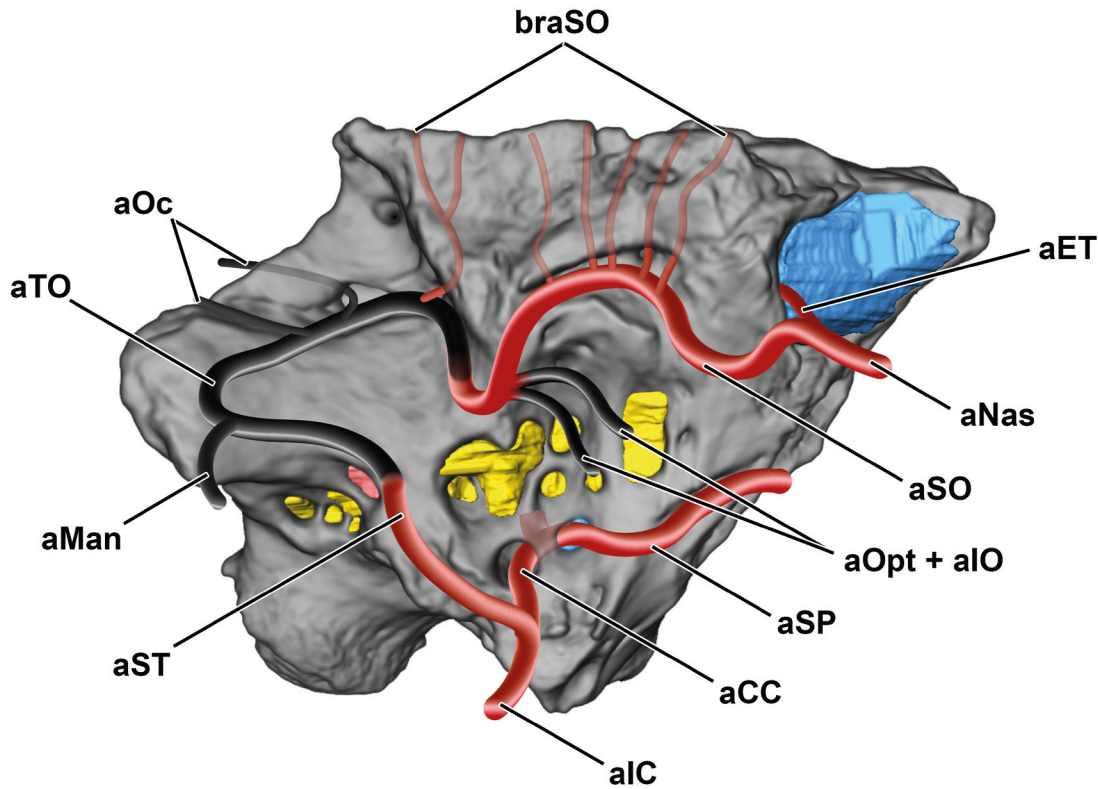
Fig. 8. ZIN PH 1/16, holotype of *Bissektipelta archibaldi* from the Bissekty Formation (Turonian), Uzbekistan. CT-based model of the braincase in right lateral view showing reconstructed pattern of arteries. Red vessels are reconstructed upon corresponding osteological correlates. Black vessels inferred from broader studies of diapsid vascular patterns. Not to scale. Abbreviations: **aCC**, cerebral carotid artery; **aET**, ethmoidal artery; **aIC**, internal carotid artery; **aMan**, mandibular artery; **aNas**, common nasal artery; **aOc**, occipital artery; **aOpt+aIO**, ophthalmotemporal and infraorbital arteries; **aSO**, supraorbital artery; **aSP**, sphenopalatine artery; **aST**, stapedial artery; **aTO**, temporoorbital artery; **braSO**, dorsal branches of supraorbital artery.

venous communications with endocranial dural veins (mainly, the dorsal longitudinal sinus with its tributaries and the cerebrotectal sinus, see Fig. 9). The supraorbital artery/vein canal also receives a number of small canals from the lateral surface of the braincase. The anterior course of the supraorbital vessels is marked by an anteroventrally directed groove and the orbitonasal foramen in the preorbital septum (Fig. 8). The latter structure is broken in the holotype but preserved in the referred specimen ZIN PH 2329/16 (Fig. 15). The communication of the supraorbital and ethmoid vessels (situated dorsal to the olfactory tract and bulbs in extant taxa; Almeida and Campos, 2010, 2011; Porter et al., 2016; Porter and Witmer, 2016a) occurred through some of the small canals piercing the lateral wall of the braincase (Figs. 6A and 7A) and further anterior to the orbitonasal foramen (see Figs. 8–9). The latter communication of the supraorbital and ethmoid vessels gave rise to the nasal vessels that supplied and drained the nasal cavity.

The encephalic vessels seldom leave direct traces on the endocranial surface (with some notable exceptions; see Evans [2005]); however, their basic pattern appears to be rather conservative among known diapsids (Bruner, 1907; Dendy, 1909; Sedlmayr, 2002; Witmer et al., 2008; Porter, 2015; Porter and Witmer, 2015, 2016; Porter et al., 2016). Major endocranial veins are recognized as swellings on the endocast surface that communicate with external vasculature via vascular or nervous canals (Hopson, 1979; Sampson and Witmer, 2007; Witmer et al., 2008; Porter, 2015). The latter are important landmarks that trace the course of the vessel. The digital endocast of the holotype of *Bissektipelta* allows recognition of several dural venous vessels/sinuses and their communications with external vasculature (Fig. 9).

The dorsal longitudinal sinus appears as a shallow but broad prominence on the top of the endocast that extends from the olfactory tract anteriorly to the level of the otic capsules posteriorly (Figs. 7, 9). Anterior to the olfactory tract, the dorsal longitudinal sinus apparently splits into a pair of vessels (olfactory veins in Dendy [1909]; ethmoid vein in Porter and Witmer [2016]; Porter et al., 2016) that overlaid the olfactory bulbs and continued forward to drain the olfactory cavity as nasal veins (vET + vNas in Fig. 9). A large number of neurovascular grooves are preserved around the olfactory bulbs/posterior portion of the olfactory region of the nasal cavity in ZIN PH 1/16 (Fig. 2F). These grooves indicate the presence of a vascular plexus around the ol-
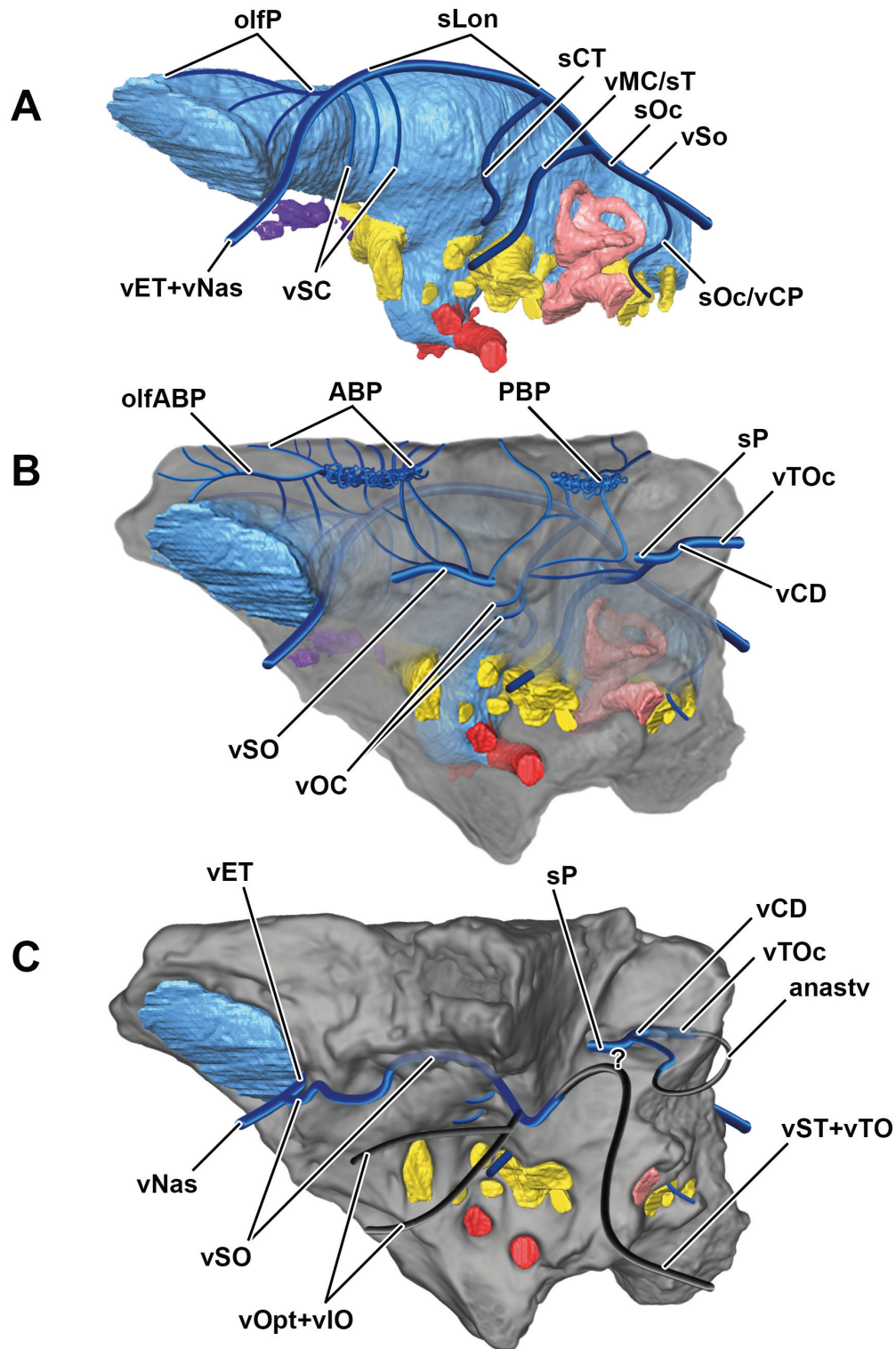
Fig. 9. ZIN PH 1/16, holotype of *Bissektipelta archibaldi* from the Bissekty Formation (Turonian), Uzbekistan. CT-based models of the cranial endocast and braincase in left lateral view showing reconstructed pattern of veins. A, encephalic veins that drain endocranial cavity, labeled on the endocast; B, semitransparent view of the braincase showing veins within the skull roof and lateral braincase wall (solid), encephalic veins (transparent), and their intercommunications; C, non-transparent view of the braincase showing external braincase veins (solid) and their parts within canals (transparent). Note controversial interpretation of veins at the supratemporal fossa; see Discussion for the preferred reconstruction. Blue vessels are reconstructed upon corresponding osteological correlates. Black vessels inferred from broader studies of diapsid vascular patterns. Not to scale. Abbreviations: **ABP**, anterior branching plexus; **anastv**, circum-occipital anastomotic loop between dorsal head vein, transverso-occipital vein, and parietal venous sinus; **olfABP**, olfactory part of the anterior branching plexus; **olfP**, olfactory plexus; **PBP**, posterior branching plexus; **sCT**, cerebrotectal sinus; **sLon**, dorsal longitudinal sinus; **sOc**, occipital venous sinus; **sOc/vCP**, occipital venous sinus/posterior head vein; **sP**, parietal venous sinus; **vCD**, dorsal head vein; **vET**, ethmoidal vein; **vMC/sT**, middle cerebral vein and transverse venous sinus; **vNas**, common nasal vein; **vOC**, orbitocerebral vein; **vOpt+vIO**, ophthalmotemporal and infraorbital veins; **vSC**, superior cerebral veins; **vSo**, supraoccipital vein; **vSO**, supraorbital vein; **vST+vTO**, stapedial and temporoorbital veins; **vTOc**, transverso-occipital vein.

factory bulbs that drained into the ethmoid vein and the anterior branching plexus (olfP in Figs. 6–7, 9). In extant birds, the olfactory bulbs are surrounded by a dense venous plexus that eventually drains into the longitudinal sinus via the ethmoidal veins and/or the olfactory sinus and their anastomoses (Sedlmayr, 2002; Porter and Witmer, 2016a).

A conspicuous median vessel arises sagittally at the top of the endocast of *Bissektipelta*, dorsal to the cerebral hemispheres (medVs, Fig. 7). The vessel extends dorsally within a canal inside the bone and opens through a foramen on the dorsal surface of the skull roof. Along the way, it issues left and right major branches as well as smaller branches in a slightly asymmetrical manner; each major branch communicates with a corresponding anterior branching plexus (Fig. 7A). The median vessel was apparently connected to the dorsal longitudinal sinus ventrally. Undoubtedly this structure was vascular (most likely, venous), as it commences from the endocast at the inferred position of the longitudinal sinus and connects to vascular branching plexuses. We are unaware of any similar dorsal extensions of the encephalic vessels in extant diapsids. As noted earlier in the description of the endocast, the position of the median vessel in *Bissektipelta* generally corresponds to the position of the pineal complex in extant lepidosaurs and birds. In extant diapsids, the pineal complex is well vascularized, supplied by branches of the posterior cerebral artery and drained by the dorsal longitudinal sinus (Dendy, 1909; Ralph, 1970). We doubt that the canal housed the pineal/parapineal organ itself but hypothesize that the median vessel and its branches may represent dorsal continuations of the pineal complex vasculature.

The dorsal longitudinal sinus is most prominent posteriorly where it received the middle cerebral veins and appears as a broad triangle in the dorsal view (torcular Herophili; Dendy, 1909; Sedlmayr, 2002; sOc, Fig. 7A). Posterior to this, the dorsal longitudinal sinus likely bifurcated into two sinus-like posterior cerebral veins (vena cerebralis posterior, vena cephalica posterior, vagal vein, occipital venous sinus of different authors) (sOc, Fig. 7A; sOc/vCP, Fig. 9A). The posterior cerebral veins likely left the endocranial cavity through the foramen magnum, as in most extant diapsids (Bruner, 1907; Sedlmayr, 2002; Witmer et al., 2008; Porter and Witmer, 2015, 2016; Porter et al., 2016). However, *Sphenodon* shows an important variation of the course of the posterior cerebral vein, which leaves the endocranial cavity through the metotic foramen (Dendy, 1909). The same route for the posterior cerebral vein through the metotic foramen was reconstructed for basal crocodylomorphs (Walker, 1990) and other pseudosuchians (Gower, 2002; Gower and Nesbitt, 2006; Sulej, 2010). Both pathways for the venous drainage (via the metotic foramen/foramen magnum) are likely traced in extant

crocodylians through their development (Dendy, 1909; Sedlmayr, 2002). For *Bissektipelta*, we imply that most, if not all, of the venous blood left the endocranial cavity posteriorly through the foramen magnum, with possible additional venous drainage through the metotic foramen via the posterior cerebral vein (sOc and sOc/vCP, Fig. 9A). Sobral et al. (2012) arrived at a similar conclusion regarding the pathway of the posterior cerebral vein in the ornithopod *Dysalotosaurus*.

A pair of small foramina (fvSo in Fig. 1) directly above the foramen magnum of *Bissektipelta* apparently transmitted small veins and accompanying arteries (supraoccipital veins; vSo in Figs. 6A, 7A and 9A). In *Sphenodon*, these vessels drain from the dura matter and the dorsal part of the occipital sinus extracranially through similarly distributed foramina (Dendy, 1909).

Along its course, the dorsal longitudinal sinus receives several transverse veins that drained lateral aspects of the endocranial cavity. We assume the presence of a number of superior cerebral veins that extended along the lateral aspects of the olfactory tract and the anterior cerebrum, dorsal to CN II, as was described for *Sphenodon* (venae cerebrales superiores; Dendy, 1909) (vSC, Fig. 9A). Additionally, the presence of corresponding but unidentified vessels dorsal to CN II was discussed for *Caiman* and reported for fossil endocasts (Hopson, 1979). The presence of superior cerebral veins in *Bissektipelta* is established by numerous small vascular canals that connected the anterior branching plexus and the canal for supraorbital vessels with endocranial dural veins (Fig. 7A). These veins joined the corresponding ethmoid vein/dorsal longitudinal sinus dorsally.

Posteriorly, at the level of CN IV, conspicuous swellings on the endocast and a pair of the orbitocerebral veins on each side indicate the course of a transverse venous sinus (sCT, Fig. 9A, B). The latter received confusing terminology in the literature: vena cerebri posterior in Hopson (1979); sphenotemporal sinus in Sedlmayr (2002); sphenoparietal sinus in Witmer et al. (2008); and cerebrotectal sinus in Porter et al. (2016) and Porter and Witmer (2016). In extant archosaurs, this venous sinus extends dorsally along the tentorial crest to join the dorsal longitudinal sinus and wedges in between the posterior region of the cerebrum and the optic tectum (Hopson, 1979; Sedlmayr, 2002). A series of veins on each side of the brain in the same region (venae begimenales superiores) was described for *Sphenodon* (Dendy, 1909). We use the term "cerebrotectal sinus", as it clearly reflects the anatomical position of the vessel. In *Bissektipelta*, the cerebrotectal sinus extends transversally as a swelling on the posterior aspect of the cerebral endocast (compare Figs. 4C, 6A, and 9A). The orbitocerebral veins drain into the cerebrotectal sinus from the orbital cavity (vOC in Figs. 6A, 9B). The cerebrotectal sinus directly communicates via small vascular canals with the

middle cerebral vein and dorsal head vein/parietal sinus, the posterior branching plexus, and the canal for supra-orbital vessels (Figs. 6, 9).

The succeeding large transverse tributary of the dorsal longitudinal sinus with complicated nomenclature is the middle cerebral vein (vena cerebralis media in Bruner [1907]; transverse sinus in Dendy [1909] and Porter and Witmer [2015]; recessus lateralis of longitudinal sinus in Hopson [1979]; rostral petrosal sinus in Sedlmayr [2002]; cerebellotectal sinus in Porter and Witmer [2016] and Porter et al. [2016]) (vMC, Fig. 9). In extant diapsids, it is a large vessel that extends between the optic tectum and cerebellum, just in front of the otic capsule. At the point of its divergence from the longitudinal sinus, the middle cerebral vein is sinus-like and broad, and thus its dorsal portion was designated the transverse, rostral petrosal, or cerebellotectal sinus (Dendy, 1909; Sedlmayr, 2002; Sampson and Witmer, 2007; Porter and Witmer, 2016a; Porter et al., 2016). Ventrally, the sinus drains into one or several smaller and more defined veins (= middle cerebral vein sensu stricto, e.g., Sampson and Witmer, 2007; transversotrigeminal vein of Porter and Witmer [2015]; rostral middle cerebral vein in Paulina-Carabajal et al. [2016]) that frequently pass through the trigeminal foramen extracranially. We use the simpler term "middle cerebral vein" for both portions of the vessel (the transverse sinus and its continuations) in an effort to keep the terminology as concise as possible and to ensure compatibility with previous accounts on dinosaurian cranial vasculature (Sampson and Witmer, 2007; Witmer et al., 2008; Miyashita et al., 2011; Leahey et al., 2015; Paulina-Carabajal et al., 2016, and others).

In *Bissektipelta*, the middle cerebral vein/transverse sinus extends dorsally from the foramen for CN V as a bulge on the endocast surface, then arches posterodorsally, parallel to the anterior semicircular canal, and finally joins the dorsal longitudinal sinus (Figs. 6A and 9). In *Bissektipelta*, there is no separate branch of the middle cerebral vein that passes extracranially in the lateral direction through its own canal (= rostral middle cerebral vein of some authors). Thus, the middle cerebral vein likely exited the braincase via the large foramen of CN V. Dorsally, a conspicuous posterodorsally curved swelling on the endocast marks the course of the middle cerebral vein. Here, the middle cerebral vein is laterally confluent with the dorsal longitudinal/occipital sinus (Fig. 9A). Three short vascular branches extend posterodorsally and laterally from the middle cerebral vein on each side of ZIN PH 1/16 (Fig. 7A). These vascular branches connect the middle cerebral vein with the external veins of the temporal and occipital regions of the skull (dorsal head vein, transversooccipital vein, parietal sinus; Figs. 6A, 7A, 9B). Additionally, a separate vessel extends from the anteriormost of the three described vascular branches and connects with the cerebrotectal sinus anteriorly (precisely,

with the dorsal orbitocerebral vein, Figs. 6A, 9B). As described, the course of the middle cerebral vein in *Bissektipelta* is consistent with observations on extant diapsids (Bruner, 1907; Dendy, 1909; Porter and Witmer, 2015; Porter and Witmer, 2016a; Porter et al., 2016) and various dinosaurs (see Discussion).

The dorsal head vein and the transverso-occipital vein (caudal middle cerebral vein of some authors) exit the braincase of *Bissektipelta* via separate foramina on the lateral (nvr+g, Fig. 2B; vCD, Fig. 6B, C) and occipital (ptf, Fig. 1; vTOc, Fig. 7B) surfaces of the skull, correspondingly. However, their endocast suggests that they either represent a single vessel or a continuous anastomotic loop that extends from the temporal to the occipital region of the skull and maintains the connection with the middle cerebral vein/transverse sinus (Fig. 7A). In *Bissektipelta*, the groove passes anterior from the foramen of the dorsal head vein (nvr+g in Fig. 2B). This groove corresponds to the continuation of the dorsal head vein; we term this continuation as the parietal sinus (sP, Figs. 6B, 7A, 9B–C) following the terminology of extant squamates (Bruner, 1907; Porter and Witmer, 2015; see also Discussion).

Numerous small openings at the dorsal surface of the skull roof of *Bissektipelta* lead into the canals within bones that eventually converge ventrally (Fig. 7). This pattern of vascular canals is herein referred to as branching plexus. There are paired anterior and posterior branching plexuses that supplied and drained the skull roof and overlying dermis in *Bissektipelta* (ABP, Figs. 6–7 and 9). The anterior branching plexus can be subdivided into two parts: one part that lies above the olfactory bulb and the olfactory cavity and is connected ventrally to the ethmoid vessels (olfABP in Fig. 9B) and the other part that lies posteriorly and communicates with the supraorbital vessels ventrally and dural veins medially (ABP in Fig. 9B). Some parts of these canals likely transmitted small branches of the supraorbital artery that pierce the frontal and emerge onto the outer surface of the skull in extant birds (Porter and Witmer, 2016a) and some dinosaurs (Porter, 2015) in a similar way (braSO in Fig. 8). The posterior plexus is situated above the dorsal head vein (PBP in Figs. 6, 9); it is less distinct compared to the anterior plexus and was not visualized on the right side of ZIN PH 1/16. As previously described, small vascular canals integrate the anterior and posterior branching plexuses as well as various endo- and extracranial vessels into a single vascular network around the brain (see Discussion for physiological implications).

Description of ZIN PH 281/16 (Figs. 10–14)

General comments. ZIN PH 281/16 is exquisitely preserved, with fine features of the external and endocranial surfaces and clear sutures and facets. It appears to

be only slightly smaller compared to the holotype; most of its measurements are only 5–15 % smaller than those for ZIN PH 1/16 (Table 1). The braincase is externally and internally non-pneumatic, as is evident from the CT data.

Skull roof. ZIN PH 281/16 does not preserve bones of the skull roof and has slightly rugose fine facets on its dorsal surface (Figs. 10A, 11A). This indicates that the skull roof was not completely co-ossified with the braincase in this particular specimen. A lack of fusion between the skull roof and braincase is present in adults of *Pinacosaurus* (Maryańska, 1977; Tumanova, 1987) and *Minotaurasaurus* (Miles and Miles, 2009; Penkalski and Tumanova, 2017), and the two cranial components are strongly sutured in adult individuals of other ankylosaurs. The unfused skull roof in ZIN PH 281/16, along with open sutures between individual neurocranial elements, indicates that the specimen probably represents a somatically subadult individual.

Ventral surface of the basicranium. The ventral aspect of the specimen is formed by the basioccipital posteriorly and the parabasisphenoid anteriorly; the suture between these bones is clearly visible on both the lateral and ventral surfaces (Fig. 10C). Unlike in the holotype, the two bones join at an obtuse angle of approximately 120°. The ventral surface of the basioccipital is smoothly arched and bears a vascular foramen (basioccipital fenestra). The triangular ventral surface of the parabasisphenoid bears the base of the fused parabasisphenoid rostrum-interorbital septum anteriorly and small, bump-like basipterygoid processes (left one is broken off), which are offset posteriorly, close to the suture between the basioccipital and parabasisphenoid (Fig. 10D).

Occipital surface. The occipital surface of the specimen is formed by the supraoccipital, basioccipital, and paired otoccipitals; the sutures between these bones are easily recognized, unlike in the holotypic cranium and most other known ankylosaurs (Fig. 11C). The occipital surface forms the same angle of about 125° with the skull roof (inferred from the plane of corresponding facets) as in the holotype. The occipital condyle barely projects beyond the occipital plane. It has a more rounded shape compared to those of the holotype and ZIN PH 2329/16. The otoccipitals form the dorsolateral portions of the condyle. The otoccipital-basioccipital suture is evident on both sides of the specimen (Figs. 11C, 12). The suture extends onto the lateral and endocranial surfaces, where it gradually disappears toward the external and internal openings of the metotic foramen, respectively. The foramen magnum is bounded by the basioccipital ventrally and by the otoccipitals laterally and dorsally. The supraoccipital was probably excluded from the dorsal margin of the foramen magnum by a short dorsal contact between the otoccipitals; however, the latter is

not preserved. The supraoccipital-otoccipital suture is apparent dorsal to the foramen magnum and further anterolaterally where the supraoccipital reaches the prootic and probably the laterosphenoid on either side (Figs. 12A, 13A).

The supraoccipital bears a clear sagittal crest with two depressions on its sides (scr, Fig. 11D). These depressions could correspond to the ventral border of the posttemporal fenestra (ptf? in Fig. 11D) and the course of the transverso-occipital vein; they are, however, too close to the sagittal plane compared to the position of the posttemporal fenestra in the holotype (Fig. 1F). Paired canals within the paroccipital processes, just ventral to the contact with the parietal and lateral to the suture with the supraoccipital, almost certainly transmitted vascular elements. These canals could have transmitted some tributaries of the dorsal head/transverso-occipital veins or the occipital artery (vf in Figs. 11D, 12B, 13B). The latter canals are absent in the holotype ZIN PH 1/16; thus, the arrangement of vascular foramina on the occipital surface is variable among the specimens assigned to *Bissektipelta*. Small paired foramina for the supraoccipital vein are present at the suture between the supraoccipital and otoccipital (fvSo, Fig. 11D).

Lateral braincase wall. In general, the structure of the lateral wall of the braincase of ZIN PH 281/16, including the distribution of the neurovascular foramina, closely matches that of the holotype. The neurovascular foramina are grouped into anterior and posterior clusters divided by a flattened crista prootica.

The otoccipital forms most of the posterior aspect of the lateral wall of the braincase and encloses much of the posterior cluster of foramina: the undivided metotic foramen (MF), two or three external foramina of the CN XII (varying between the two sides of the specimen), and partly the fenestra ovalis (FO) and the columellar recess (Fig. 12). These openings are incised ventral to the broad base of the paroccipital process. A pair of grooves begins from the FO and MF and extends distally on the ventral surface of the paroccipital process. The openings for CN XII and the MF are completely enclosed by the otoccipital; the basioccipital is apparently excluded from the external ventral border of the MF (Fig. 12E). The MF is separated from the foramina for CN XII by a lamina-like process of the otoccipital that descends anteroventrally toward the basal tuber. The metotic foramen is separated from the anteriorly situated FO by an oblique crista interfenestralis (= ventral ramus of opisthotic in more basal archosauriforms). The crista interfenestralis is a minor process that is not visible in occipital view. The columellar recess and the FO are bounded by the prootic anteriorly and by the otoccipital posteriorly, which is a common condition for diapsids in general (e.g., Sobral and Müller, 2016). The columellar recess is more open laterally that in the holotype ZIN PH 1/16. It leads into
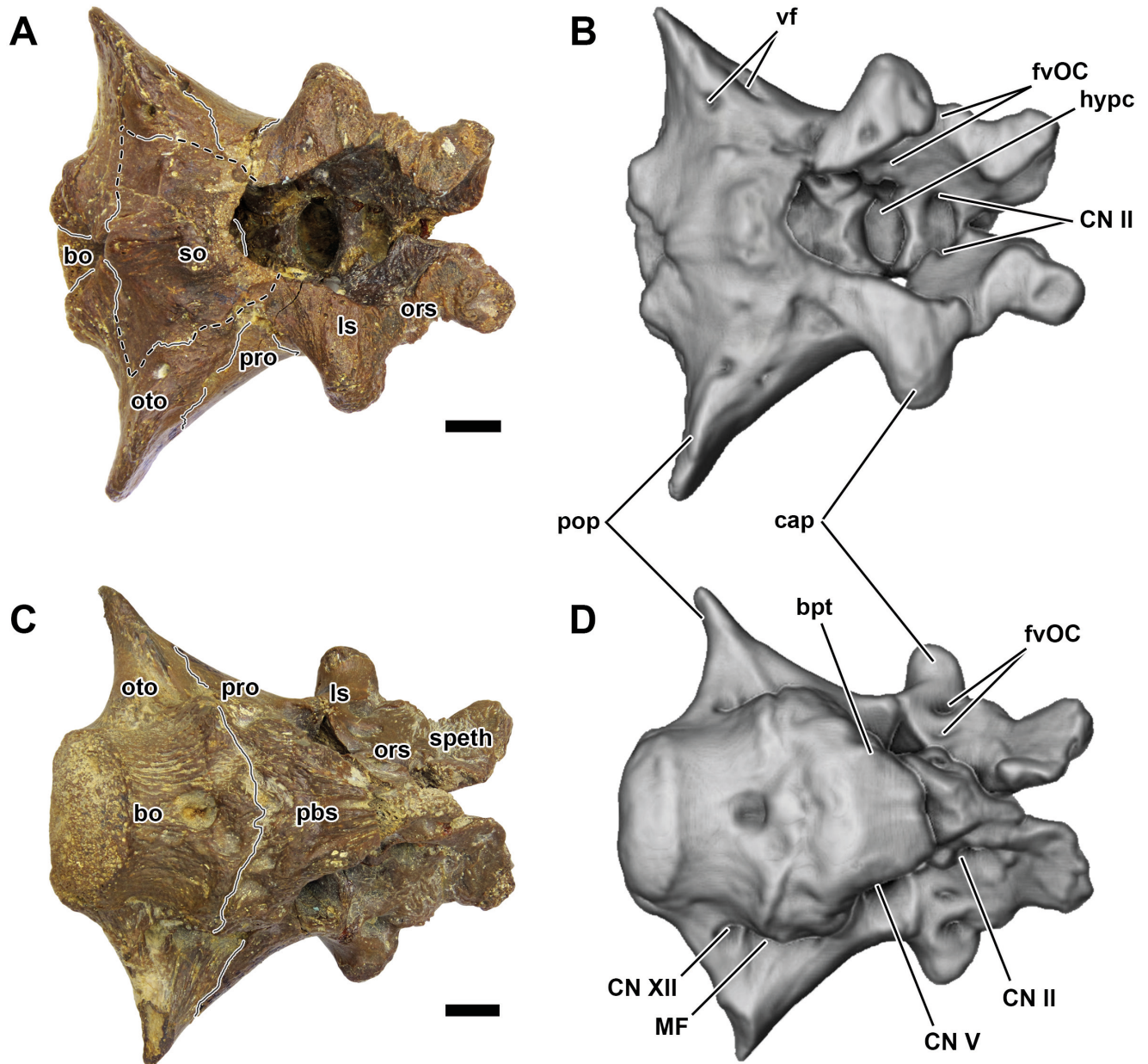
Fig. 10. ZIN PH 281/16, referred specimen of *Bissektipelta archibaldi* from the Bissekty Formation (Turonian), Uzbekistan. Photographs and corresponding CT-based models in dorsal (A, B) and ventral (C, D) views. Scale bars each equal 1 cm. Sutures are represented by solid lines; possible sutures are represented by dashed lines. Abbreviations: **bo**, basioccipital; **bpt**, basipterygoid process; **cap**, capitate process; **CN II — XII**, cranial nerve foramina; **fvOC**, foramen for orbitocerebral vein; **hypc**, hypophyseal cavity; **ls**, laterosphenoid; **MF**, metotic foramen; **ors**, orbitosphenoid; **oto**, otoccipital; **pbs**, parabasisphenoid; **pop**, paroccipital process; **pro**, prootic; **so**, supraoccipital; **speth**, sphenethmoid; **vf**, vascular foramen.

the FO; the latter communicates medially with the vestibular recess of the inner ear via a foramen (Fig. 13C).

The prootic forms the posterior border of the foramen for CN V, encloses the foramen for CN VII, and partially bounds the columellar recesss/FO (Fig. 12A, C, E). It broadly adheres to the anterior surface of the paroccipital process, as in various archosauriforms except crocodylomorphs (character 105 in Nesbitt [2011]). The anterior contact of the prootic with the laterosphenoid is evident on both sides of the specimen. The prootic-supraoccipital contact is not clearly observable, and the ventral contacts of the prootic with the parabasisphenoid

are obliterated. The prootic forms a triangular projection that descends from the dorsal margin of the foramen for CN V and partially subdivides it.

The suture between the laterosphenoid and prootic and a prominent capitate process (cap in Figs. 11B, 12B) mark the posterior extent of the laterosphenoid. The latter participates in the anterior margin of the foramen for CN V. It is likely that the laterosphenoid also encloses the orbitocerebral vein openings and the foramen for CN IV. A pair of foramina for the orbitocerebral veins is present on both laterosphenoids; additionally, a groove at the presumed laterosphenoid-frontal contact on both

Fig. 11. ZIN PH 281/16, referred specimen of *Bissektipelta archibaldi* from the Bissekty Formation (Turonian), Uzbekistan. Photographs and corresponding CT-based models in anterior (A, B) and posterior/occipital (C, D) views. Scale bars each equal 1 cm. Sutures are represented by solid lines; possible sutures are represented by dashed lines. Abbreviations: **ameth**, articular surface for mesethmoid; **bo**, basioccipital; **bpt**, basipterygoid process; **bt**, basal tuber; **cap**, capitate process; **CN V**, trigeminal cranial nerve foramen; **oc**, occipital condyle; **cvn?**, cavity for vomero-nasal bulb?; **fCC**, cerebral carotid artery and vein foramen; **fm**, foramen magnum; **fvSo**, supraoccipital vein foramen; **ls**, laterosphenoid; **oto**, otoccipital; **pbs**, parabasisphenoid; **pbsro-ios**, fused parabasisphenoid rostrum and interorbital septum; **pop**, paroccipital process; **proaf**, proatlas facet; **ptf?**, posttemporal fenestra?; **scr**, sagittal crest; **so**, supraoccipital; **speth**, sphenethmoid; **vf**, vascular foramen.

sides of the specimen marks the course of a similar vascular element (fvOC in Fig. 12D). An internal vascular canal for the supraorbital vessels was reconstructed for the holotype at this region; the canal is absent in ZIN PH 281/16, indicating a lesser degree of ossification of the braincase wall. The capitate process is stout and bears a rounded head with an unfinished articular surface (Fig. 12A). The facet on its dorsal surface and round head indicate a synovial joint between the laterosphenoid and the postorbital (Holliday and Witmer, 2008) that was nevertheless akinetic, as in extant crocodylians. The blunt crista antotica (Sampson and Witmer, 2007, and references therein; laterosphenoid buttress in Holliday and Witmer [2009]) descends from the capitate process and subdivides the orbital and adductor aspects of the external surface of the laterosphenoid (Fig. 12B,

D). On the left side of ZIN PH 281/16, a groove passes through the crista antotica. It likely indicates the course of the temporoorbital artery/vein (gTO in Fig. 12D).

Sutures cannot be distinguished between the preserved elements of the sphenethmoidal complex and between them and the parabasisphenoid. The medial septum that separated the olfactory bulbs is broken off in ZIN PH 281/16, but the preserved surface is symmetrical on both sides and most likely represents a facet (ameth, Fig. 11A). Thus, this medial septum was a separate element (mesethmoid in Miyashita et al. [2011]). It contacted the elements of the lateral wall of the braincase laterally, the parabasisphenoid ventrally, and the skull roof dorsally (based on the holotype that preserves both the medial septum and the skull roof) and was probably continuous anteriorly with the ossified nasal septum as

Fig. 12. ZIN PH 281/16, referred specimen of *Bissektipelta archibaldi* from the Bissekty Formation (Turonian), Uzbekistan. Photographs and corresponding CT-based models with cranial endocast in right lateral (A, B) and oblique left lateral (C, D) views, with a close-up of the posterior cranial nerve foramina (E). Scale bars each equal 1 cm; E not to scale. Sutures are represented by solid lines; possible sutures are represented by dashed lines. Abbreviations: **bo**, basioccipital; **bpt**, basipterygoid process; **bt**, basal tuber; **cap**, capitate process; **CN II — XII**, cranial nerve foramina; **cvn?**, cavity for vomero-nasal bulb?; **faCC**, cerebral carotid artery and vein foramen; **faSP?**, sphenopalatine artery and vein foramen?; **CR+FO**, columellar recess and fenestra ovalis; **fvOC**, foramen for orbitocerebral vein; **gTO**, temporoorbital artery and vein groove; **ls**, laterosphenoid; **MF**, metotic foramen; **ors**, orbitosphenoid; **oto**, otoccipital; **pbs**, parabasisphenoid; **pro**, prootic; **so**, supraoccipital; **speth**, sphenethmoid; **vf**, vascular foramen.
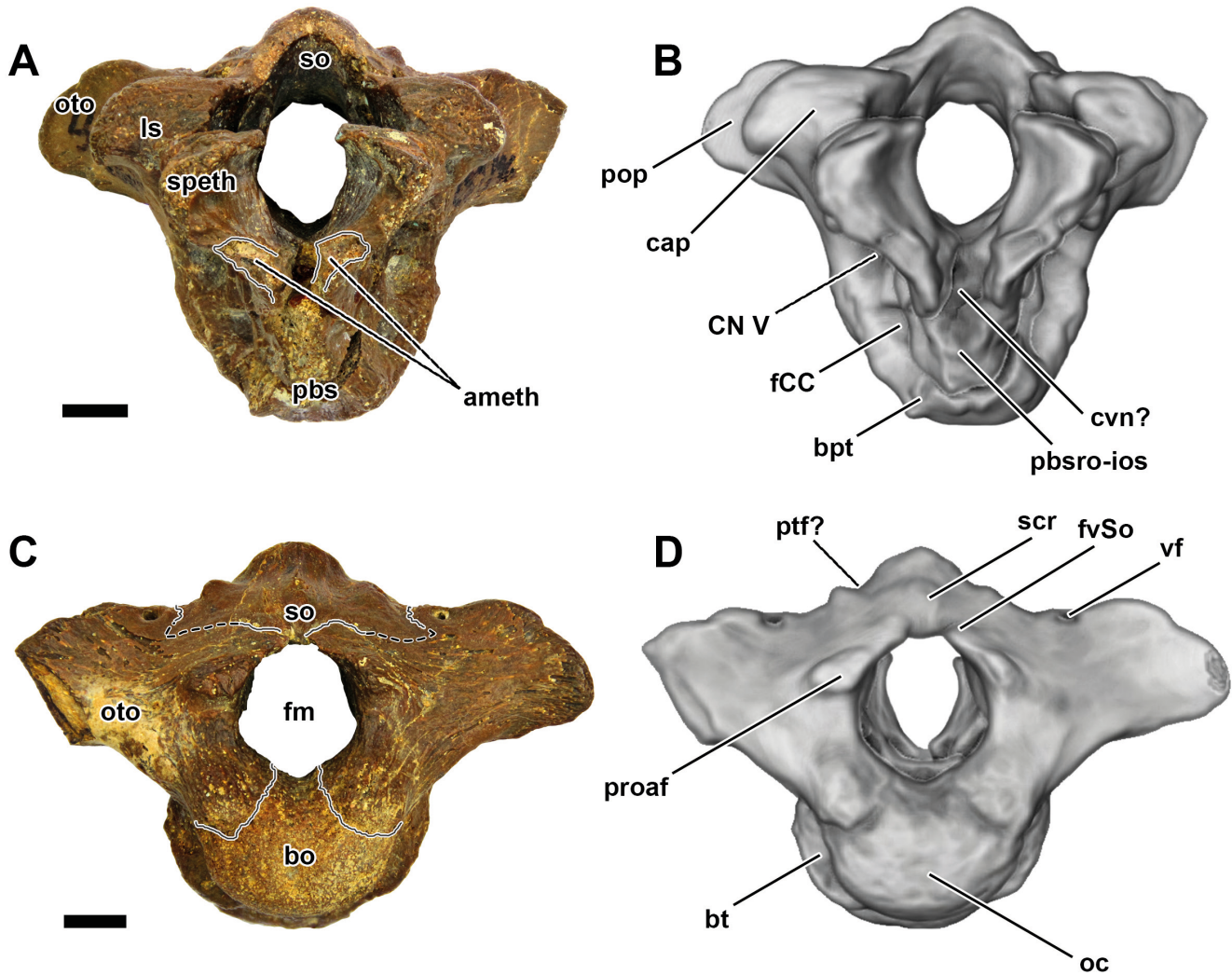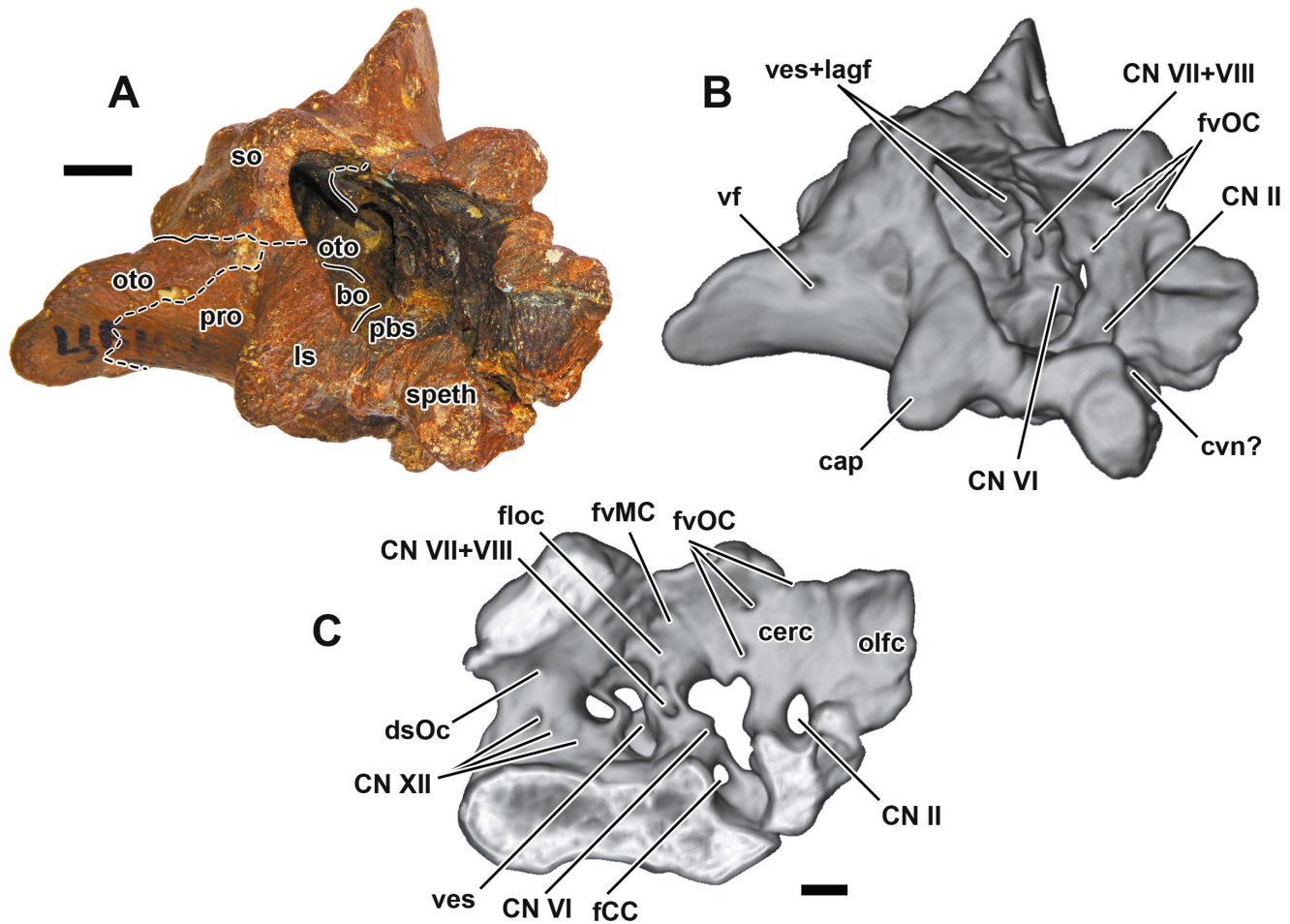
Fig. 13. ZIN PH 281/16, referred specimen of *Bissektipelta archibaldi* from the Bissekty Formation (Turonian), Uzbekistan. Photograph and corresponding CT-based model in oblique anterodorsal view (A, B) and parasagitally sectioned CT-based model showing left endocranial surface in medial view (C). Scale bars each equal 1 cm. Sutures are represented by solid lines; possible sutures are represented by dashed lines. Abbreviations: **bo**, basioccipital; **cap**, capitate process; **cerc**, cerebral cavity; **CN II — XII**, cranial nerve foramina; **cvn?**, cavity for vomero-nasal bulb?; **dsOc**, occipital venous sinus depression; **fCC**, cerebral carotid artery and vein foramen; **floc**, floccular fossa; **fvMC**, middle cerebral vein foramen; **fvOC**, foramen for orbitocerebral vein; **lagf**, lagenar fossa; **ls**, laterosphenoid; **olfc**, olfactory cavity; **oto**, otoccipital; **pbs**, parabasisphenoid; **pro**, prootic; **so**, supraoccipital; **speth**, sphenethmoid; **ves**, vestibular cavity; **vf**, vascular foramen.

in other ankylosaurs (Miyashita et al., 2011). Features of the complex external surface of the sphenethmoidal complex include prominent vertical striations dorsal to the foramen for CN II (possible site of attachment of the preorbital septum; ectethmoid in Miyashita et al. [2011]) and multiple grooves, ridges, and bumps around the foramen for CN II (indicating courses of neurovascular elements and possible attachment sites of ocular musculature).

The parabasisphenoid constitutes most of the anteroventral aspect of the lateral surface of the braincase (Fig. 12A, C). Paired grooves mark the course of CN VI from the dorsum sellae toward the external surface of the braincase, bypassing the hypophyseal cavity (Figs. 12D, 13). The participation of the prootic in the canal for CN VI is not clear. A large foramen for the cerebral carotid artery is present on either side of the specimen (faCC in Fig. 12B, D). The breakage of the specimen anterior to the cerebral carotid foramen on both sides makes the interpretation of certain foramina challenging. On the left side, the anterior rounded margin of a foramen is preserved (faSP?, Fig. 12D). This opening is comparable in size to the foramen for the cerebral carotid artery. Dorsal to it, the bone is broken, and no additional foramina could be identified. On the right side, the margin of a small-sized foramen is preserved anterior to the foramen for CN VI (faSP?, Fig. 12B). It is half as large as the abovementioned foramen on the left side but is located at the same level as the latter. Considering the position of these foramina, both of them could equally likely represent foramina for the sphenopalatine artery or foramina for CN III. In the latter case, the sphenopalatine artery would have branched off from the cerebral carotid artery before the latter entered the hypophyseal cavity in ZIN PH 281/16. However, as the nature of foramen for CN III is controversial in the holotype (see above), we assume that these foramina represent exits of the sphenopalatine artery (faSP?, Fig. 12B, D). Thus, the
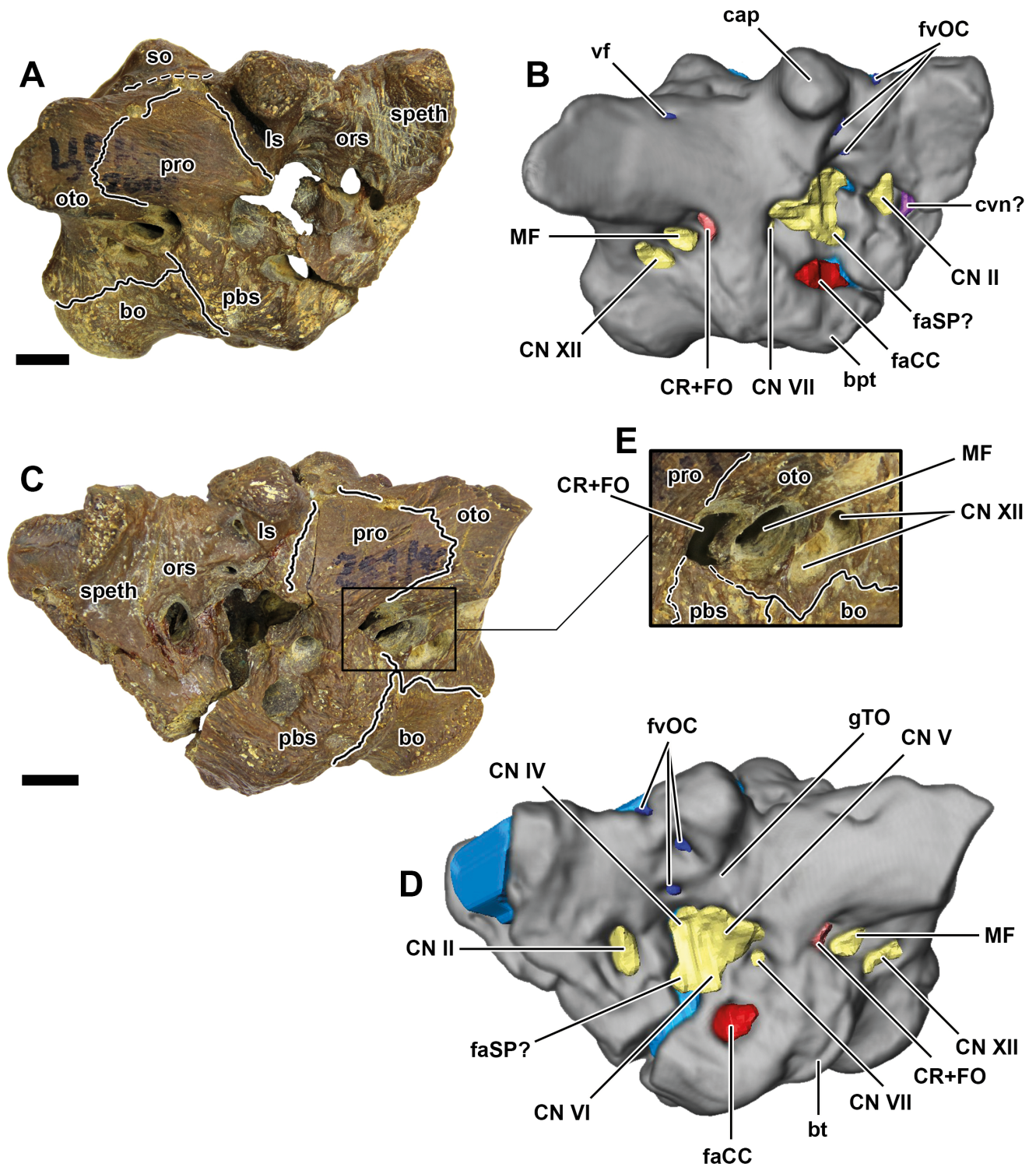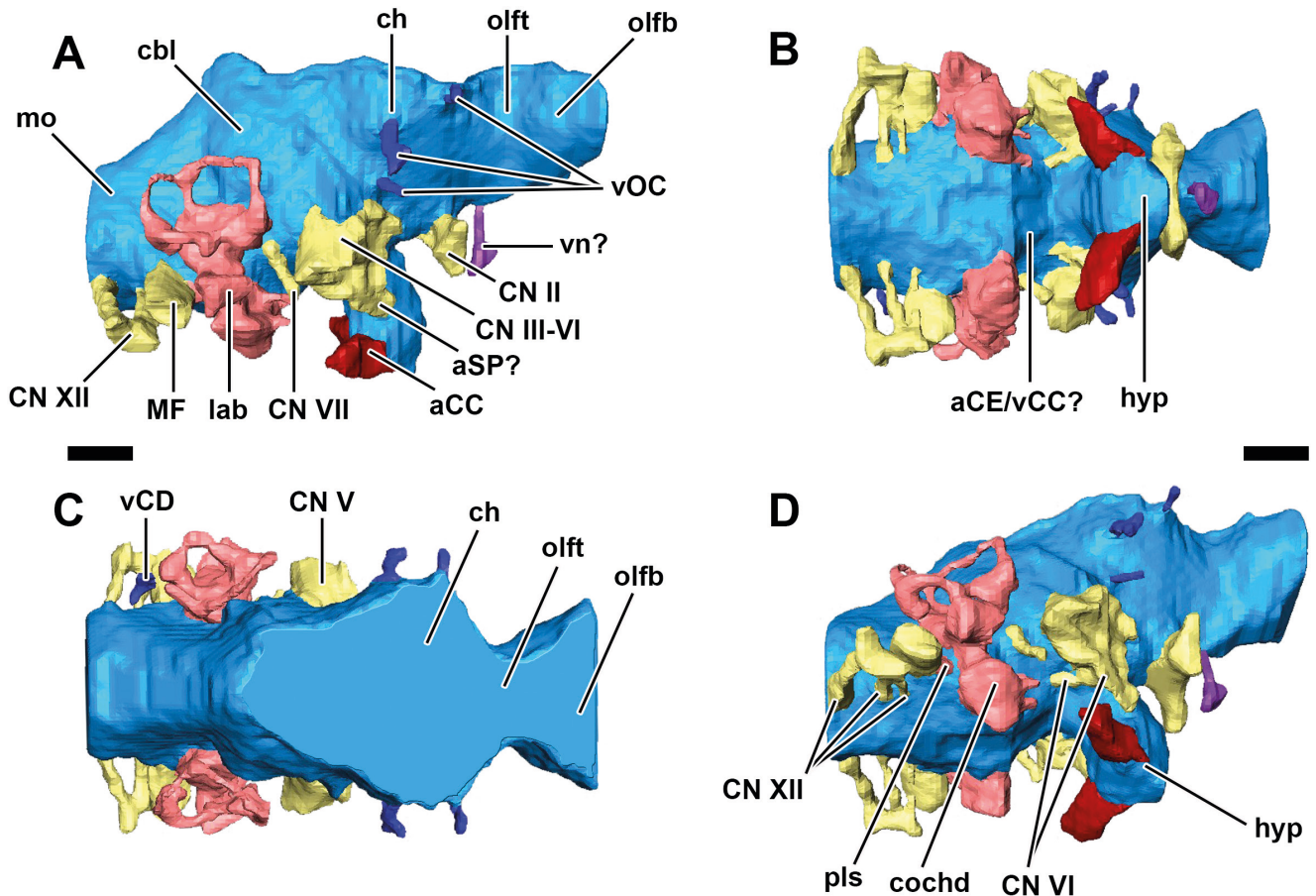
Fig. 14. ZIN PH 281/16, referred specimen of *Bissektipelta archibaldi* from the Bissekty Formation (Turonian), Uzbekistan. Cranial endocast with endosseous labyrinth of the inner ear in right lateral (A), ventral (B), dorsal (C), and oblique ventrolateral (D) views. Scale bars each equal 1 cm. Abbreviations: **aCC**, cerebral carotid artery and vein; **aCE/vCC?**, caudal encephalic artery/caudoventral cerebral vein; **aSP?**, sphenopalatine artery and vein; **cbl**, cerebellum; **ch**, cerebral hemisphere; **CN II — XII**, cranial nerves; **cochd**, endosseous cochlear duct; **hyp**, hypophysis (pituitary); **lab**, endosseous labyrinth; **MF**, metotic passage; **mo**, medulla oblongata; **olfb**, olfactory bulb; **olft**, olfactory tract; **pls**, perilymphatic sac; **vCD**, dorsal heard vein; **vn?**, vomero-nasal bulbs?; **vOC**, orbitocerebral veins.

presence and position of separate foramina for CN III in ZIN PH 281/16 are uncertain.

Endocranial surface. The endocranial surface of ZIN PH 281/16 does not differ significantly from that of the holotype in the general division into regions or the distribution of neurovascular foramina (Fig. 13). Its surface is mostly smooth, indicating a loose infilling by the brain. Vertical striations at the surface of the cavity for the olfactory tract probably result from a closer contact between the brain and its dura with the walls of the braincase (Fig. 13A). Most sutures on the endocranial surface are obliterated; however, the basioccipital-otoccipital, basioccipital-parabasisphenoid, and prootic-otoccipital sutures are visible (Fig. 13A). The straight basioccipital-otoccipital sutures extend ventral to the internal foramina for CN XII and disappear towards the MF and lagenar fossae. The suture between the basioccipital and parabasisphenoid extends transversally between large, unossified lagenar fossae. The basioccipital apparently forms most of the ventral endocranial surface. Possible

prootic-otoccipital sutures extend as ridges on the preserved surface of both otic capsules.

A single transverse canal for CN II opens laterally on either side in a separate foramen (Fig. 13C). The hypophyseal cavity is comparatively shallow, nearly half the dorsoventral depth of the cerebral cavity above it. The tentorial crest separating the cerebral and cerebellar cavities appears to be prominent and sharp at its dorsal part; it is broken off ventrally on both sides and the canal for CN VI is exposed (Fig. 13B). The dorsum sellae preserves the central triangular projection. Posterodorsally in the prootic, a foramen leads into two canals, one anteroventral (for CN VII) and the other posterodorsal into the otic capsule (for CN VIII) (Fig. 13C). The medial walls of both otic capsules are largely unossified, and two huge lagenar fossae are present on the floor of the endocranium (ves+lagf in Fig. 13B). Anterodorsal to the otic capsule, a distinct fossa is present on either side, which is not particularly evident in the holotype (floc, Fig. 13C). These depressions correspond in their position to the

floccular (auricular) fossae in other archosaurs (Gower, 2002; Sampson and Witmer, 2007; Witmer et al., 2008; Sobral et al., 2016). Each fossa has a pair of sediment-filled openings at the bottom that apparently connect to the inner ear cavities within the bone (the CT data offer insufficient resolution to trace these structures with confidence). These foramina likely transmitted vessels to the inner ear labyrinth. Although the external foramina for CN XII vary in number (two or three) between both sides of the specimen, there are three internal openings on either side (Fig. 13C).

Endocast. The digital endocranial cast of ZIN PH 281/16 is relatively complete except its dorsal part (due to the absence of the skull roof) (Fig. 14). It has a steeper slope posterodorsally above the medulla oblongata (mo, Fig. 14A) than in the holotype. The region corresponding to the olfactory bulbs expands anteriorly and narrows posteriorly (olfb, Fig. 14C). The olfactory bulbs are not separated on the endocast, as the midline septum is not preserved in ZIN PH 281/16; however, the lateral margins of their endocast form an angle of 67º in dorsal view that is comparable to the divergence angle for the olfactory bulbs in ZIN PH 1/16 (approximately 80º). This suggests that the olfactory bulbs of ZIN PH 281/16 were divided anteriorly and did not touch medially, as in the holotype and in other ankylosaurs (see Discussion). The olfactory tract of ZIN PH 281/16 is short and constricted (half the lateromedial breadth of the region of the olfactory bulbs in dorsal view); it merges posteriorly into an expanded cerebral region of the endocast (olft, Fig. 14C). The cerebral hemispheres are clearly visible as rounded expansions on the lateral surface of the endocast (ch, Fig. 14A, C, D). The endocast of ZIN PH 281/16 is broadest at the cerebral hemispheres; the endocast of the olfactory bulbs has a slightly smaller breadth (similar to ZIN PH 1/16, although both regions are almost equally broad in the latter). The constriction posterior to the cerebral hemispheres is more pronounced on the endocast of ZIN PH 281/16 compared to that of ZIN PH 1/16 (Fig. 14A). The cerebellar region is more defined than in ZIN PH 1/16 as a slight roundish bulge on the lateral surface of the endocast (cbl, Fig. 14A). It has relatively small projections that protrude into the anterior semicircular canal and are comparable to the larger flocculi in other dinosaurs (e.g., Sampson and Witmer, 2007; Witmer et al., 2008; Miyashita et al., 2011; Paulina-Carabajal et al., 2018). The brainstem is as broad transversely as deep dorsoventrally and has a flat ventral surface with an incision posterior to the pituitary (Fig. 14D). The endocast of the hypophyseal cavity (pituitary) projects ventrally and slightly anteriorly. The pituitary fossa is oval in cross-section; it is broader mediolaterally than long anteroposteriorly (Fig. 14B).

The endocast of CN II is oval in cross-section and perpendicular to the sagittal plane. Each CN II left the braincase through its own foramen laterally, similar to ZIN PH 1/16. Due to the damage to the lateral wall of the braincase, cranial nerves III–VI and the sphenopalatine artery (on the left side) were visualized as a single large entity; individual bundles of some cranial nerves are, nevertheless, apparent (Fig. 14A). The greater part of this artificial neurovascular endocast belongs to CN V, which is the largest among cranial nerves. The endocast of CN V is circular in cross-section and only slightly lobate distally (compared to the strongly pronounced three external lobuli of CN V in ZIN PH 1/16). CN VI extends anteroventrally, bypassing the hypophyseal cavity (Fig. 14D). The ventralmost portion is interpreted as the sphenopalatine artery. A separate stalk of the cerebral carotid artery is evident on either side of the hypophyseal endocast ventrally (aCC, Fig. 14A). CN IV corresponds to the anterodorsal part of the artificial neurovascular endocast. A separate CN III bundle is not evident due to the breakage of the specimen. Cranial nerves VII and VIII emerge together on the lateral surface of cranial endocast and then diverge (visualized only on the left side). The endocast of CN VII extends anteroventrally and laterally from below the inner ear cast. Cranial nerve VIII passes posterodorsally and enters the vestibular part of the endosseous labyrinths. The metotic foramen is undivided and is as large as the endocast of CN II. Three branches of CN XII are apparent on either side posterior to MF. Two smaller anterior branches extend parallel to one another and converge laterally.

Vascular elements of the cranial endocast include a series of small venous branches emerging from around the cerebral hemispheres (two posterior branches are usually referred to as orbitocerebral veins; e.g. Witmer et al., 2008), comparatively large curved stalks of the cerebral carotid arteries that merge with the hypophyseal endocast at its ventral extremity, a possible cast of the sphenopalatine arteries just anterodorsal to the cerebral carotid casts, and short sections of the tributaries of the transverso-occipital/dorsal head veins or the occipital artery enclosed in canals within the paroccipital processes (vCD, Fig. 14C).

Endocasts were produced for both endosseous labyrinths (lab, Fig. 14), but they are partly incomplete and have some artifacts (e.g., coiled lateral semicircular canal of the right inner ear) due to the poor resolution of the original CT images. Nevertheless, together these casts appear to faithfully represent the structure of the inner ear in ZIN PH 281/16. Semicircular canals appear narrower compared to those of ZIN PH 1/16. The anterior semicircular canal is the largest of the three and has an oval course. The posterior semicircular canal of the right endosseous labyrinth is better preserved and is nearly circular. The ampullae are better defined than in ZIN PH 1/16; they appear as two rounded expansions at the bases of semicircular canals. The ampullae of the

anterior and lateral semicircular canals are not separated from each other. The auditory portion of the inner ear (endosseous cochlear duct; cochd in Fig. 14D) is set apart from the vestibular portion by a prominent constriction ventral to the semicircular canals. The cochlear duct is relatively elongate (13.1 to 14.4 mm, Table 3) and comprises 45–52 % of the overall height of the endosseous labyrinth. As is the case in ZIN PH 1/16, the length of the endosseous cochlear duct could be overestimated, as large unossified spaces below the endocranial cavity on both sides of ZIN PH 281/16 were segmented as parts of the inner ear labyrinth. As already discussed above, these spaces could have contained large compartments of the perilymphatic labyrinth and/or neurovascular elements, and the actual cochlea was possibly less elongated. ZIN PH 281/16 preserves notches on the endocranial surface between the inner ear cavities and corresponding MF. These notches are possibly the osteological correlates of the extracapsular perilymphatic sacs and were segmented as parts of the inner ear.

Description of ZIN PH 2329/16 (Fig. 15)

General comments. ZIN PH 2329/16 appears to be similar in size to the holotype ZIN PH 1/16 (Table 1). It preserves a substantial portion of the posterior skull roof, which is described in detail below. Overall, the specimen is crushed and covered by matrix that obscures much of the osteological detail. ZIN PH 2329/16 was not CT scanned. Thus, we do not provide an extended description of the features of its braincase.

Skull roof. ZIN PH 2329/16 preserves much of the right side of the posterior region of the skull roof (Fig. 15A). The preserved region corresponds to portions of the parietal, frontal, squamosal, postorbital, and the supraorbital ossification(s) (Maryańska, 1977; Carpenter et al., 2001; Hill et al., 2003; Leahey et al., 2015). The supratemporal fenestrae are closed. The skull roof has a relatively flat dorsal surface and lacks any prominent horns, bumps, or other ornamental features. The base of a small posterodorsally inclined projection is present on the nuchal shelf, but the structure is largely broken off. The skull roof is essentially flat in the center, above the braincase, slightly domed above the orbit, and has shallow depressions antero- and posterolaterally. The nuchal shelf (nus, Fig. 15A) overhangs the occiput and obscures it in dorsal view. No transverse groove is present anterior to the shelf. There are no discrete caputegulae, although the skull roof is partially covered by matrix.

The roofing of the orbit is incompletely preserved in ZIN PH 2329/16 (Fig. 15B, C). It is slightly domed in lateral view. The orbital cavity is, at least partially, separated from the adductor cavity posteriorly by the postocular shelf (Maryańska, 1977; Vickaryous et al., 2004; Carpenter et al., 2011; pos in Fig. 15) and from the nasal cavity

anteriorly by the preorbital septum (Maryańska, 1977; ectethmoid in Miyashita et al. [2011]; pros in Fig. 15). Both the postocular shelf and the preorbital septum are anteroposteriorly thin ridges nearly perpendicular to the sagittal axis of the skull. The postocular shelf is more pronounced and is more laterally extensive than the preorbital septum. The posterior surface of the postocular shelf forms the anterior wall of the adductor cavity and has two depressions (d, Fig. 15D); its anterior surface is smooth, slightly concave, and forms the posterior wall of the orbital cavity. The preorbital septum is a thin sheet of bone that separates the orbital cavity from the anteriorly situated olfactory region of the nasal cavity (a similar structure was identified as ectethmoid by Miyashita et al. [2011]). It is almost perpendicular to the sagittal plane of the skull in *Bissektipelta* and differs from the more anterolaterally oriented and elongated structure in *Euoplocephalus* (Miyashita et al., 2011). The preorbital septum bears a small foramen between the orbital cavity and the olfactory region (onf, Fig. 15B, D). The foramen appears to be genuine but its edges are partially eroded. A small foramen was noted in a similar position in *Euoplocephalus* as a possible orbitonasal foramen (Miyashita et al., 2011). Both the postocular shelf and the preorbital septum are developed as the ventral outgrowths of the skull roof that merge with the lateral wall of the braincase medially. The postocular shelf also contacts the braincase in *Euoplocephalus* and *Talarurus* but not in *Saichania* (Carpenter et al., 2011). The extensive matrix cover precludes direct observations of the contacts with the braincase wall in ZIN PH 2329/16, the only studied specimen that preserves these structures. In the holotype ZIN PH 1/16, both these structures are broken off, and only their bases could be identified. The smaller-sized specimen ZIN PH 281/16 shows no signs of the co-ossification between the lateral wall of the braincase and the postocular shelf or the preorbital septum.

Braincase. The occipital condyle is prominent, crescent-shaped, and transversely extended (Table 1; Fig. 15E). Both basipterygoid processes are partially preserved (bpt, Fig. 15C). They are short, stout, and displaced posteriorly, close to the basioccipital-parabasisphenoid contact. The fused parabasisphenoid rostrum-interorbital septum is preserved as a sharp sagittal lamina that dorsally merges with the medial septum between the olfactory bulbs (pbsro-ios in Fig. 15). The configuration of neurovascular foramina on the lateral wall of the braincase is difficult to determine due to the state of preservation. The neurovascular foramina are disposed as two distinct clusters separated by a flat crista prootica. Posteriorly, the FO, MF, and XII foramina are apparently situated ventral to the base of the paroccipital process. Only the posterior outline of a large partially subdivided foramen for CN V is visible anteriorly (Fig. 15C). Among the preserved endocranial features
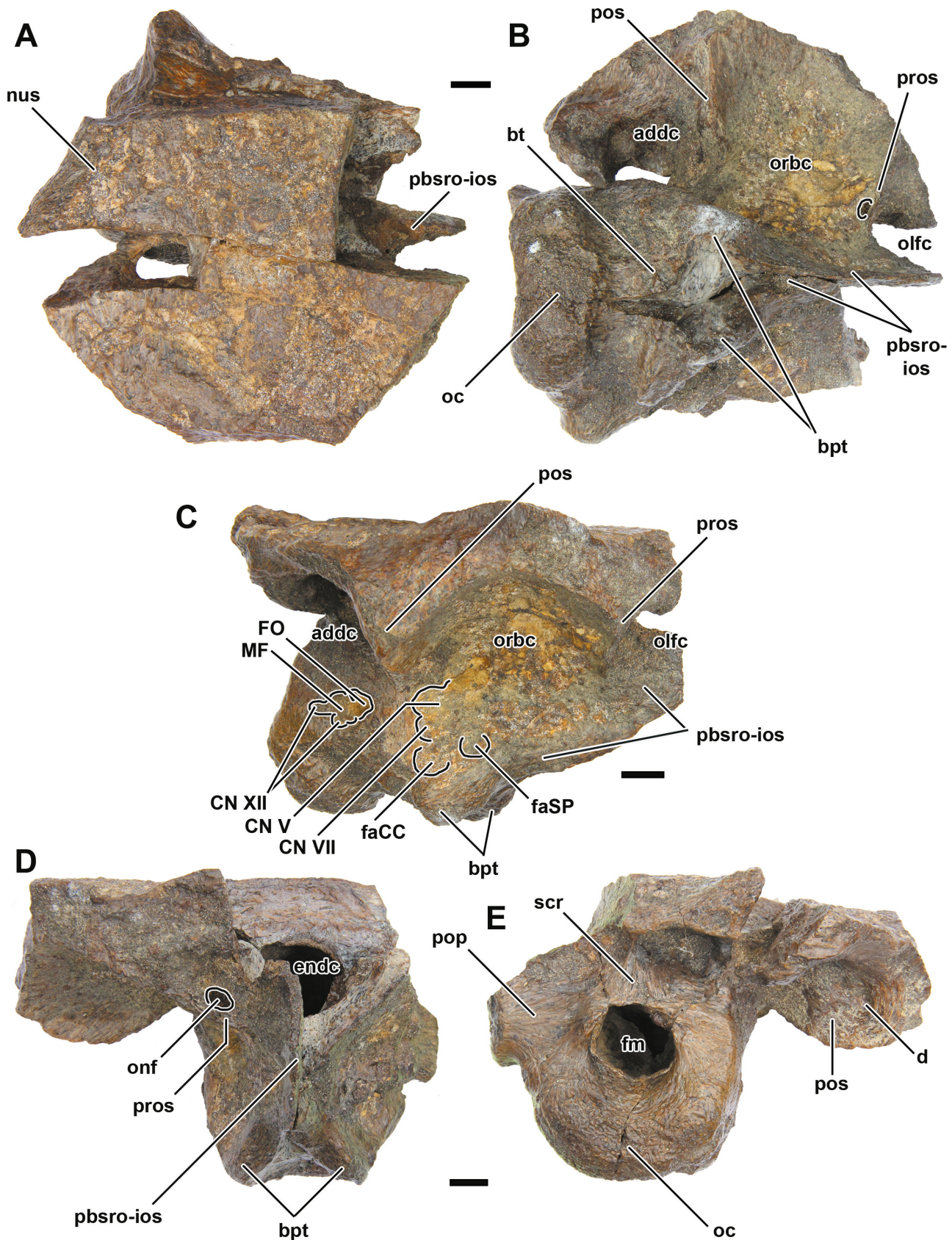
Fig. 15. ZIN PH 2329/16, referred specimen of *Bissektipelta archibaldi* from the Bissekty Formation (Turonian), Uzbekistan. Photographs in dorsal (A), ventral (B), right lateral (C), anterior (D), and posterior/occipital (E) views. Scale bars each equal 1 cm. Abbreviations: **addc**, adductor cavity; **bpt**, basipterygoid process; **bt**, basal tuber; **CN V-XII**, cranial nerve foramina; **d**, depression; **endc**, endocranial cavity; **faCC**, cerebral carotid artery and vein; **faSP**, sphenopalatine artery and vein; **fm**, foramen magnum; **FO**, fenestra ovalis; **MF**, metotic foramen; **nus**, nuchal shelf; **oc**, occipital condyle; **olfc**, olfactory cavity; **onf**, orbitonasal fenestra; **orbc**, orbital cavity; **pbsro-ios**, fused parabasisphenoid rostrum and interorbital septum; **pop**, paroccipital process; **pos**, postocular shelf; **pros**, preorbital septum; **scr**, sagittal crest.

are a partially preserved median septum between the cavities of the olfactory bulbs, large internal foramina for CN V posterior to the tentorial crest, small foramina for CN VI piercing the dorsum sellae ventral to CN V, and incompletely ossified otic capsules. Notably, the dorsum sellae appears to form a complete sheet of bone between both tentorial crests (the medial part of this sheet is not preserved). It is not incised like a U as in ZIN PH 1/16 and ZIN 281/16.

Comparison and taxonomic attribution of the studied ankylosaurian braincases from the Upper Cretaceous Bissekty Formation of Uzbekistan

Skull roof. Portions of the skull roof are preserved in two specimens — the holotype ZIN PH 1/16 and ZIN PH 2329/16. In both specimens, it is co-ossified with the braincase without clear sutures. The boundaries between the skull roof and the braincase are discernible in ZIN PH 1/16 through the position of neurovascular foramina, surficial grooves, and other features (Figs. 1, 2). On the other hand, obvious facets for bones of the skull roof are preserved on dorsal margins of ZIN PH 281/16, which suggests a sutural contact instead of fusion (Fig. 10). We suggest that co-ossification of the skull roof and the braincase is ontogenetically variable in *Bissektipelta* because ZIN PH 281/16 is generally slightly smaller than the rest of the specimens (Table 1) and retains open sutures between other bones.

ZIN PH 1/16 and ZIN PH 2329/16 share closed supratemporal fenestrae and secondary modified sculpture on the dorsal surface of the skull roof; there are no sutures between individual bones of the skull roof. A prominent transverse groove (frontoparietal depression of Godefroit et al., 1999) anterior to the nuchal ornamentation found in some derived ankylosaurids (Carpenter et al., 2011) is absent in ZIN PH 1/16 and ZIN PH 2329/16. Both specimens have a relatively flat posterior surface of the skull roof without prominent ornamentation, similar to *Shamosaurus* and *Gobisaurus* (Tumanova, 1983; Vickaryous et al., 2001b; Arbour and Currie, 2016).

ZIN PH 1/16 and ZIN PH 2329/16 strongly differ in the type of cranial roof ornamentation. ZIN PH 1/16 possesses a truncated Y-shaped groove that separates three distinct caputegulae (Fig. 1A, B). The presence of this groove was suggested as the only autapomorphy of *Bissektipelta archibaldi* by Parish and Barrett (2004; see also Arbour and Currie [2016]). On the other hand, ZIN PH 2329/16 has a rugose amorphous sculpture with no caputegulae (Fig. 15A). As most recent analyses of ankylosaurian phylogeny (e.g., Arbour and Currie, 2016; Arbour and Evans, 2017; Zheng et al., 2018) used features of cranial ornamentation as charac-

ters, and the existing diagnosis of *Bissektipelta* includes the single autapomorphy concerning cranial ornamentation, the difference between ZIN PH 1/16 and ZIN 2329/16 could be considered an argument for the latter specimen representing a separate taxon (see "Taxonomic attribution" below).

Ventral surface of the basicranium. All three studied specimens share a basioccipital with an undifferentiated neck that is as broad as the parabasisphenoid and a short parabasisphenoid with an anterodorsally inclined rostrum. The basipterygoid processes of the studied specimens are short, stout, and posteriorly displaced, lying close to the basal tubera. The rounded tips of the basipterygoid processes indicate a sutural rather than fused contact with the pterygoid.

The most prominent difference between the holotype ZIN PH 1/16 and two other specimens is the angle between the ventral surfaces of the parabasisphenoid and the basioccipital. It equals approximately 90º in ZIN PH 1/16, 110º in ZIN PH 2329/16, and 120º in ZIN PH 281/16 (Figs. 2, 12, 15C). The right angle between these bones in the holotype was used by Averianov (2002) to distinguish *Bissektipelta archibaldi* from other Asian ankylosaurids. The angle is actually created between the anterior and posterior surfaces of the parabasisphenoid in ZIN PH 281/16. Ontogenetic or intraspecific variability of this character is possible but, to our knowledge, has never been discussed for ankylosaurs. However, extant crocodylians have a well-known change of the parabasisphenoid during ontogeny: hatchlings have a plate-like parabasisphenoid that expands dorsoventrally and becomes vertical during growth (Tarsitano, 1985).

The relief of the ventral surface of the basioccipital differs slightly between ZIN PH 1/16 and ZIN PH 281/16 (ZIN PH 2329/16 is damaged in this area): the holotype possesses a pair of coarse ridges that converge ventrally, with two depressions flanking the ridges (Fig. 1C, D). ZIN PH 281/16 has a central rounded bump with depressions on its sides (Fig. 10C, D). The general topography seems to be comparable between specimens, and the coarser ridges of ZIN PH 1/16 are probably due to ontogeny. The ventral surface of the basioccipital shows notable variability among Asian ankylosaurids (Tumanova, 1987) and Late Cretaceous taxa from North America closely related to *Euoplocephalus* (Penkalski, 2018).

Occipital surface. The occiput of the three studied specimens has the same general structure: it is lateromedially wider than dorsoventrally deep, with a massive occipital condyle, triangular proatlas facets, and the occipital surface sloping at about 125º relative the horizontal plane. The shape and relative size of the occipital condyle differ between all three specimens. Overall, the condyle is oval to crescent-shaped, but more rounded in the smallest specimen ZIN PH 281/16 and strongly dor-

soventrally compressed in ZIN PH 2329/16 (Table 1). We surmise that this variation of shape of the occipital condyle represents an intraspecific difference. Intraspecific variability in shape and length of the condylar neck was noted for some ankylosaurs (e.g., *Cedarpelta*; Carpenter et al., 2001). The diameter of condyle and its position relative to the main portion of the bone ("offset") are variable among specimens of *Euoplocephalus* sensu lato (Penkalsi, 2001), although this possibly represents a taxonomically significant difference between closely related species (Penkalski, 2018).

ZIN PH 1/16 and ZIN PH 281/16 vary in the disposition of vascular foramina on the occipital surface. In the holotype ZIN PH 1/16, the circular posttemporal fenestrae are present at the level of lateral margins of the foramen magnum. The posttemporal fenestra in ZIN PH 1/16 is apparently located at the contact of the supraoccipital, paroccipital process, and parietal (Fig. 1E, F). In ZIN PH 281/16, there are small vascular canals completely surrounded by paroccipital processes. They are placed relatively laterally compared to the posttemporal fenestrae of ZIN PH 1/16. We consider these canals as supplementary vascular features that are not present in the holotype. There are also depressions at the lateral margins of the supraoccipital in ZIN PH 281/16 that could correspond to ventral borders of the posttemporal fenestrae; they are, however, too close to the sagittal plane compared to the condition in the holotype (Fig. 11C, D).

Lateral braincase wall. The three studied specimens completely lack paratympanic pneumaticity, as is common for ornithischians (Witmer, 1997). The holotype ZIN PH 1/16 and ZIN PH 281/16 share an identical pattern of distribution of neurovascular openings: there are two clusters of foramina separated by a flattened crista prootica. The relative size of foramina is also very similar in both specimens. The number of lateral openings for CN XII varies between sides in ZIN PH 281/16, but its endocast shows that there were three roots of the nerve on both sides, similar to the condition in the holotype. The only possible difference between the two specimens is the presence of a putative foramen for CN III; however, ZIN PH 281/16 is damaged in the corresponding area. In addition, ZIN PH 281/16 shows a lesser degree of ossification of the lateral wall of the braincase: some sutures are still open, there is no supraorbital artery canal embedded within bone, the fenestra ovalis and its recess are not as deep as in ZIN PH 1/16, and the preorbital septum is not fused and/or ossified, with only the rugose texture of the lateral surface present anterior to the capitate process of the laterosphenoid.

The lateral wall of the braincase in ZIN PH 2329/16 is damaged and covered by matrix, precluding detailed observations. From what is evident, ZIN PH 2329/16 is similar to both other specimens in terms of the distribution of neurovascular foramina. Unfortunately, the number of roots/foramina for CN XII could not be assessed in ZIN PH 2329/16.

Endocranial surface. The endocranial surface of the studied specimens is identical in many aspects. The pattern of the neurovascular foramina is similar. All three specimens share an unossified medial wall of the otic capsule and a pit ventral to it, a rounded and relatively shallow hypophyseal cavity, and prominent tentorial crests. ZIN PH 2329/16 differs in the structure of the dorsum sellae: whereas the holotype and ZIN PH 281/16 have a U-shape incision between the tentorial crests with a small triangular process, there is a continuous bony sheet between the bases of the tentorial crest in ZIN PH 2329/16. The differences in the structure of the dorsum sellae were noted for several Late Cretaceous Asian ankylosaurids (*Pinacosaurus*, *Tarchia*, and *Saichania*) by Maryańska (1977). Additionally, ZIN PH 281/16 has a more pronounced depression anterodorsal to the otic capsule compared to ZIN PH 1/16. This depression has usually been interpreted as housing the flocculus of the cerebellum (e.g., Miyashita et al., 2011; Paulina-Carabajal et al., 2018); however, much of this depression may have actually housed vasculature (Walsh et al., 2013), and thus intraspecific variation of its size is conceivable.

Taxonomic attribution. The comparisons show that the three ankylosaur braincases from the Bissekty Foramation are comparable in a large number of features but show differences in some other aspects. Each of the specimens is undoubtedly referable to Ankylosauria (or one of its less inclusive subclades) based on the presence of at least several of the following features: closed supratemporal fenestrae; cranial roof with secondarily remodeled surface and obliterated sutures; presence of the postocular shelf between the orbit and the adductor cavity; presence of two separate foramina for CN II; laterally displaced canal for CN VI that bypasses the hypophyseal cavity; low and massive basicranium; posteroventrally oriented surface of the basioccipital; straight, ventrally projecting pituitary cavity; medially separated olfactory bulbs; and cerebral carotid canal extending transversely to enter the pituitary fossa laterally rather than posteroventrally (Maryańska, 1977; Tumanova; 1987; Vickaryous et al., 2004; Paulina-Carabajal et al., 2018; see Discussion for further details).

Attribution to Ankylosauridae (or one of its less inclusive subclades) of each of the specimens is possible based on the presence of the following features (see Discussion for further details): semilunar to ellipsoidal basioccipital condyle; basioccipital wide and with undifferentiated neck; ridge-like basitubera; basipterygoid processes small and not fused with pterygoids; closely spaced external foramina for CN V and CN VII; three internal foramina for CN XII; mostly laterally directed

paroccipital processes; and flat endocranial floor. This taxonomic assumption was corroborated by the results of a formal phylogenetic analysis (see below).

The difference in the ornamentation of the skull roof between ZIN PH 1/16 and ZIN PH 2329/16 is the most taxonomically significant variation documented among the studied specimens. Features of the cranial ornamentation have been used in recent phylogenetic analyses of ankylosaurs (e.g., Hill et al., 2003; Thompson et al., 2012; Arbour and Currie, 2016) and were employed to distinguish closely related taxa of the *Euoplocephalus* complex (Penkalsi, 2018). The only autapomorphy that currently diagnoses *Bissektipelta* is the presence of a Y-shaped groove separating polygons of remodeled bone (caputegulae) in the holotype (Parish and Barrett, 2004; Arbour and Currie, 2016).

However, although taxonomically significant patterns of cranial ornamentation exist among ankylosaurs, some taxa represented by a number of specimens show intraspecific variation of certain features. Variability in frontoparietal and nuchal caputegulae was noted for *Euoplocephalus tutus* and closely related species from the Late Cretaceous of North America (Penkalski, 2001; Arbour and Currie, 2013a). Larger skulls of *Euoplocephalus* tend to have a more rugose and amorphous dorsal surface, blunter squamosal horns, and wider and less distinct nuchal caputegulae (Penkalski, 2001). Arbour and Currie (2016) hypothesized that these differences may be due to ontogeny. The gradual development of cranial ornamentation is known from numerous specimens of *Pinacosaurus* from the Late Cretaceous of Asia representing an ontogenetic sequence (Hill et al., 2003). In juveniles of the latter taxon, sutures between individual bones are clearly apparent, and the parietals are paired (Maryańska, 1971). In other specimens, the parietals appear to be fused (Hill et al., 2003; Burns et al., 2011), and, in the largest (holotype) skull, sutures are completely obscured due to development of ornamentation (Gilmore, 1933). The aforementioned data indicate that the cranial ornamentation in ankylosaurs differs not only between taxa but also within species and is likely subject to ontogenetic and intraspecific variation.

The absence of caputegulae on the dorsal surface of ZIN PH 2329/16 may be due to poor preservation, ontogenetic/intraspecific variability of the cranial ornamentation in *Bissektipelta*, or taxonomic separation. Given a sample size of merely two specimens compared with each other, it is hard to choose a single hypothesis at present. The dorsal surface of the holotype is textured with a vast array of vascular foramina and grooves. The Y-shaped groove is irregular on closer look: it is interrupted on the left side and has an offshoot oblique groove extending anteromedially on the left side but not on the right. All these suggest active bone remodeling in ZIN PH 1/16. Thus, the hypothesis of the variability of

cranial ornamentation in *Bissektipelta* cannot be ruled out.

Ankylosaurian teeth, vertebrae, and limb bones are known from the Bissekty Formation. These remains have not yet been formally described, but preliminary observations (by A. O. Averianov) suggest the presence of a single taxon. Given that all three studied braincases are from a single locality, share anatomical features, and each belong to an ankylosaurid, we tentatively refer all of them to a single taxon *Bissektipelta archibaldi*. The referral of additional specimens modifies the diagnosis of *Bissektipelta*: no autapomorphies can be hypothesized at present. The structure of the braincase appears to be highly conservative at low taxonomic levels among ankylosaurs (Burns, 2015; Paulina-Carabajal et al., 2018; see Discussion). This hampers the diagnosis of *Bissektipelta archibaldi*, a monospecific taxon presently based solely on isolated braincases. Additional study of the ankylosaurian material from the Bissekty Formation is needed.

Phylogenetic analysis

Previous work on the phylogenetic position and diagnosis of Bissektipelta. Averianov (2002) established "*Amtosaurus*" *archibaldi* on the basis of a single specimen, ZIN PH 1/16, which until now was the only known ankylosaur braincase from the Bissekty Formation. He referred ZIN PH 1/16 to Ankylosauridae based on the crescent-shaped basioccipital condyle without a defined neck and directed posteroventrally (versus a hemispherical condyle with a constricted neck and directed ventrally in nodosaurids) (Averianov, 2002). The comparison between ZIN PH 1/16 and Asian ankylosaurids with known braincase structure led Averianov to suggest a close affinity with "*Amtosaurus magnus*", a monospecific genus based upon a single braincase (Kurzanov and Tumanova, 1978). Averianov (2002) provided a species-level diagnosis of "*Amtosaurus*" *archibaldi* that listed differences between the two species: three rather than two exteral foramina for CN XII, a smaller angle between ventral surfaces of the parabasisphenoid and basioccipital, and the more posteriorly placed basipterygoid processes.

The validity of "*Amtosaurus*" has been questioned by a number of authors (Coombs and Maryańska, 1990; Parish and Barrett, 2004). Based on the most recent published revision, "*Amtosaurus magnus*" should be regarded as a *nomen dubium* and Ornithischia indet. (Parish and Barrett, 2004). A new genus, *Bissektipelta*, was proposed for "*Amtosaurus*" *archibaldi*, which was considered a valid taxon of ankylosaur (Parish and Barrett, 2004). The authors stated that the fragmentary nature of ZIN PH 1/16 precludes its assignment to any particular subclade and placed *Bissektipelta* as Ankylosauria

incertae sedis. The diagnosis was significantly modified from that of Averianov (2002) and included a single autapomorphy — a distinctive pattern of the skull roof ornamentation with a truncated Y-shaped groove that separates three flat polygonal areas of remodeled bone, combined with three exits for CN XII (Parish and Barrett, 2004).

In a recent revision of ankylosaur materials from Russia and adjacent countries, Tumanova (2012) listed *Bissektipelta* within Ankylosaurinae but without any specific comments regarding that attribution. She provided a diagnosis similar to that of Averianov (2002) except for the exclusion of the number of foramina for CN XII. Additionally, Tumanova (2012) questioned features of the skull roof ornamentation as reliable for the inclusion in the diagnosis. Later, Arbour and Currie (2016) listed *Bissektipelta* as a valid ankylosaurid taxon and adopted the diagnosis of Parish and Barrett (2004).

In summary, there is no current consensus on the phylogenetic position of *Bissektipelta archibaldi*. The taxon has never been included in a formal phylogenetic analysis, and its affinities and taxonomic status are in flux.

Dataset and taxon selection. To assess the phylogenetic position of *Bissektipelta*, we added it in the recently published taxon-character matrix by Zheng et al. (2018), which itself is a modification of the matrix compiled by Arbour and Currie (2016). Character scores were mainly based on the holotype ZIN PH 1/16, with only 2 out of 27 characters based on observations of ZIN PH 2329/16 (characters 42 "Development of the postocular shelf" and 54 "Posterior projection of the nuchal shelf"). These features are not observed on the holotype as they were broken off with only their bases remaining.

We added 12 new morphological characters concerning braincase and endocranial features (see Supplementary File 1 and Discussion below). Additionally, we added two new outgroup taxa (*Kentrosaurus aethiopicus* and *Stegosaurus* spp.), for which the morphology of the braincase and endocast is well known (Gilmore, 1914; Galton, 1988, 2001; Leahey et al., 2015: Fig. 10), in contrast to *Huayangosaurus taibaii*, the only stegosaurian taxon included in the original dataset. We coded these new taxa based on the available published accounts (Gilmore, 1914; Hennig, 1925; Galton, 1982, 1988, 2001; Berman and McIntosh, 1986; Galton and Upchurch, 2004; Maidment et al., 2006, 2015). Additionally, we revised some previous scores for outgroup and ingroup taxa based on recently published revisions (see Supplementary File 1 for details). In total, the obtained matrix contains 62 taxa (including 5 outgroup taxa) and 189 characters.

Analytical methods. The final datasets (Supplementary Files 2 and 3) were assembled in NEXUS Data Editor 0.5.0 and analysed in TNT version 1.5 (Golo-

boff and Catalano, 2016). All characters were treated as unordered and of equal weight. The tree searching procedure follows those of Arbour and Currie (2016) and Zheng et al. (2018). The maximum trees setting in memory was set to 10000. The analysis was carried out using the Traditional search option, with random seed 1 and 1000 replicates of Wagner trees and the tree bisection reconnection (TBR) swapping algorithm (holding 10 trees per replication).

Results. As was noted by Wiersma and Irmis (2018), the dataset from Arbour and Currie (2016) and its modified versions (Arbour and Evans, 2017; Zheng et al., 2018; current analysis) are extremely sensitive to taxon and character sampling. For example, Zheng et al. (2018) had to prune out a posteriori four ingroup taxa (*Aletopelta*, 'Paw Paw scuteling', *Sauroplites*, and '*Zhejiangosaurus*') to receive a resolved strict consensus tree. In the present study, we have run the analysis multiple times with different types of the dataset (e.g., prior to inclusion of new braincase characters, before inclusion of *Stegosaurus* and *Kentrosaurus* as additional outgroup taxa, and prior to revision of various character states) and a posteriori pruning of certain taxa. Overall, we have observed two most frequently encountered tree topologies. Both are reported and further used in the discussion of braincase evolution in Ankylosauria here.

The first topology (Fig. 16) is recovered using the first taxon-character matrix (Supplementary File 2). The analysis resulted in 20 most parsimonious trees, each with a length of 620 steps, a consistency index (CI) of 0.387, and a retention index (RI) of 0.674. The strict consensus tree is relatively well resolved. Among outgroup taxa, the analysis failed to obtain a monophyletic Stegosauria, and *Huayangosaurus* is placed as a sister taxon to a monophyletic clade composing *Stegosaurus* + *Kentrosaurus* and Ankylosauria. Ankylosauria is monophyletic. *Kunbarrasaurus* from the Lower Cretaceous of Australia is basal to a monophyletic Ankylosauridae + Nodosauridae. Several taxa with a large number of missing scores (e.g., Paw Paw scuteling, *Liaoningosaurus*, *Hylaeosaurus*, *Chuanqilong*) are thrown off to basal positions within Ankylosauria. "Polacanthinae" or "Polacanthidae" is not found as a monophyletic clade; instead, its constituent taxa are scattered near the base of Ankylosauria and Ankylosauridae. A monophyletic clade comprising recognized nodosaurids is present and resolved to some extent. Ankylosauridae is monophyletic and relatively well resolved except crownward ankylosaurines. *Bissektipelta* is placed among basal ankylosaurines.

An additional tree topology (Fig. 17) is recovered when a slightly different taxon-character matrix is used (state for character 77 is "0/1" instead of "1" for *Talarurus*; Supplemetary File 3) and *Ahshislepelta* is pruned. The analysis results in 10 optimal trees, each with a length of 616, CI of 0.390, and RI of 0.678. The strict consensus tree
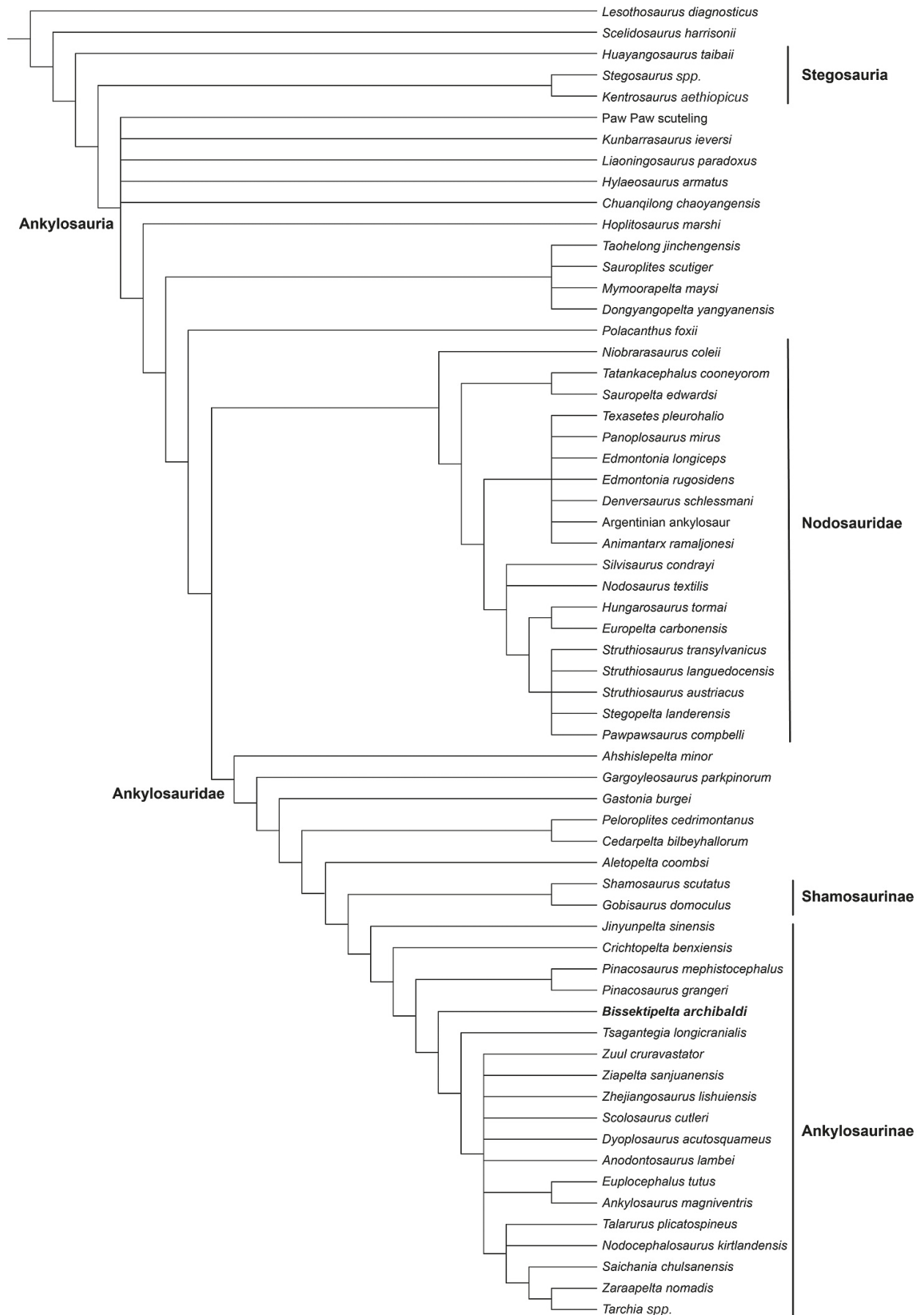
Fig. 16. Strict consensus of 20 optimal trees recovered from the phylogenetic analysis using TNT v.1.5 and modified taxon–character matrix from Zheng et al. (2018) (first topology; Supplementary file 2; all taxa included). Length = 620 steps; Ci = 0.387; Ri = 0.674.
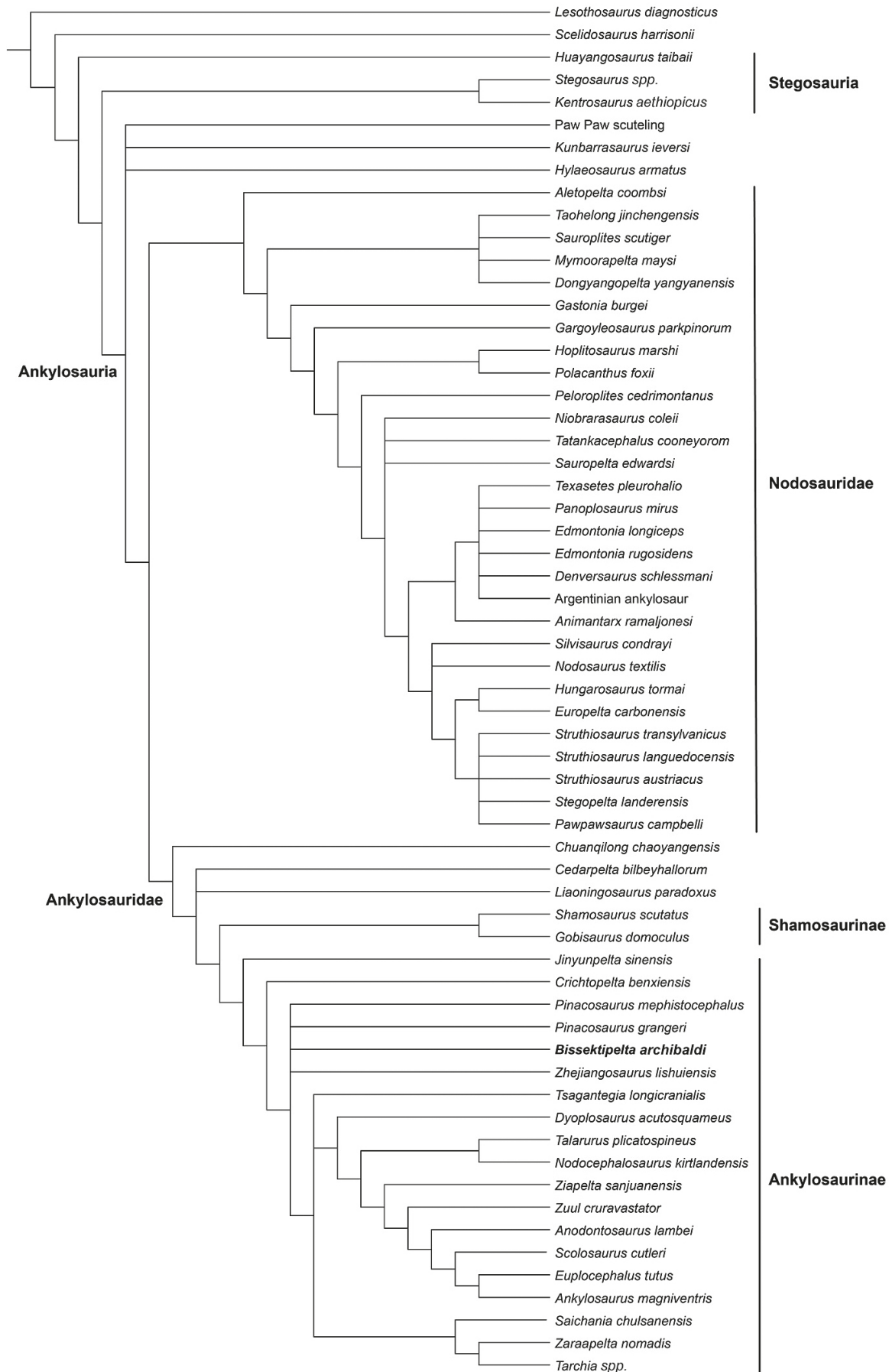
Fig. 17. Strict consensus of 10 optimal trees recovered from the phylogenetic analysis using TNT v.1.5 and modified taxon–character matrix from Zheng et al. (2018) (second topology; Supplementary file 3; *Ahshislepelta minor* is pruned out). Length = 616 steps; Ci = 0.390; Ri = 0.678.

is reasonably resolved and similar overall to the previous one. However, "polacantines" are now revealed as a series of basal taxa within a branch of Nodosauridae. A less inclusive clade (Nodosauridae sensu stricto) is identical to the previously reported tree topology. *Chuanqilong, Liaoningosaurus*, and *Cedarpelta* are basal ankylosaurids, a result that is consistent with most published studies (e.g., Arbour and Currie, 2016; Arbour and Evans, 2017). Crownward Ankylosaurinae is largely resolved compared to the previous tree topology, but the interrelationships of taxa are slightly different. *Bissektipelta* is found as a relatively basal ankylosaurine in a polytomy with *Pinacosaurus* spp. and "*Zhejiangosaurus*".

Comments on the phylogenetic position of Bissektipelta. Based on the results of the phylogenetic analysis, we conclude that *Bissektipelta archibaldi* is an undisputed ankylosaurid, contra Parish and Barrett (2004) and in agreement with Averianov (2002). The agreement position for *Bissektipelta* throughout the course of the present analysis was among basal ankylosaurines, corroborating the suggestion of Tumanova (2012). This result is consistent with the morphological comparison of braincases (see Discussion) and overall geographic and stratigraphic distribution of ankylosaurids (e.g., Arbour and Currie, 2016). In addition, a relatively flat skull roof with possibly rugose and irregular (inferred from ZIN PH 2329/16) ornamentation in *Bissektipelta* is similar to that of shamosaurines, *Crichtonpelta* from "mid"-Cretaceous of China and *Pinacosaurus* from the Late Cretaceous of Mongolia (Tumanova, 1987; Vickaryous et al., 2001b; Arbour and Currie, 2016). All this evidence supports a relatively basal position of *Bissektipelta* among Ankylosaurinae. Additional study of the ankylosaurian remains from the Bissekty Formation is needed to test this hypothesis.

Systematic paleontology

Dinosauria Owen, 1842
Ornithischia Seeley, 1887
Thyreophora Nopsca, 1915
Ankylosauria Osborn, 1923
Ankylosauridae Brown, 1908
Ankylosaurinae Brown, 1908
Bissektipelta Parish and Barrett, 2004

Type species: *Amtosaurus archibaldi* Averianov, 2002
Diagnosis: as for the type and only known species.

Bissektipelta archibaldi (Averianov, 2002)

Holotype: ZIN PH 1/16, fully ossified braincase with the posterior part of the skull roof (Figs. 1–9).

Referred material: ZIN PH 281/16, partial braincase of a smaller individual (Figs. 10–14); ZIN PH 2329/16, partial braincase with the posterior portion of the skull roof (Fig. 15).

Type locality: Dzharakuduk, Central Kyzylkum Desert, Uzbekistan. Bissekty Formation, Upper Cretaceous (Turonian).

Revised diagnosis. Referred to Ankylosauria based on closed supratemporal fenestrae; cranial roof with secondarily remodeled surface and obliterated sutures; presence of postocular shelf between the orbit and adductor cavity; presence of two separate foramina for CN II; laterally displaced canal of CN VI that bypasses the hypophyseal cavity; low and massive basicranium; posteroventrally oriented occipital condyle; straight ventrally projecting pituitary fossa; medially separated olfactory bulbs; and cerebral carotid canal extending transversely to enter pituitary fossa laterally rather than posteroventrally.

Referred to Ankylosauridae based on basioccipital wide and with an undifferentiated neck; ridge-like basitubera; basipterygoid processes small and not fused with pterygoids; closely spaced foramina for CN V and CN VII; and flat endocranial floor and linearly arranged cranial endocast with low angles of cerebral and pontine flexures.

Referred to Ankylosaurinae based on semilunar to ellipsoidal basioccipital condyle; three internal foramina for CN XII; and laterally directed paroccipital processes.

Differs from all ankylosaurids except *Pinacosaurus* by having relatively short (less than twice the diameter of the foramen magnum) and straight paroccipital processes. Differs from other Late Cretaceous ankylosaurines from Asia (*Crichtonpelta, Pinacosaurus, Tsagantegia, Minotaurasaurus, Saichania, Tarchia, Talarurus*) by having a flat posterior region of the skull roof and lacking a prominent nuchal ridge and frontoparietal depression. Differs from *Talarurus, Saichania, Tarchia*, and *Zaraapelta* by having large FO and MF and by having two or three external openings for CN XII separated from MF. Differs from *Euoplocephalus, Scolosaurus*, and *Tarchia* by lacking a flocculus of the cerebellum on the endocast.

No autapomorphies can currently be identified for *Bissektipelta*.

Discussion

Comments on the previous studies of the braincase and endocast of Bissektipelta

Averianov (2002) described the osteology of the holotype ZIN PH 1/16 of *Bissektipelta archibaldi* in detail, and, more recently, Alifanov and Saveliev (2019) independently worked on an artificial endocast made from ZIN PH 1/16. Here we summarize our comments on these earlier studies.

The osteological description of ZIN PH 1/16 provided by Averianov (2002) is comprehensive and accu-

rate. The present reexamination of the holotype is mostly built on the initial study of Averianov (2002) and seeks to update and expand this account by applying CT scanning and imaging techniques. We disagree with only a few interpretations made in that work: the incomplete state of ossification of some structures (basal tubera, occipital condyle, basipterygoid process) and the course of the otoccipital-basioccipital suture. The aforementioned structures (supposed as unossified in the holotype of *Bissektipelta archibaldi*) are variably preserved and frequently broken in the three studied specimens; ZIN PH 281/16, which is smaller overall than the holotype, has them. A break on the posterior surface of the paroccipital process was misinterpreted as the suture between the otoccipital and the basioccipital; a remnant of the actual suture is evident on the right side of the occipital condyle of ZIN PH 1/16 and is clearly present and having the same route on both sides of ZIN PH 281/16. Additionally, Averianov (2002) claimed that the preserved flat dorsal surface of the skull is devoid of osteoderms. We regard this as a problematical assumption; the dorsal surface of the skull roof of ZIN PH 1/16 is undoubtedly remodeled and lacks any sutures, but the nature of this condition is impossible to assess using the present sample of specimens (e.g., the involvement of osteoderms in the remodeling of the skull roof; see Vickaryous et al. [2001a]).

Recently, a study of the endocast of *Bissektipelta* was conducted by Alifanov and Saveliev (2019). The quality of the endocast produced during that study appears to reveal subtle surface details, especially in the region of the olfactory bulbs. Overall, the artificial and digital endocasts of *Bissektipelta* are congruent in their structure. Alifanov and Saveliev (2019) described in detail the olfactory complex of *Bissektipelta* and claimed the importance of the olfaction in ankylosaurs, with which we agree. The authors identified a vessel ("vena orbitocerebralis") that is not evident on the digital endocast. Corresponding grooves are present on either side of the endocranial cast of ZIN PH 1/16; they extend from the upper part of the hypophyseal cavity to the olfactory region, just above the canal for CN II. Although the term "orbitocerebral vein" is inappropriate, these structures are most likely vascular.

However, a large number of the anatomical interpretations made by Alifanov and Saveliev (2019), and biological conclusions based on them, are either in error or highly subjective. Most of the cranial nerves were misinterpreted. A small twig that extends anterolaterally was identified as CN 0 (nervus terminalis) in *Bissektipelta* by Alifanov and Saveliev (2019). Overall, the terminal cranial nerve has been observed only in a number of amniotes (Johnston, 1913). CN 0 is a small nerve that leaves the brain at the anteromedial terminus of the cerebral hemisphere; its fibers extend anteriorly (into the nasal cavity), adjacent to the medial fibers of the olfactory nerve (CN I). CN 0 is distributed to the vomeronasal organ or parts of the olfactory sac corresponding to it (Johnston, 1913). Thus, the identification of a twig passing anterolaterally into the orbit on the endocast of *Bissektipelta* as CN 0 is in error. If present, CN 0 was a part of the olfactory complex along with CN I in *Bissektipelta* and other ankylosaurs. Concerning CN 0, Alifanov and Saveliev (2019) stated that other workers "either do not see it or confuse it with blood vessels". On the contrary, the interpretation of this structure as the orbitocerebral vein in dinosaurs is more reliable, as extant birds possess vascular structures in the corresponding region (Witmer et al., 2008; Porter and Witmer, 2016a; see the description of ZIN PH 1/16 above).

The identification of CN III (oculomotor), IV (trochlear), and VI (abducens) by Alifanov and Saveliev (2019) is not congruent with the initial study of Averianov (2002) or with published studies on the brain and endocast structure in birds, crocodylians, and dinosaurs (e.g., Hopson, 1979; Tumanova, 1987; Witmer et al., 2008; and other, more specific accounts). The inference of "low functional weight of visual system" in *Bissektipelta* based upon these anatomical interpretations is misleading. Alifanov and Saveliev (2019) described two separate parts of CN VII; we interpret one of these as a branch of CN VIII. That branch was not visualized due to the resolution of the CT scans but was observed both in ZIN PH 1/16 and ZIN PH 281/16 (see description above). A partial endocast of the vestibular recess was interpreted by Alifanov and Saveliev (2019) as a large but weakly structured ganglion of CN VIII. The authors inferred an undeveloped auditory system and imperfect vestibular system, both of which we do not accept (see discussion of paleobiology below). The presence of a separate branch of CN IX (glossopharyngeal nerve) and combined branches of CN XI (accessory nerve) and XII (hypoglossal nerve) is not supported either by osteological evidence from *Bissektipelta* or the extant phylogenetic bracket approach. It is usually assumed that CN XI is combined with CN X in lower amniotes; for example, the three cranial nerves IX, X, and XI exit the braincase through a single foramen in crocodylians (e.g., Hopson, 1979). CN IX can exit the braincase through a separate foramen in diapsids (e.g., squamates; Willard, 1915; Oelrich, 1956), but there is no such opening in *Bissektipelta*.

Alifanov and Saveliev (2019) described three dorsal projections of the forebrain of *Bissektipelta* and referred to a similar condition in elasmobranchs. We identify these dorsal projections as swellings corresponding to encephalic veins; they probably mark the position of the epiphysis. Dorsal projections (dural peaks) of the endocast are known in most dinosaurs (Hopson, 1979; Witmer et al., 2008), and the presence of epiphysis-like protuberances was discussed for a number of ankylosaurs

(e.g., Coombs, 1978b; Pereda-Suberbiola and Galton, 1994; Miyashita et al., 2011; Burns, 2015; Leahey et al., 2015).

Throughout their study, Alifanov and Saveliev (2019) claim that *Bissektipelta* has an archaic and in many ways primitive brain structure. However, their inferences concerning primitive and derived features lack an explicit phylogenetic framework, both in terms of comparison among ankylosaurs or vertebrates as a whole. The authors refer to the anatomy of elasmobranchs several times but did not compare *Bissektipelta* with crocodylians, birds, or squamates, which constitute the proximal phylogenetic bracket for dinosaurs. Thus, despite the good-quality endocast and some useful observations and conclusions, the work of Alifanov and Saveliev (2019) on the endocast of *Bissektipelta* is problematic in many ways.

Distribution of braincase characters in Ankylosauria

The braincase structure of dinosaurs is poorly studied in terms of relevant characters for phylogenetic analyses. Ankylosaurian braincases and endocasts have been studied and compared to each other by a number of authors (Maryańska, 1977; Coombs, 1978a; Kurzanov and Tumanova, 1978; Tumanova, 1987; Pereda-Suberbiola and Galton, 1994; Lee, 1996; Norman and Faiers, 1996; Carpenter et al., 2001; Averianov, 2002; Vickaryous et al., 2004; Parsons and Parsons, 2009; Miyashita et al., 2011; Ösi et al., 2014; Leahey et al., 2015; Kinneer et al., 2016; Paulina-Carabajal et al., 2016, 2018). Paulina-Carabajal et al. (2018) recently concluded that the braincase structure of ankylosaurs is highly conservative and showing little variability, although it may be informative regarding deeper evolutionary relationships among Ankylosauria (Burns, 2015). The number of characters that concern features of the braincase is comparatively low (e.g., 11 out of 177 characters in Arbour and Currie [2016]), and scores for these characters appear to be controversial. This limits the ability to assess the taxonomic attribution, phylogenetic position and affinities of taxa represented by isolated braincase material (e.g., "*Amtosaurus*" and *Bissektipelta*; Parish and Barrett, 2004). Here we comment in detail on the updated taxon-character matrix with a broader sampling of braincase features that was used in the present study. We discuss new characters added to the dataset, modifications made to previous character descriptions, and character optimizations. This allows assessment of the distribution of the braincase features within Ankylosauria and hypothesizing diagnostic characters for different subclades within that group. Some of the characters discussed here were not included in the current matrix because they either have poor sampling and would hamper the resolution of the consensus tree or were considered of little taxonomical utility.

Otoccipital contribution to the occipital condyle (character 73). There is a notable inconsistency in the literature regarding this character. Sereno (1999) provided the following scores for the character 82 "Occipital condyle, composition: basioccipital and exoccipitals (0); basioccipital only (1)": 0 — for *Gargoyleosaurus*, *Shamosaurus*, *Minmi* (= *Kunbarrasaurus* sensu Leahey et al., 2015), *Gastonia*, and *Pinacosaurus*; 1 — for *Pawpawsaurus*, other nodosaurines, other Ankylosaurines. Citing Sereno's assessment, Averianov (2002) concluded that "derived nodosaurids and ankylosaurids independently acquired an occipital condyle composed entirely of the basioccipital", and that was referred to by Vickaryous et al. (2004). A large number of ankylosaur taxa is currently scored as having the occipital condyle composed solely from the basioccipital (Vickaryous et al., 2001b; Arbour and Currie, 2016; Arbour and Evans, 2017; Zheng et al., 2018). On the contrary, Thompson et al. (2012) coded only nodosaurids as having the derived state "1".

Participation of the otoccipitals in dorsolateral corners of the occipital condyle appears to be the basal condition for Ankylosauria (state 0). This feature is documented in the outgroup taxon *Lesothosaurus* from the Early Jurassic of Africa (a small contribution was noted by Porro et al., 2015), as well as in the basal thyreophorans *Scelidosaurus* and *Emausaurus* from the Early Jurassic of Europe (Owen, 1861; Haubold, 1990). Among stegosaurs, this character state has been documented at least for some specimens of *Stegosaurus* (Gilmore, 1914), and *Huayangosaurus* appears to have an otoccipital contribution to the condyle based on published reconstructions (Sereno and Dong, 1992). *Tianchiasaurus nedegoapeferima*, a putative primitive ankylosaur from the Middle Jurassic of China, and *Kunbarrasaurus ieversi* from the Lower Cretaceous of Australia both have the primitive state of a composite condyle (Dong, 1993; Leahey et al., 2015).

In *Gastonia* (Kinneer et al., 2016) and *Gargoyleosaurus* (Kilbourne and Carpenter, 2005), an otoccipital contribution has been documented. In the nodosaurids *Sauropelta* (Ostrom, 1970; Carpenter and Kirkland, 1998; Parsons and Parsons, 2009: Figs. 11B, 14B; Paulina-Carabajal et al., 2018), *Pawpawsaurus* (Lee, 1996), *Silvisaurus* (Eaton, 1960), *Europelta* (Kirkland et al., 2013), *Struthiosaurus* (Pereda-Suberbiola and Galton, 1994), and *Hungarosaurus* (Ösi et al., 2014), it was explicitly stated that the condyle is composed only of the basioccipital. This is a derived condition that appears to be also present in other nodosaurids (e.g., *Edmontonia*, Russell, 1940; Carpenter and Breithaupt, 1986; *Panoplosaurus*, Burns, 2015: Figs. 4.36, 4.47; Paulina-Carabajal et al., 2018: Fig. 9B, C; *Denversaurus*, Burns, 2015). This feature was used to diagnose Nodosauridae (Carpenter, 2001). The problem with assessing this character state in known nodosaurid specimens is the absence of clear

sutures between bones due to complete co-ossification (Eaton, 1960; Pereda-Suberbiola and Galton, 1994; Kirkland et al., 2013; Ösi et al., 2014). Probable OTO-BO boundaries were indicated for *Silvisaurus* (Eaton, 1960), *Pawpawsaurus* (Lee, 1996), *Edmontonia* (Russell, 1940), and *Tatankacephalus* (Parsons and Parsons, 2009) as extending from the ventrolateral margin of the foramen magnum, just above the condyle. It was claimed that neurovascular foramina (MF and CN XII) occur along the line of the OTO-BO suture (Russell, 1940; Lee, 1996; Parsons and Parsons, 2009). That may be indeed apomorphic for nodosaurids; however, our study of ZIN PH 281/16 indicates that at least in ankylosaurids, MF and foramina for CN XII are enclosed mainly by the otoccipital and lack a basioccipital contribution ventrally. A nicely preserved cranium referred to *Denversaurus* (Burns, 2015: Fig. 5.1) shows ventrolateral protuberances of the otoccipitals at the contact with the basioccipital. It appears that the otoccipitals may have participated in the dorsolateral corners of the occipital condyle; this may be the case for other nodosaurids as well. However, the participation of the otoccipitals is less than in ankylosaurids and almost negligible.

The otoccipital contribution was previously scored as present for *Shamosaurus* (Sereno, 1999; Thompson et al., 2012; Arbour and Currie, 2016) and *Gobisaurus* (Thompson et al., 2012; Arbour and Currie, 2016) and absent for *Cedarpelta* (Arbour and Currie, 2016). However, the basis for this is not entirely clear. Neither the original description of *Shamosaurus* (Tumanova, 1983) nor subsequent revisions (Tumanova, 1987, 2012) reported or illustrated the OTO-BO suture on the condyle. Similarly, this feature was not explicitly mentioned and coded as unknown in the original description of *Gobisaurus* (Vickaryous et al., 2001b) and for *Cedarpelta* (Carpenter et al., 2001). We revised corresponding character states for these taxa in our dataset as unknown.

The otoccipitals clearly contribute to dorsolateral corners of the condyle in *Bissektipelta*, *Pinacosaurus* (Maryańska, 1977), *Tarchia* (Paulina-Carabajal et al., 2018), *Ankylosaurus* (Carpenter, 2004), and probably *Euoplocephalus* and *Scolosaurus* (Penkalski, 2018). We revised the corresponding character states (see Supplementary File 1). Other ankylosaurines were described and coded as having the occipital condyle composed entirely of the basioccipital (e.g., *Saichania*, Maryańska, 1977; *Zaraapelta*, Arbour et al., 2014; *Zuul*, Arbour and Evans, 2017). This may merely reflect complete obliteration of sutures; we did not change the corresponding character states in our dataset. Given that *Ankylosaurus, Tarchia,* and some specimens of *Euoplocephalus* and *Scolosaurus* have compound condyles, as do basal ankylosaurines (*Bissektipelta*, *Pinacosaurus*), we posit that ankylosaurids inherited the plesiomorphic character

state present in the outgroups and in basal ankylosaurs. A great disparity, especially between closely related taxa previously referred to *Euoplocephalus* (e.g., *Anodontosaurus*, *Scolosaurus*; Arbour and Currie, 2013a; Penkalski, 2018), appears to be doubtful. Derived Asian ankylosaurids (e.g., *Saichania*, *Talarurus*) may have independently acquired a condyle solely formed by the basioccipital, but this should be verified.

We conclude that basal thyreophorans, basal ankylosaurs (*Kunbarrasaurus*), "polacanthines" (*Gastonia*, *Gargoyleosaurus*), certain basal (*Bissektipelta*, *Pinacosaurus*) and derived (*Ankylosaurus*, *Tarchia*, *Euoplocephalus*) ankylosaurines share a compound condyle with otoccipitals forming one third to a quarter of it. Character states for other ankylosaurids should be verified on the original specimens. Nodosaurids appear to have the derived character state of a condyle composed only or mostly of the basioccipital, but this should be checked against the material with the preserved sutures.

Shape and orientation of the occipital condyle (character 184). The shape (spherical/rounded versus crescentic/reniform/oval), the presence of a neck, and the orientation of the occipital condyle were traditionally used to define ankylosaurs and their subclades. Nodosaurids are frequently diagnosed by a spherical condyle, which is offset on a short, posteroventrally or ventrally directed neck (Coombs, 1978a; Pereda-Suberbiola and Galton, 1994; Carpenter, 2001; Hill et al., 2003). Crescent-shaped or reniform condyles were considered characteristic of ankylosaurids (Coombs, 1978a; Averianov, 2002; Vickaryous et al., 2004).

We have added character 184 ("Basioccipital condyle: (0) reniform or oval, with a constricted neck; (1) spherical/rounded; (2) reniform or oval, without a constricted neck") to our dataset to assess distribution of this feature in Ankylosauria. It is broadly similar to character 35 in Vickaryous et al. (2001b) and character 29 in Hill et al. (2003), with an addition of the primitive state "0" observed in the outgroup taxon *Lesothosaurus* (Porro et al., 2015). Optimization of the character on strict consensus trees shows that the spherical condyle appears to be diagnostic and apomorphic for nodosaurids. The reniform/oval condyle is optimized as the basal condition for Ankylosauria, and it is present in *Kunbarrasaurus* (Leahey et al., 2015). Although similarly scored with the rest of ankylosaurids, *Gargoyleosaurus* (Kilbourne and Carpenter, 2005), *Gastonia* (Kinneer et al., 2016), and cf. *Polacanthus* (Norman and Faiers, 1996) possibly share a transversally expanded and dorsoventrally compressed, lip-shaped occipital condyle that is slightly offset posteriorly. Previously, Carpenter (2001) listed "occipital condyles crescent-shaped and set on very short neck" as diagnostic for "polacanthids", and our comparison corroborates this. However, ZIN PH 2329/16 has a similar condition.

Most ankylosaurids have a robust reniform to oval occipital condyle without a defined neck (e.g., Maryańska, 1977; Tumanova, 1987; Carpenter, 2004). This is the case in *Bissektipelta* and was used by Averianov (2002) to support ankylosaurid affinities of this taxon (see also Comparison for differences between specimens). Notably, the basal ankylosaurids *Cedarpelta* (Carpenter et al., 2001) and *Shamosaurus* (Tumanova, 1983) have rounded condyles, although unlike those of nodosaurids. Given that the condyle shape in a particular taxon might be subjectively defined (e.g., *Cedarpelta* — hemispherical in Carpenter et al. [2001] and crescent-shaped in Carpenter et al. [2008]) and reversibly assigned to one or other character state, we suggest to apply formal approaches to shape determination (e.g., geometric morphometrics) instead of a simple descriptive character in future analyses.

We have not formally tested the significance of the condyle orientation with our dataset. It is apparent from the literature and previous analyses that most but not all (e.g., *Cedarpelta*; Carpenter et al., 2001) ankylosaurs have posteroventrally or even ventrally inclined condyles (Maryańska, 1977; Tumanova, 1987; ch. 36 in Vickaryous et al. [2001b]; ch. 32 in Hill et al. [2003]; ch. 61 in Thompson et al. [2012]).

Structure of the ventral surface of the basioccipital. The concave ventral surface of the basioccipital in ankylosaurs may variably possess the basioccipital fenestra and different ridges/depressions, which are probably attachment sites for cervical muscles (Tumanova, 1987). These differences in the structure of the ventral surface of the basioccipital were noted for Asian (Tumanova, 1987) and Laramidian ankylosaurids (Penkalski, 2018) and converted into separate characters in some datasets (e.g., ch. 55 in Thompson et al. [2012]; ch. 13 in Penkalski [2018]). We suggest that the observed differences in the degree of these ridges between ZIN PH 1/16 and 281/16 is likely due to ontogenic or intraspecific variability in *Bissektipelta*; potentially, this is also the case for other ankylosaurs. Additionally, we interpret the basioccipital fenestra as an osteological correlate for a small vein (based on comparison with extant crocodylians; Owen, 1850). Thus, we see little taxonomic utility for these characters at present.

Structure of the basal tubera (character 75). The basal tubera (= basisphenoidal tuberosities of Thompson et al. [2012]; sphenoccipital tubera in Tumanova [1987]) are formed at the junction between the basioccipital and the parabasisphenoid. A character concerning their structure (paired stubs or continuous ridge) is implemented in most phylogenetic datasets of ankylosaurs (character 32 in Vickaryous et al., 2001b; ch. 57 in Thompson et al., 2012; ch. 75 in Arbour and Currie, 2016). Optimization of this character on consensus trees shows that the plesiomorphic condition for Ankylosauria are two rounded rugose stubs projecting ventrally or posteroventrally and separated medially by a depression (e.g., *Kunbarrasaurus*, Leahey et al., 2015; *Gargoyleosaurus* Kilbourne and Carpenter, 2005). In *Gastonia*, the basal tubera are prominent, swollen and elongated (Kinneer et a., 2016). Paired basal tubera are retained in Nodosauria. Whereas they remain stubby and rounded in some nodosaurids (e.g., *Silvisaurus*, Eaton, 1960: Fig. 3; *Tatankacephalus* and *Sauropelta*, Parsons and Parsons, 2009), the basal tubera look more like elongated bulbous convexities in *Pawpawsaurus* and *Panoplosaurus* (Lee, 1996; Paulina-Carabajal et al., 2018: Fig. 9), are flange-like in *Struthiosaurus* and *Hungarosaurus* (Pereda-Suberbiola and Galton, 1994; Ösi et al., 2014), and particularly so in *Niobrarasaurus* (Carpenter and Everhart, 2007). These variations have not been previously discussed, to the best of our knowledge. Further use of geometric morphometric techniques will probably help to evaluate if there is taxonomic significance in basituberal shape variation among nodosaurids. Ankylosaurids (save *Gobiosaurus*, Vickaryous et al., 2001b) appear to have highly modified, transversely continuous, and ridge-like basal tubera.

Relative length of the parabasisphenoid and basioccipital (character 74). This character was found to support a clade *Scelidosaurus* + Eurypoda by Sereno (1990: ch. 12), and has since been included in most datasets for ankylosaurs (ch. 31 in Vickaryous et al. [2001b]; ch. 56 in Thompson et al. [2012]; ch. 74 in Arbour and Currie [2016]). The parabasisphenoid is generally considered relatively short in Ankylosauria (Tumanova, 1987; Vickaryous et al., 2004). *Lesothosaurus* and basal thyreophoran *Emausaurus* share the basal archosaurian condition of longer parabasisphenoids (Haubold, 1990; Porro et al., 2015). Recently, the skull of *Kunbarrasaurus*, a putative basal ankylosaur from the Early Cretaceous of Australia, has been described in detail (Leahey et al., 2015). The PBS-BO suture was found posterior to the basal tubera, which makes the parabasisphenoid longer than the basioccipital (Leahey et al., 2015: Fig. 2D). Currently, this is optimized as independently acquired and autapomorphic for *Kunbarrasaurus*. *Tianzhenosaurus*, an ankylosaurid from the Late Cretaceous of China, was previously scored as having a long parabasisphenoid (Vickaryous et al., 2001b). This is probably incorrect as the parabasisphenoid appears to be longer than the basioccipital in the original drawing but was explicitly reported as a short element in the description (Pang and Cheng, 1998). *Tatankacephalus* was also erroneously coded as having a long parabasisphenoid (Thompson et al., 2012; Arbour and Currie, 2016), whereas the opposite was clearly stated in the original description (Parsons and Parsons, 2009).

Structure of the basipterygoid contact (character 66). This feature was traditionally used to distinguish

nodosaurids and ankylosaurids, the former having a fused basipterygoid joint and the latter displaying a sutural contact between the pterygoid and the basipterygoid process of the parabasisphenoid (Coombs, 1978a; Tumanova, 1987). The feature was included in most taxon-character matrices for ankylosaurs (ch. 30 in Vickaryous et al. [2001b]; ch. 44 in Thompson et al. [2012]; ch. 66 in Arbour and Currie [2016]). We revised scores for this character in our dataset based on published accounts. Optimization of the character on strict consensus trees revealed that an unfused contact between the basipterygoid processes and the pterygoids is the primitive condition for Ankylosauria, present in outgroups, "polacanthines", and most ankylosaurids. Unfortunately, the condition in the putative basal ankylosaur *Kunbarrasaurus* is not clear due to fracturing (Leahey et al., 2015). *Gastonia* and *Gargoyleosaurus* apparently have unfused basipterygoid joints, although the condition is not clear in the latter: Kilbourne and Carpenter (2005) described a short right basipterygoid process as intact but Kinneer et al. (2016) noted that both processes are lacking in *Gargoyleosaurus*.

The derived character state (fused basipterygoid joint) is optimized as a synapomorphy of a less inclusive clade within Nodosauridae comprising *Tatankacephalus*, *Struthiosaurus*, *Pawpawsaurus*, and *Panoplosaurus*. Fusion of the pterygoids and the basipterygoid processes was explicitly described for these taxa (Pereda-Suberbiola and Galton, 1994; Lee, 1996; Parsons and Parsons, 2009) or was observed in the available CT-scan data (*Panoplosaurus* ROM 1215, Witmer and Ridgely, 2008). In *Sauropelta*, the parabasisphenoid "butts closely against the posterior surface of the pterygoid" and is normally concealed by pterygoids (Ostrom, 1970), suggesting a fused basipterygoid joint. However, an isolated braincase referred to *Sauropelta* (Parsons and Parsons, 2009: Figs. 11B, 15B; Paulina-Carabajal et al., 2018: Fig. 9A) has a vestige of the basipterygoid process and was considered to be insufficiently preserved to assess whether the process was fused to the pterygoid (Parsons and Parsons, 2009). In *Europelta*, the basipterygoid joint is concealed by crushed pterygoid fragments (Kirkland et al., 2013). Eaton (1960) suggested slight mobility of the basipterygoid joint in *Silvisaurus*, as "the connection between pterygoids and basisphenoid is not yet firm". This is doubtful based on the current optimization of the character. We coded *Sauropelta*, *Europelta*, *Silvisaurus*, and some other nodosaurid taxa for which we were unable to find an explicitly described state (e.g., *Edmontonia*) as uncertain at the moment.

Several ankylosaurids (e.g., *Shamosaurus*, *Saichania*, *Zaraapelta*) independently acquired a fused basipterygoid joint (Maryańska, 1977; Tumanova, 1983, 1987; Arbour et al., 2014). However, there is some uncertainty in the literature. For example, a fused basipter-ygoid joint was described in *Saichania* by Maryańska (1977). Carpenter et al. (2011) described an additional specimen and referred it to *Saichania*, noting that "the basisphenoid processes contact, but do not fuse with the pterygoids". Later, Arbour and Currie (2013b) provided additional comments on the specimen described by Carpenter et al. (2011): it is not referable to *Saichania*, lacks the skull, and was supplied with the cast of the holotype skull of *Saichania chulsanensis*. We thus score *Saichania* as having fused basipterygoid joint based on the original description by Maryańska (1977). Additionally, the holotype of *Gobisaurus domoculus* has robust processes that are separated from the pterygoid by matrix, and the contact was likely sutural (Vickaryous et al., 2001b). Arbour and Currie (2016) referred an additional specimen (holotype of "*Zhongyuansaurus luoyangensis*" Xu et al., 2007) to *Gobisaurus*. In the latter specimen, the pterygoid base and the basipterygoid process were described as completely fused (Xu et al., 2007), making the condition in *Gobisaurus* uncertain. We score this taxon based on the description by Vickaryous et al. (2001b).

Size of the basipterygoid processes (character 76). The basipterygoid processes are generally considered stout, short, and massive in the majority of ankylosaurs (Maryańska, 1977; Tumanova, 1987; character 58 in Thompson et al. [2012]; ch. 76 in Arbour and Currie [2016]). *Gastonia* from the Early Cretaceous of the United States with two recognized species (*G. burgei* and *G. lorriemcwhinneyae*) is characterized by an unusually elongated basipterygoid processes (Vickaryous et al., 2004; Kinneer et al., 2016). This feature is currently optimized as autapomorphic for *Gastonia*.

Relative position of the basipterygoid processes and basal tubera (character 187). The basipterygoid processes of ankylosaurs appear to be modified and are posteriorly displaced relative to those of basal ornithischians (e.g., *Lesothosaurus*, Porro et al., 2015). We have added a corresponding character to explore distribution of this feature in the phylogenetic context. Presently, the posteriorly displaced basipterygoid processes lying close to the basal tubera are optimized as a derived condition characteristic for Eurypoda (but uncertain in *Huayangosaurus*). The outgroup taxon *Lesothosaurus* and the basal thyreophoran *Emausaurus* show a primitive condition with an anteriorly placed basipterygoid processes (Haubold, 1990; Porro et al., 2015). The condition of *Scelidosaurus* has not yet been clearly described. Nevertheless, there is some detailed variability among ankylosaurs that has not been sampled for the present character. For example, in *Gastonia* (Kinneer et al., 2016) or *Sauropelta* (Paulina-Carabajal et al., 2018: Fig. 9A), the basipterygoid processes and the basal tubera are more broadly spaced than in *Bissektipelta* and other ankylosaurines.

Length of the paroccipital processes (character 186). This feature varies between taxa and was added

as a new character in the current dataset. Most taxa included in the analysis have long paroccipital processes, the length of which is twice the diameter of the foramen magnum or more. The distal tips of the processes are usually bent downwards and hook-like (e.g., Maryańska, 1977; Tumanova, 1987; Lee, 1996; Carpenter, 2004; Parsons and Parsons, 2009). Short paroccipital processes are present in *Bissektipelta* (based on ZIN PH 281/16), *Pinacosaurus* (Maryańska, 1971), *Minotaurasaurus* (Miles and Miles, 2009), *Gargoyleosaurus* (Kilbourne and Carpenter, 2005), and *Gastonia* (Kinneer et al., 2016). The taxonomic significance of this character cannot be assessed with current sampling, but it may be diagnostic for certain subclades. Included in the analysis are the putative "polacanthines" *Gargoyleosaurus* and *Gastonia* and the ankylosaurids *Pinacosaurus* and *Bissektipelta* that share short paroccipital processes and are closely positioned on the phylogenetic trees produced by our analysis and elsewhere (e.g., Carpenter, 2001; Thompson et al., 2012). Short, distally expanded paroccipital processes were recently used to diagnose Polacanthidae (Kinneer et al., 2016). Additionally, the oblique distal margin of the paroccipital process of *Pinacosaurus* (Maryańska, 1971, 1977) appears to be similar to that of ZIN PH 281/16. Both taxa share a relatively straight profile of the process and the absence of the downward bend distally.

Orientation of the paroccipital processes (character 72). This character is included in most recent taxon-character matrices (e.g., ch. 33 of Vickaryous et al. [2001b]; ch. 27 in Hill et al. [2003]; ch. 51 in Thompson et al. [2012]; ch. 72 in Arbour and Currie [2016]). It is generally assumed that ankylosaurids have a derived state of laterally directed paroccipital processes and nodosaurids usually have posterolaterally directed processes (Coombs and Maryańska, 1990). Optimization of this character on consensus trees with our sampling (which is mostly consistent with that of Arbour and Currie, 2016) indicates that the North American clade Panoplosaurinae (sensu Burns, 2015) apparently independently acquired the derived state of laterally projecting paroccipital processes. This variability was previously observed among nodosaurids (e.g., Pereda-Suberbiola and Galton, 1994).

Contacts between the paroccipital process (POP), quadrate (Q), and skull roof (sutural/articulation-like or fused; character 63). Coombs (1978a) implies a notable taxonomical significance for this character in distinguishing the traditional families Ankylosauridae and Nodosauridae: members of the former usually have an articular or sutural contact, whereas the paroccipital process, quadrate, and the skull roof are indistinguishably fused in the latter. This character is included in some character-taxon matrices for Ankylosauria, including that used in the present study. Several

ankylosaurids from the Cretaceous of Asia — *Shamosaurus*, *Crichtonpelta*, *Saichania*, and *Tarchia kielanae* — are important exceptions with a fused POP-Q contact (Maryańska, 1977; Tumanova, 1987; Lü et al., 2007; Carpenter et al., 2011; Penkalski and Tumanova, 2017; Yang et al., 2017). Interestingly, a second, recently named species of *Tarchia*, *T. teresae*, has a POP-Q contact typical for ankylosaurids (Penkalski and Tumanova, 2017). Tumanova (1987) hypothesized that differences in ossification of the palatoquadrate cartilage could account for the observed variation, and thus this feature may not be a reliable diagnostic character for ankylosaurids.

The state of this character is difficult to evaluate in *Bissektipelta*. In the holotype ZIN PH 1/16, only an incomplete right paroccipital process is preserved, and it lacks its distal end. ZIN PH 2329/16 completely lacks the processes. The right paroccipital process is preserved in ZIN PH 281/16 and appears to be complete, although the distal margin shows some breakage and abrasion. Anteriorly, the paroccipital process has a smooth surface suggestive of a possibly loose contact with the quadrate. Loose POP-Q-skull roof joints were reported in a skull of a juvenile *Pinacosaurus* (Maryańska, 1971, 1977), and the condition of ZIN PH 281/16 may also be due to ontogeny.

Development of the postocular shelf (character 42). The postocular shelf is a transverse wall between the orbit and the adductor cavity that is formed by the jugal, postorbital, laterosphenoid, and possibly the frontal (Maryańska, 1977; Vickaryous et al., 2004). Sereno (1990, ch. 104) found the presence of the postocular shelf as a synapomorphy for Ankylosaurinae. Vickaryous et al. (2004) considered this state as ambiguously diagnostic for Ankylosauridae, and Thompson et al. (2012, ch. 15) — as an ambiguous synapomorphy of Ankylosauria. Our current sampling reveals results similar to those of Thompson et al. (2012); optimization of this character state indicates that it is diagnostic for Ankylosauria. The putative basal ankylosaur *Kunbarrasaurus* has a postocular shelf that partially separates the orbital and adductor cavities (Leahey et al., 2015).

Previously, variability in the contact between the postocular shelf and the lateral wall of the braincase was reported. For example, *Pinacosaurus* has a loose contact, whereas the shelf is fused to the braincase in *Saichania* and *Tarchia* (Maryańska, 1977). Similar variation is reported here for the larger specimens of *Bissektipelta* (ZIN PH 1/16 and ZIN PH 2329/16) and the smaller ZIN PH 281/16. We interpret these differences as ontogenetic in nature and of little taxonomic utility.

Presence of the posttemporal fenestrae. Generally, ankylosaurs lack posttemporal fenestrae. Slit-like posttemporal fenestrae were noted for *Pinacosaurus* (Maryańska, 1971; Tumanova, 1987). We report the posttemporal fenestrae in *Bissektipelta*. The posttempo-

ral fenestrae in ZIN PH 1/16 are rounded and appear to lie at the junction of the paroccipital processes, parietals, and the supraoccipital. However, there are notable differences between ZIN PH 1/16 and ZIN PH 281/16 in this feature (see comparison above). Small paired openings in the dorsal region of the occiput have occasionally been described in ankylosaurs (e.g., *Crichtonpelta*, where they were erroneously interpreted as foramina for CN XII by Yang et al. [2017]). Though apparently homologous to the posttemporal fenestrae of other archosaurs, these foramina in ankylosaurs are slit-like vascular remnants enveloped by hyperossified bones of the skull roof, far diverging from the typical diapsid condition.

Number of external foramina for CN II (character 180). As far as we know, this character has only been discussed by Sobral (2014) and has never been previously included in a formal phylogenetic analysis of any ornithischian group. Our sampling indicates that the primitive condition for Ankylosauria is the presence of a single medial foramen for passage of CN II. A single medial foramen for CN II is present in *Kentrosaurus* (Galton, 1988) and *Stegosaurus* (Galton, 2001; Leahey et al., 2015), as well as in the basal ankylosaurid *Kunbarrasaurus* (Leahey et al., 2015). We concur with Leahey et al. (2015) that the condition of *Kunbarrasaurus* is primitive for Ankylosauria. It supports the basal position of this taxon within the clade. All other ankylosaurs share the presence of the derived character state of separate lateral openings for CN II.

Course of CN VI (character 179). This character was previously discussed by Sobral (2014). CN VI entering the hypophyseal cavity was considered the primitive condition for archosaurs in general and dinosaurs in particular. The lateral deviation of the nerve canal with CN VI bypassing the hypophyseal cavity was noted for Ankylosauria and some other archosaurian groups. We have tested this hypothesis by including this character in our dataset. Optimization with our sampling indicates that the lateral course of CN VI appears to be a putative synapomorphy of Ankylosauria that corroborates the results of Sobral (2014). Stegosaurs have the primitive condition (Galton, 1988, 2001; Leahey et al., 2015), and basal thyreophorans (e.g., *Emausaurus*; Haubold, 1990) and the outgroup taxon *Lesothosaurus* (Porro et al., 2015) are currently treated as uncertain. However, character optimization by Sobral (2014) indicates only a single change within Ornithischia (at the base of Ankylosauria), and the lateral deviation of the CN VI course appears to be autapomorphic for Ankylosauria among Ornithischia.

Subdivision of CN V. In extant and probably extinct archosaurs, CN V has a large and complex trunk that ultimately gives off three main branches either extracranially or endocranially. The ophthalmic, maxillary, and mandibular branches diverge from the Gasserian

ganglion (Holliday and Witmer, 2007, 2009). This results in the presence of either a single, sometimes subdivided foramen for CN V on the lateral wall of the braincase or a pair of foramina (because the ophthalmic branch has a different embryonic origin and sometimes leaves the braincase separately from the maxillomandibular trunk; Sobral, 2014). Subdivision of the external foramina for CN V in dinosaurs was discussed by Sobral (2014) and Burns (2015). We have not directly tested the distribution of this feature within Ankylosauria by the inclusion of a corresponding character in the analysis but briefly discuss it a posteriori. Most ankylosaurs have a single large foramen for CN V; thus, the branches apparently split extracranially (e.g., Miyashita et al., 2011). *Bissektipelta* clearly shows a partial subdivision of CN V into branches; a triangular projection of bone partially separates the foramen for CN V_I from that for CN V_{II}+V_{III}. A similar morphology seems to be present in the holotype of *Tarchia kielanae* (Penkalski and Tumanova, 2017: Fig. 2). Two separate foramina are present in the nodosaurid *Denversaurus* (Burns, 2015) and ankylosaurids *Saichania* (Maryańska, 1977) and *Zaraapelta* (Arbour et al., 2014: Fig. 11; the second foramen for CN V is apparently incorrectly labeled as CN VII and the actual foramen for CN VII is located just posteriorly). The condition of *Saichania* and *Zaraapelta* is closely comparable to that of *Bissektipelta* but the wall between two foramina is completely ossified in the two Mongolian taxa. Currently, the character appears to be homoplastic but may prove informative for small subclades such as derived Mongolian ankylosaurines.

Structure of the crista prootica. We have not included this feature in our phylogenetic analysis but provide a brief discussion here. The crista prootica (otosphenoidal crest of some authors) in the general diapsid condition is a curved crest that extends from the basipterygoid process posterodorsally onto the anterior surface of the paroccipital process on either lateral wall of the braincase. This crest separates the foramen for CN V and FO and frequently forms a lamina projecting slightly laterally and covering FO externally to some degree. The crista prootica is much more prominent in theropods and sauropodomorphs compared to most ornithischians. However, more or less prominent crests on the lateral surface of the prootic posterior to the foramen for CN V are present in most ornithischian taxa. The basal ornithischian *Lesothosaurus* has the general diapsid condition of the lateral surface of the prootic with a prominent and lamellar crista prootica (Porro et al., 2015). Most eurypods appear to lack a prominent crista prootica. In stegosaurs (e.g., *Kentrosaurus*, *Stegosaurus*; Galton, 1988, 2001), there is a flattened and rounded crest or crest-like sheet of bone that is more developed in *Stegosaurus* (Galton, 2001: Fig. 5.2D). Most ankylosaurs lack a crest in a corresponding region of the prootic and

instead have a flat or concave sheet of bone between the foramen for CN V and FO (e.g., *Bissektipelta*, *Euoplocephalus*, *Tarchia*, *Talarurus*, *Panoplosaurus*, *Sauropelta*; Miyashita et al., 2011; Paulina-Carabajal et al., 2018). A prominent exception is *Gastonia*; the corresponding part of the braincase of this taxon has a typical diapsid appearance with a distinct crista prootica (Kinneer et al., 2016: Fig. 8A). The nodosaurid *Pawpawsaurus* also has some ridges between the external openings for CN V and CN VII and FO (Paulina-Carabajal et al., 2016: Fig. 3). We tentatively consider the lack of a prominent crista prootica as potentially diagnostic for Eurypoda in general and Ankylosauria in particular. Previously, this feature was used by Pereda-Suberbiola and Galton (1994) to dismiss theropod affinities of the type material of *Struthiosaurus*.

Position of CN VII external foramen (character 178). The variability of distribution of the foramina for CN VII has been for the first time observed and used in a formal phylogenetic analysis of Ankylosauria. A broad survey of archosaurian braincase morphology (Kuzmin, unpubl. data) indicates that a primitive condition for Archosauria generally and Ornithischia specifically is the position of the foramen for CN VII close to the fenestra ovalis, with both structures covered laterally by the lamellar crista prootica. This condition is present in the outgroup taxon *Lesothosaurus diagnosticus* (Porro et al., 2015) and was independently acquired by the "polacanthine" *Gastonia* (Kinneer et al., 2016). Character optimization reveals that stegosaurs (Galton, 1988, 2001) and some nodosaurids (e.g., *Sauropelta*, Fig. 9A in Paulina-Carabajal et al., 2018; *Denversaurus*, Burns, 2015) independently acquired an intermediate condition when the foramen for CN VII is not covered by the crista prootica and lies in between the foramen for CN V and FO. A similar condition is present in cf. *Polacanthus* (Norman and Faiers, 1996), which was not included in the formal analysis. There is some variability between the specimens assigned to *Kentrosaurus*; the foramen for CN VII appears to be between that for CN V and FO in some of them and closer to that for CN V in others (Galton, 1988). Ankylosaurids and certain nodosaurids (e.g., *Silvisaurus*, Eaton, 1960; *Pawpawsaurus*, Paulina-Carabajal et al., 2016) have the foramen for CN VII situated adjacent to the foramen for CN V, with both nerve exits frequently sharing a similar recess. Thus, the position of the foramen for CN VII may be a homoplastic character but appears to be diagnostic for certain subclades within Ankylosauria, e.g., all Ankylosauridae with known braincase structure share closely spaced foramina for CN V and VII, respectively. Overall, in Eurypoda, there is a tendency of anterior displacement of the foramen for CN VII from FO closer to that for CN V.

Number of external foramina for CN VII (character 181). Generally, in dinosaurs and archosaurs, CN VII exits the braincase through a single foramen, although the presence of two separate foramina for the palatine and hyomandibular branches of CN VII is known in some dinosaur taxa (see discussion in Sobral [2014]). Among the taxa sampled here, a single foramen for CN VII is present in the outgroup taxon *Lesothosaurus* (Porro et al., 2015) and in all ankylosaurs. Two separate foramina for branches of CN VII were noted for *Kentrosaurus* (Galton, 1988) and *Stegosaurus* (Galton, 2001; Leahey et al., 2015). We suggest that this feature might represent a new braincase synapomorphy for Stegosauria or some subclades among the latter but the sampling is scant and should be extended.

Composition of the posterior CN foramina and number of foramina for CN XII (characters 77 and 182). Although these characters are treated as separate in the current dataset, we discuss the distribution of the posterior CN foramina as a single feature. Disposition of the foramina for CN IX–XII as several separate openings (state 0) or as a single foramen (state 1) was included in the datasets of Thompson et al. (2012, ch. 59) and Arbour and Currie (2016, ch. 77). There is a great disparity in the literature regarding the interpretation of external foramina in the posterior part of the braincase, both among Ankylosauria in general (Vickaryous et al., 2004; Miyashita et al., 2011, Paulina-Carabajal et al., 2016) and among the Late Cretaceous Mongolian taxa *Saichania*, *Tarchia*, and *Talarurus* (Maryańska, 1977; Tumanova, 1987; Carpenter et al., 2011; Penkalski and Tumanova, 2017; Paulina-Carabajal et al., 2018).

A broad comparison reveals a common pattern of distribution of the braincase foramina. In most taxa except *Gastonia* (Kinneer et al., 2017), the foramen for CN VII lies adjacent to that for CN V. A flattened strip of bone (crista prootica) extends from the basal tubera ventrally to the paroccipital process dorsally. The crista prootica separates two more or less defined clusters of neurovascular foramina, and here we discuss the posterior cluster — the fenestra ovalis (FO), the metotic foramen (MF), and the foramina for CN XII. Following Gower and Weber (1998) and Sobral et al. (2012), we suggest avoiding the terms "jugular vein" and "jugular foramen". It appears that ankylosaurs plesiomorphically share an undivided MF that was traversed by CN IX–XI, the perilymphatic duct, and probably the posterior cerebral vein. The rest of the posterior CN foramina are more reliably interpreted as for CN XII based on the available comparative data and phylogenetic framework.

Even the most derived Late Cretaceous Mongolian ankylosaurines (*Tarchia*, *Saichania*, *Talarurus*, *Zaraapelta*) follow the aforementioned pattern. Recently, Paulina-Carabajal et al. (2018) described in detail the braincases of two of these taxa (*Tarchia teresae* and *Talarurus plicatospineus*) and presented interpretations similar to those that we further discuss here. Comparing

the published data and images of the lateral surface of the braincase, one can observe a uniform general picture: posterior to the crista prootica, there is a small, frequently questionable or unnoticed foramen followed by a single large and sometimes clearly subdivided opening with an addition of a small foramen posteriorly (*Tarchia*: Penkalski and Tumanova, 2017: Fig. 2, Paulina-Carabajal et al., 2018: Fig. 6; *Talarurus*: Paulina-Carabajal et al., 2018: Fig. 4; *Saichania*: Maryańska, 1977: Fig. 7, the anterior smallest foramen is not drawn, but it is nevertheless cited by Carpenter et al., 2011: Fig. 8; *Zaraapelta*: Arbour et al., 2014: Fig. 11). The anteriormost and the smallest foramen in question is best interpreted as FO. Although its connection to the inner ear cavity could not be undoubtedly demonstrated even with the aid of CT scanning, the position of this small opening directly corresponds to FO in, for example, *Tarchia teresae* (Paulina-Carabajal et al., 2018: Fig. 8; the foramen in question appears posterodorsal to the endosseous cochlear duct = lagena and ventral to the remnants of the semicircular canals). Posterior to FO, a large, sometimes subdivided recess likely contains separate CN foramina internally and broadly corresponds to MF. This was best shown by Paulina-Carabajal et al. (2018) and, in part, by Penkalski and Tumanova (2017) for *Tarchia* spp. The anterior foramen within the recess is here interpreted as the passage of the perilymphatic duct from the inner ear recess. In *Bissektipelta*, the perilymphatic duct apparently extended from the inner ear recess into the ventral part of MF and notched the endocranial wall, following the primitive diapsid pattern (Gower and Weber, 1998; Sobral et al., 2016). The small foramen within a recess in *Tarchia teresae* is in a comparable position and appears to be anteromedially directed (Paulina-Carabajal et al., 2018). Whereas this hypothesis is hard to assess at present (as the CT scanning of *Tarchia teresae* failed to show this passage extending into the inner ear recess/endocranial cavity), it appears like the most reasonable inference, and logically corroborates the interpretation of this foramen as connected to the inner ear by Paulina-Carabajal et al. (2018). The dorsal foramen within the recess corresponds to the passage of CN IX–XI and likely the posterior cerebral vein. The posteroventral foramen corresponds to a separate opening for CN XII, as was shown by Penkalski and Tumanova (2017) and Paulina-Carabajal et al. (2018). The holotype of *Tarchia teresae* diverges from this pattern (Penkalski and Tumanova, 2017: Fig. 6) but there appears to be some matrix in the area of these small foramina, and the specimen should be reassessed with the aid of CT scanning.

We hypothesize that the small size of FO and the enclosure and subdivision of several separate openings (MF and CN XII) within a single recess are due to extensive ossification of the lateral wall of the braincase in adults of these Mongolian taxa. It appears to be diag-

nostic, but in light of the above discussion, we propose to update character 59 from Thompson et al. (2012) and character 77 from Arbour and Currie (2016) and subsequent analyses. Instead of "Form of the cranial nerve foramina IX–XII: separate foramina (0), single foramen shared with the jugular vein (1)", we propose following wording: "Fenestra ovalis and posterior neurovascular foramina of the braincase: nearly equal in size and subdivided into 4 or 5 separate openings (0), fenestra ovalis reduced in size, other foramina tend to coalesce, no more than 3 separate openings (1)". The derived state currently is optimized as a putative synapomorphy of *Saichania*, *Tarchia*, *Zaraapelta*, and probably *Talarurus*.

Considering the number of openings for CN XII, we suggest avoidance of the count of external foramina as a reliable character due to intraspecific variability and a tendency of separate roots of CN XII to converge laterally (see the description of ZIN PH 281/16 above; Paulina-Carabajal et al., 2018). The number of internal foramina (= roots) of CN XII is variable among Ankylosauria and was formally assessed by inclusion of a corresponding character in the present phylogenetic analysis. We discriminate between the presence of one or two foramina for CN XII as a primitive character state and three foramina as a derived character state (ch. 182). Our review of the literature on the braincases of Ornithischia indicates that the presence of three internal foramina for CN XII is not a common character state for the group and is potentially diagnostic (e.g., Norman and Faiers, 1996). Currently, it is optimized that a derived character state was independently acquired by the putative basal ankylosaur *Kunbarrasaurus* (Leahey et al., 2015) and some derived ankylosaurines (e.g., *Bissektipelta*, *Talarurus*, *Tarchia*, some specimens of *Euoplocephalus* sensu lato; Coombs, 1978b; Miyashita et al., 2011; Penkalski, 2018; Paulina-Carabajal et al., 2018). Miyashita et al. (2011) and Penkalsi (2018) noted the variability of foramina for CN XII number between the closely related ankylosaurines (*Euoplocephalus* sensu lato) from the Late Cretaceous of North America. The latter implies caution, but currently, three internal foramina for CN XII appear to be diagnostic for a derived subclade within Ankylosaurinae.

Structure of the endocast (character 185). The variability of endocranial morphology in ankylosaurs was recently discussed in Paulina-Carabajal et al. (2018). The authors concluded that nodosaurids tend to have a stronger flexed, sigmoidal endocast with a ventrally convex region corresponding to the medulla oblongata; ankylosaurids, on the other hand, have a straighter endocast with a flat medulla oblongata (Tumanova, 1987; Paulina-Carabajal et al., 2018). We have included this feature in our dataset. Previously, Thompson et al. (2012) included a similar character in their analysis (ch. 60, "Degree of endocranial flexure: strong (0); weak (1)").

Optimization of the character with current sampling corroborated previous results and indicates that a more flexed endocast with a ventrally convex medulla oblongata is a basal condition for Ankylosauria (e.g., *Kunbarrasaurus*, Leahey et al., 2015), and it was retained and became even more strongly pronounced in Nodosauridae (e.g., *Struthiosaurus*, Pereda-Suberbiola and Galton, 1994; *Hungarosaurus*, Ösi et al., 2014; *Pawpawsaurus*, Paulina-Carabajal et al., 2016) and "polacanthines" (cf. *Polacanthus*, Norman and Faiers, 1996; *Gastonia*, Kinneer et al., 2016). Ankylosaurids share a derived condition of a lesser endocast flexure and ventrally flat region of the medulla oblongata (*Cedarpelta*, Carpenter et al., 2001; *Euoplocephalus*, Miyashita et al., 2011; *Talarurus* and *Tarchia*, Paulina-Carabajal et al., 2018). However, we suggest using a formal geometric morphometric approach to assess differences in the endocranial morphology of ankylosaurs more quantitavely.

Projection of the hypophyseal (pituitary) endocast (character 189). Leahey et al. (2015) and Paulina-Carabajal et al. (2018) discussed that most ankylosaurs (and even maybe eurypods) except *Kunbarrasaurus* have a pituitary that projects more or less directly ventrally from the endocast. Additionally, the canal for the cerebral carotid artery opens into the ventral terminus of the hypophyseal cavity in these taxa. We have incorporated the angle of the pituitary endocast as a discrete character in our dataset. Character optimization indicates that a ventrally projecting pituitary endocast may indeed represent an endocranial synapomorphy of Eurypoda, although sampling is poor in outgroup taxa (known only in *Stegosaurus* and *Kentrosaurus*). There is variability in the pituitary inclination between the endocasts of *Kentrosaurus* (Galton, 1988). The structure of the basisphenoid is known for *Lesothosaurus* (Porro et al., 2015) and *Emausaurus* (Haubold, 1990), but the angle of the pituitary inclination was not precisely stated. Ventrally projecting pituitary endocasts appear to be diagnostic for ankylosaurs, but endocasts of some taxa have a slightly anteroventrally (e.g., *Struthiosaurus austriacus*, Pereda-Suberbiola and Galton, 1994) or posteroventrally (cf. *Polacanthus*, Norman and Faiers, 1996) deflected cast of the hypophyseal cavity. The condition in *Kunbarrasaurus* (strongly posteroventrally projecting pituitary with the cerebral carotid merging at half the pituitary depth; Leahey et al., 2015) is currently optimized as autapomorphic.

Divergence of olfactory bulbs (character 188). Short divergent olfactory bulbs are known for Triassic pseudosuchians and for pachycephalosaurs and ankylosaurs among dinosaurs (Hopson, 1979). We have included this character in our formal phylogenetic analysis. Character optimization indicates that divergent olfactory bulbs are synapomorphic for most ankylosaur taxa more derived than *Kunbarrasaurus* (not known

in *Hylaeosaurus* and the 'Paw Paw scuteling'). This corroborates the initial statement by Leahey et al. (2015) that *Kunbarrasaurus* has a primitive condition (medially contacting olfactory bulbs) present in stegosaurs (Galton, 1988, 2001) and, indeed, most other ornithischians.

Presence of the flocculus (character 183). The flocculus is a part of the cerebellum that plays a role in vestibular-ocular reflex and gaze stabilization (e.g., Paulina-Carabajal et al., 2016). Recently, Paulina-Carabajal et al. (2018) hypothesized that a flocculus is present in the cranial endocast of ankylosaurids, as it was observed in *Euoplocephalus* sensu lato (Hopson, 1979; Miyashita et al., 2011), *Tarchia*, and *Talarurus* (Paulina-Carabajal et al., 2018), but not in any nodosaurid so far. We tested this hypothesis by the inclusion of a corresponding character (presence/absence of the flocculus) in our character-taxon matrix. Optimization of the character on the strict consensus trees revealed that the presence of the flocculus is diagnostic for a less inclusive subclade within Ankylosaurinae that comprises *Tarchia* and *Ankylosaurus* and derived taxa closely related to them. Thus, this feature has a more limited distribution than previously hypothesized by Paulina-Carabajal et al. (2018).

Ossification of the medial wall of the otic capsule. We have not used this character in the final character-taxon matrix but briefly disscuss it here (see also Sobral, 2014). A number of ankylosaurian taxa, ranging from relatively basal ones (e.g., *Kunbarrasaurus*, *Polacanthus*, *Gastonia*) to derived representatives (*Bissektipelta*, *Euoplocephalus* sensu lato, *Panoplosaurus*, *Pawpawsaurus*, *Pinacosaurus*, *Silvisaurus*, *Talarurus*), have an incompletely ossified medial wall of the otic capsule (Eaton, 1960; Tumanova, 1987; Hill et al., 2003; Leahey et al., 2015; Kinneer et al., 2016; our observations of the available CT data of ankylosaur skulls from the works of Witmer and Ridgely, 2008 and Paulina-Carabajal et al., 2016). The incompletely ossified wall of the otic capsule was observed in *Stegosaurus* (Hill et al., 2003) and *Kentrosaurus* (Galton, 1988). The condition in more basal taxa has not yet been explicitly described. *Lesothosaurus* may have a medially unossified otic capsule (Porro et al., 2015: Fig. 9B). It appears that an incompletely ossified wall of the otic capsule is a common feature present in ankylosaurs and stegosaurs, and it might be plesiomorphic for Ornithischia as a whole (Sobral, 2014; Kuzmin, unpubl. data), but currently sampling is scarce at the base of the clade.

Final comments. We conclude that the braincase structure of ankylosaurs is more variable in terms of character evolution than was previously supposed. Though not all the braincase characters have a straightforward distribution, and some are likely homoplastic, there are features that diagnose certain subclades among Ankylosauria (Figs. 18–21).
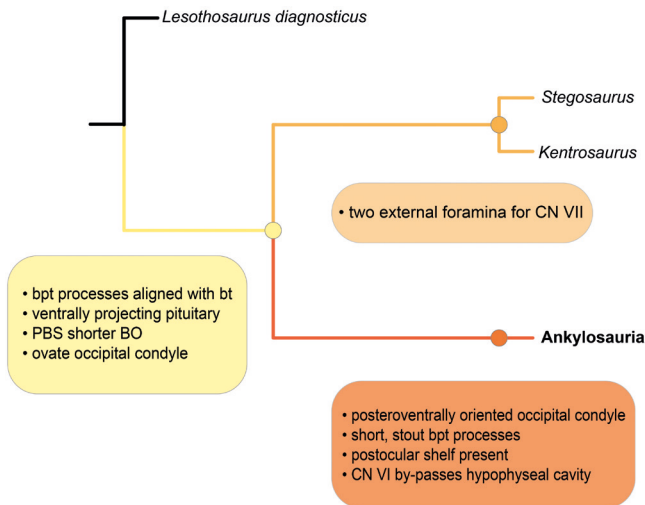
Fig. 18. Simplified phylogenetic hypothesis for *Lesothosaurus* and Eurypoda (Stegosauria plus Ankylosauria). Hypothesized braincase synapomorphies for Eurypoda in yellow, for Stegosauria — in pale orange, for Ankylosauria — in bright orange. Abbreviations: BO, basi-occipital; bpt, basipterygoid; bt, basal tuber; CN VI, abducens nerve; CN VII, facial nerve; PBS, parabasisphenoid.

Fig. 19. Simplified phylogenetic hypothesis for basal ankylosaurs and the Ankylosauridae/Nodosauridae split. Hypothesized braincase synapomorphies for all Ankylosauria except *Kunbarrasaurus* in pale red, for Ankylosauridae — in purple, for Nodosauridae — in blue. Common braincase characters for "polacanthines" in brown. Abbreviations: BO, basioccipital; bpt, basipterygoid; bt, basal tuber; CN II, optic nerve; CN V, trigeminal nerve; CN VII, facial nerve; FO, fenestra ovalis; PBS, parabasisphenoid; POP, paroccipital process; Q, quadrate; SQ, squamosal.

Fig. 20. Simplified phylogenetic hypothesis for Nodosauridae sensu stricto (the clade found in both strict consensus topologies in the present work). Hypothesized braincase synapomorphy for the Late Cretaceous clade from North America in pale-blue. A common braincase character for *Hungarosaurus* and *Struthiosaurus* in green. Abbreviations: bt, basal tuber; POP, paroccipital process.
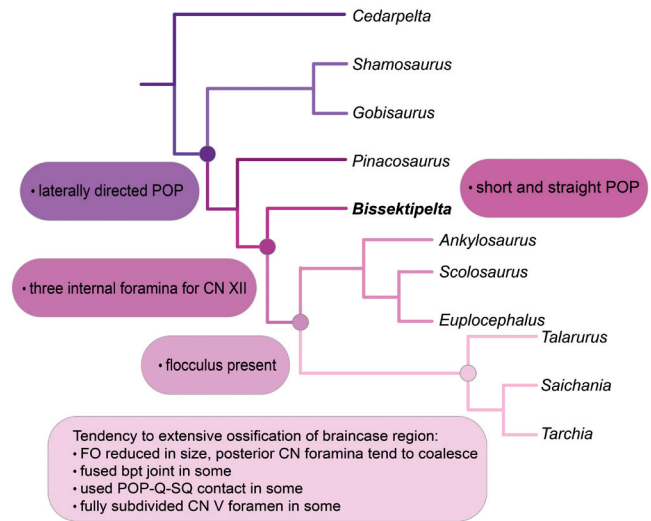
Fig. 21. Simplified phylogenetic hypothesis for Ankylosauridae sensu stricto (the clade found in both strict consensus topologies in the present work). Hypothesized braincase synapomorphies for Shamosaurinae + Ankylosaurinae in purple, for *Bissektipelta* plus derived ankylosaurins — in pale purple, for derived Ankylosaurinae — in pink; for derived Mongolian ankylosaurins — in pale pink. A common braincase feature for *Pinacosaurus* and *Bissektipelta* in dark pink. Abbreviations: bpt, basipterygoid; CN, cranial nerve; CN V, trigeminal nerve; CN XII, hypoglossal nerve; FO, fenestra ovalis; POP, paroccipital process; Q, quadrate; SQ, squamosal.

Reconstruction of the cephalic vasculature in Bissektipelta *and its implications for vascular anatomy in ankylosaurs*

Earlier researchers occasionally pointed out vascular features of the skull and the braincase of ankylosaurs in specimen descriptions (Maryańska, 1977; Kurzanov and Tumanova, 1978; Norman and Faiers, 1996; Ave-rianov, 2002) or surveyed the arterial system by comparison with squamates (Tumanova, 1987); however, the precise identification of particular vessels was not explicitly justified. A remarkable improvement in sampling and interpretation of dinosaur vascular anatomy was recently achieved with the advent of the Extant Phylogenetic Bracket (EPB) approach (Witmer, 1995), thor-

ough study of the cephalic vascular patterns in a range of extant diapsids (Sedlmayr, 2002; Porter and Witmer, 2015, 2016; Porter et al., 2016), and CT-scanning and 3D-imaging technics (Witmer et al., 2008; Miyashita et al., 2011; Leahey et al., 2015; Paulina-Carabajal et al., 2016). A synopsis of current knowledge of dinosaur vascular anatomy (Porter, 2015) presents plausible reconstructions of major head vessels and their intercommunications in various dinosaurian taxa (including *Euoplocephalus*) based on the EPB approach and extensive surveys of closely related extant taxa. Despite the extensive research, the detailed pattern of the blood vessels in the braincase region of ankylosaurs has never been reconstructed in as much detail as is possible for *Bissektipelta*. Here we discuss major vessels that were external to the lateral wall of the braincase. The internal vascular system of the braincase of *Bissektipelta* has already been described in detail above (see Figs. 6–9).

Arteries. The elements of the arterial system of *Bissektipelta* restored directly from relevant osteological correlates include the cerebral carotid, sphenopalatine, temporoorbital/occipital, and supraorbital arteries (see Fig. 8). The ramification of the common carotid artery, a major blood supplier of the head, and the course of its branch, the internal carotid artery, along the basitubera is not reflected by any obvious osteological features in *Bissektipelta* (see Porter [2015] for the discussion of the condition in dinosaurs). However, its course is particularly consistent among diapsids, with the internal carotid extending lateral to the basitubera on either side (Walker, 1990; Sedlmayr, 2002; Porter, 2015). Additionally, in *Talarurus*, there is a groove ventral to the cerebral carotid foramen, along the parabasisphenoid-basioccipital contact, that presumably reflects the course of the internal carotid artery (Paulina-Carabajal et al., 2018).

The bifurcation of the internal carotid artery into the cerebral carotid and stapedial arteries is a consistent feature among diapsids (Shindo, 1914; O'Donoghue, 1920; Walker, 1990; Sedlmayr, 2002; Porter, 2015). Generally in diapsids, the stapedial artery branches off at the level of CN X and courses medial to the middle ear epithelium (O'Donoghue, 1920; Walker, 1990; Porter, 2015). The only possible evidence of the stapedial artery course in *Bissektipelta* is a wide, dorsoventrally oriented groove at the contact between the basioccipital, parabasisphenoid, and prootic in the holotype and on the left side of ZIN PH 2329/16. The diameter of the cerebral carotid foramen and the width of the groove are congruent, large (comparable to the size of the opening for CN II and the metotic foramen) and uniform throughout the course. The groove extends over the crista prootica (= otosphenoid crest of some authors), the posterior portion of which is sometimes considered a relevant osteological correlate for the course of the stapedial artery (Sampson and Witmer, 2007). In that case, the

stapedial artery in *Bissektipelta* would have passed onto the ventromedial aspect of the paroccipital process (the common diapsid condition) in a rather unconventional way — anterior to the fenestra ovalis, the metotic foramen, and, hence, CN X. Thus, there are two alternative hypotheses: the stapedial artery branched off of the internal carotid more posteriorly and arched over the fenestra ovalis onto the medial aspect of the paroccipital process in a more general diapsid condition but leaving no osteological correlates, or that the vessel's course was modified in *Bissektipelta* (Fig. 22). A similar arrangement of ridges and grooves at the basituberal region and the relatively posterior position of the FO+MF complex in several other taxa (e.g., *Euoplocephalus*, *Talarurus*, *Tarchia*; Miyashita et al., 2011; Paulina-Carabajal et al., 2018) suggest that the modified route of the stapedial artery anterior to FO might have been shared by ankylosaurids.

In either studied specimen of *Bissektipelta*, the stapedial artery and its main branches (temporoorbital and mandibular arteries) left no distinct osteological correlates along their course through the supratemporal fossa (aST, aTO, aMan in Fig. 8). This is likely because these vessels passed through the supratemporal fossa between portions of the temporal muscles (medial to the external adductor muscles and lateral to the pseudotemporalis superficialis muscle), as in extant lepidosaurs and birds but unlike crocodylians (Holliday et al., 2019). Based on the comparison with the extant lepidosaurs and birds, we can hypothesize that the mandibular and occipital arteries branched off of the stapedial artery along its route through the supratemporal fossa (aMan and aOc, Fig. 8). The occipital artery is a branch of the temporoorbital artery that supplies the cervical musculature in extant lepidosaurs (O'Donoghue, 1920; Porter and Witmer, 2015) and birds (e.g., *Struthio camelus,* OUVC 10519, https://people.ohio.edu/witmerl/3D_ostrich.htm; external occipital artery in Sedlmayr [2002]), but it is absent in modern-day crocodylians (Sedlmayr, 2002). If it was present in *Bissektipelta*, it could have traversed the posttemporal fenestra along with the transversooccipital and the dorsal head veins or more laterally to that (Fig. 8).

An obvious groove ventral to the capitate process of ZIN PH 281/16 (gTO, Fig. 12D) likely marks the course of the temporoorbital artery near the point of its branching into the supraorbital, ophthalmotemporal, and infraorbital arteries. The latter is another consistent vascular trait in diapsids (Shindo, 1914; O'Donoghue, 1920; Walker, 1990; Sedlmayr, 2002; Porter, 2015). The ophthalmotemporal and infraorbital arteries are bounded only by soft tissues of the orbit in extant diapsids (Porter, 2015), and they left no osteological evidence in *Bissektipelta*. On the other hand, the supraorbital artery and its small branches are well documented in *Bissektipelta*.
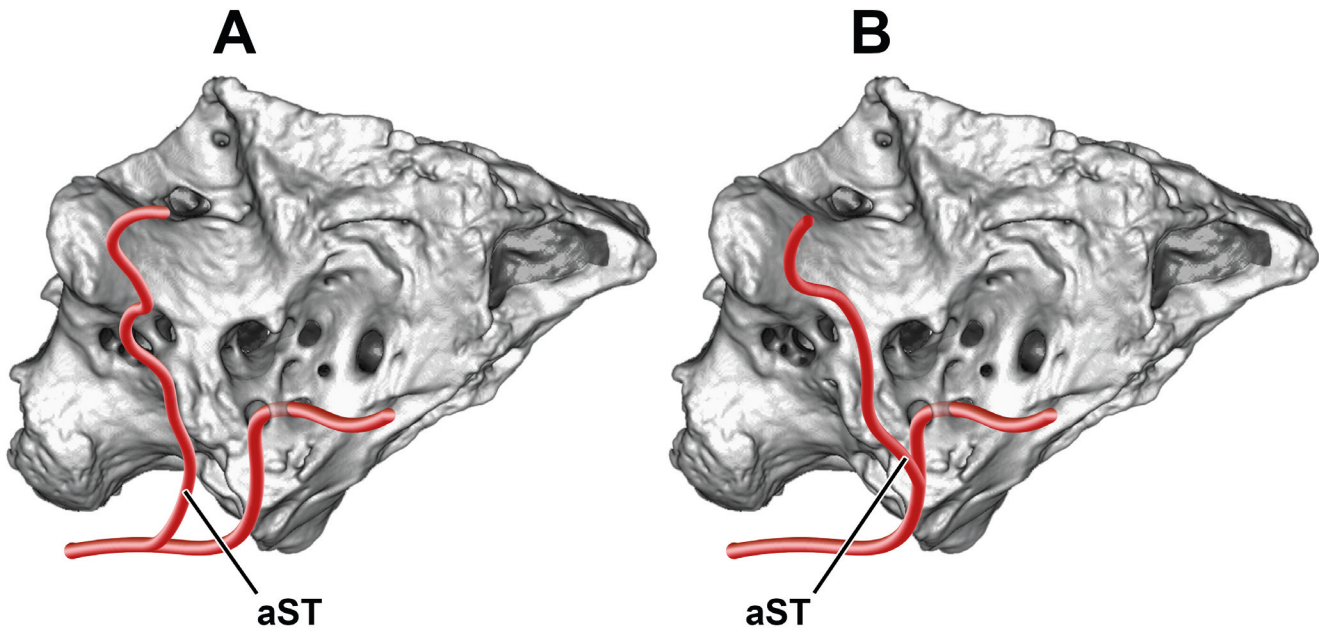
Fig. 22. Two alternative hypotheses for the branching of the internal carotid artery and the stapedial artery course in *Bissektipelta archibaldi*, with (A) representing a general diapsid pattern (stapedial artery pass posterior to the fenestra ovalis and metotic foramen), and (B) representing supposedly modified ankylosaurid patter (stapedial artery pass anterior to FO and MF). Not to scale.

A distinct curved canal dorsal to the foramina for CN II–IV in the holotype ZIN PH 1/16 possibly transmitted supraorbital artery and vein (aSO, Fig. 8). These vessels had numerous dorsally directed branches that pierced the skull roof of *Bissektipelta* (braSO, Fig. 8) and likely supplied dermis above the skull roof, as it occurs in extant birds (Porter and Witmer, 2016a). Additionally, ZIN PH 2329/16 preserves an orbitonasal foramen within the preorbital septum (Fig. 15B, D). The foramen marks the possible anterior course of the supraorbital vessels from the orbit into the nasal region to anastomose with the ethmoid vessels. The same pattern is present in extant diapsids and was reconstructed for various dinosaurs including *Euoplocephalus* (Miyashita et al., 2011; Porter, 2015). This is the first direct evidence of the course of the supraorbital artery in ankylosaurs, and it supports the vascular reconstruction for *Euoplocephalus* (Porter, 2015). Additionally, a large number of small branches of the supraorbital artery that pierce the skull roof of *Bissektipelta* and participate in the anterior branching plexus were for the first time restored in ankylosaurs. Our preliminary observations of the open access CT data for the ankylosaur skull described as *Euoplocephalus* by Miyashita et al. (2011) (*Scolosaurus* sp. sensu Penkalsi, 2018) confirm the presence of a complex system of vascular canals within the skull roof. Thus, this feature may have been more widely distributed, at least among ankylosaurids.

The interpretation of major vessels that pierce the basicranium (cerebral carotid and sphenopalatine arteries) is relatively conservative among various dinosaurs in general and ankylosaurs in particular (Maryańska,

1977; Norman and Faiers, 1996; Averianov, 2002; Miyashita et al., 2011; Porter, 2015; Paulina-Carabajal et al., 2016). Paired foramina for the cerebral carotid artery are the most obvious and universally recognized vascular features in dinosaurs (Porter, 2015). According to Kurzanov and Tumanova (1987), the opening anterior to the cerebral carotid foramen is for the pituitary vein, an interpretation not supported here. The preferred identification of this foramen is for the sphenopalatine artery (= sphenoid/palatine artery of some authors). The anterior course of the sphenopalatine artery over the fused parabasisphenoid rostrum-interorbital septum into the nasal region in *Bissektipelta* is documented by a corresponding groove in the holotype specimen ZIN PH 1/16 (aSP, Fig. 8). In extant squamates and birds, the sphenopalatine artery enters the nasal region and anastomoses with the palatine and nasal arteries (Porter and Witmer, 2015, 2016).

Encephalic arteries leave almost no osteological correlates as they lay deep under the dura (Porter, 2015). In *Bissektipelta*, numerous grooves on the rugose wall of the olfactory region probably correspond to vascular plexuses around olfactory bulbs and likely to the ethmoid artery and vein. Possible evidence of encephalic arteries includes paired grooves on the dorsum sellae and corresponding swellings on the endocast posterior to the hypophysis, interpreted as for the caudal encephalic arteries (and/or caudoventral cerebral veins; e.g., aCE/vCC? in Fig. 14B). Additionally, swellings on the lateral surface of the hypophyseal endocast extend anterodorsally from the sphenopalatine artery and open externally via a canal. The interpretation of these struc-

tures appears to be challenging. As discussed above, we interpret the canal in question as for the passage for CN III, although we note its unusually ventral position. Alternatively, the paired grooves could be interpreted as for the encephalic arteries, and the aforementioned canal could have transmitted its outbranch, the orbital artery (and corresponding vein). In extant birds, a small canal posterior to the foramen for CN II carries these blood vessels passing to and out of the orbit (Porter and Witmer, 2016a).

Veins. Endocranial veins of *Bissektipelta* were restored and described in detail above; the inferred pattern is generally consistent with the condition in other diapsids (see Vasculature in the description of the holotype and Fig. 9). The evidence for the reconstruction of major external head veins is controversial in dinosaurs, with both basal diapsid condition (orbital sinus continued by lateral head vein) and derived archosaur condition (discrete orbital veins continued by temporoorbital and stapedial veins plus temporomandibular vein) equally plausible (Porter, 2015). The level of inference for the derived archosaur condition in dinosaurs is higher according to the EPB approach (Porter, 2015) because both extant crocodylians and birds show similar venous patterns (Sedlmayr, 2002; Porter and Witmer, 2016a; Porter et al., 2016). However, extant archosaurs have a highly ossified occipital region of the skull and related apomorphic pattern of vascular arrangement, whereas various dinosaurs, stem archosaurs, non-crocodylomorph pseudosuchians, and even basal crocodylomorphs show a general diapsid, lepidosaur-like structure of the occiput. A general diapsid venous pattern with the lateral and dorsal head veins was restored for the basal crocodylomorph *Sphenosuchus* (Walker, 1990). These data suggest possibly independent acquisition of the derived vascular arrangement in extant archosaurian clades. In that case, what pattern of external cephalic veins can we infer for *Bissektipelta*?

The basal diapsid (lepidosaur-like) condition implies the presence of the lateral head vein that drained the orbital sinus and all major intracranial veins while they emerge on the external surface of the braincase (e.g., middle cerebral vein, orbitocerebral veins, and occipital/posterior cerebral vein) (Porter, 2015). In that case, the supratemporal fossa of *Bissektipelta* would have been drained by the parietal sinus that joined the dorsal head and transverso-occipital veins. These vessels would have merged with the middle cerebral vein/dorsal longitudinal sinus endocranially. The venous blood from the temporal and occipital regions of the skull would have been eventually distributed by these major veins into the lateral head vein and the spinal vein and would have left the skull.

Accepting the derived archosaur condition, one assumes that the orbital sinus and the lateral head vein were absent in *Bissektipelta*. Instead, discrete orbital veins (supra-, infraorbital, and ophthalmotemporal) ac-

companied corresponding arteries, eventually merging into the temporoorbital and stapedial veins in the temporal region. These latter veins would have drained the temporal region of the skull into the jugular vein. The intracranial veins would have been drained by the occipital sinus into the spinal vein and the caudal head vein that eventually joined the jugular vein (Porter, 2015). Thus, the derived archosaur condition does not imply a connection between the temporal and intracranial veins.

In *Bissektipelta*, relevant osteological correlates for reconstruction of the external cephalic veins include a large vascular groove and a recess in the medial wall of the supratemporal fossa (nvr+g, Fig. 2B), the posttemporal fenestra (ptf, Fig. 1F), paired external foramina for the orbitocerebral veins (fvOC; Figs. 2F, 12D), and the canal for the supraorbital vessels (ca+v and fa+vSO, Fig. 2F). In *Bissektipelta*, the presence of the supraorbital canal and orbitocerebral veins that apparently anastomosed with discrete orbital veins supports the derived archosaurian condition. On the other hand, vascular osteological correlates in the supratemporal fossa and on the occiput closely resemble those of extant lepidosaurs and basal archosauriforms. The presence of the temporoorbital/stapedial veins or the parietal sinus/dorsal head vein in the supratemporal fossa of *Bissektipelta* appears equally likely at first sight and is contradictory (Fig. 9C).

A detailed consideration of the available vascular osteological correlates in the temporal and occipital regions of the skull of *Bissektipelta* and other dinosaurs can probably resolve this contradiction. Two principal veins could be reconstructed in these regions for *Bissektipelta* and other dinosaurs: the transverso-occipital vein and the dorsal head vein. These vessels have a complex and convoluted terminology. The transverso-occipital vein (caudal middle cerebral vein or external occipital vein of different authors) is a vessel that courses from the external occipital surface of the skull into the endocranial cavity through a foramen between the parietal, supraoccipital, and the otoccipital. Intracranially, the transverso-occipital vein connects with the transverse sinus/middle cerebral vein (Sampson and Witmer, 2007; note that these authors name the vessel in question the caudal middle cerebral vein). The dorsal head vein courses from the occipital region anteriorly into the temporal region (adductor cavity) through the posttemporal fenestra, then extends intracranially through the foramen between the parietal and the supraoccipital/prootic, and also joins the middle cerebral vein/transverse sinus (Sampson and Witmer, 2007). Both these vessels could be present in the dinosaur endocast (*Bissektipelta*: present study; *Kentrosaurus*: Galton, 1988; *Stegosaurus*: Leahey et al., 2015; *Allosaurus*: Hopson, 1979; *Majungasaurus*: Sampson and Witmer, 2007; *Tyrannosaurus*: Witmer and Ridgely, 2009; *Camarasaurus*: Witmer et al., 2008) or only a single vessel is reconstructed (*Diplodo-*

PALAEONTOLOGY
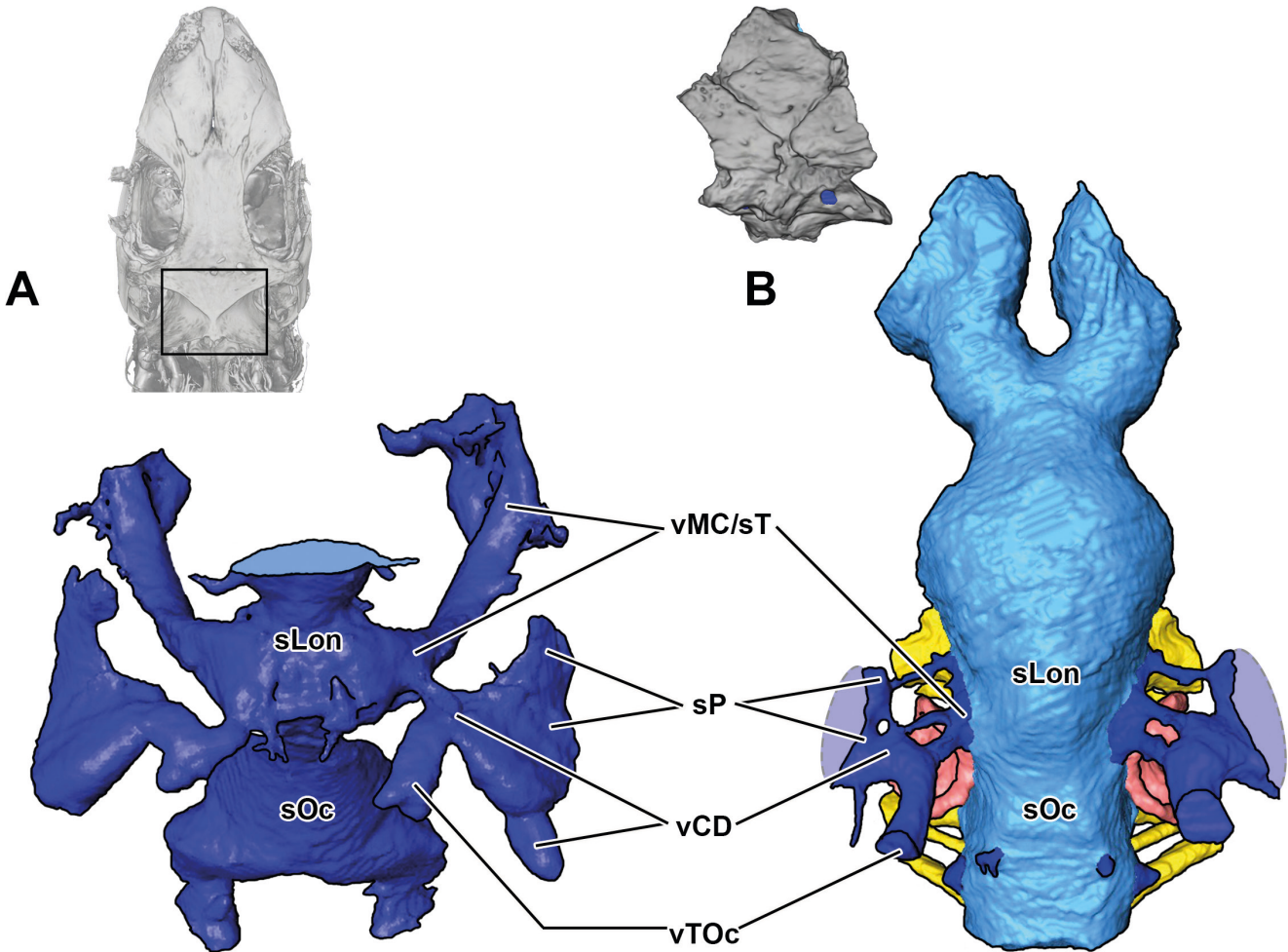
Fig. 23. Comparison of the patterns of temporal, occipital, and dural cephalic veins in (A) *Iguana iguana* (OUVC 10612) and (B) *Bissektipelta archibaldi* (ZIN PH 1/16) (B), in dorsal view. (A) is 3D renderred model of the cephalic veins of *Iguana iguana* based on the original CT scan data of the specimen with injected veins from Porter and Witmer (2016b). The region of interest is pointed in the inset above; only the dorsal dural veins and the occipital/temporal veins are shown. The dorsal longitudinal sinus is cut. (B) is the 3D renderred model of the cranial endocast of *Bissektipelta archibaldi*; only the posterior vessels are shown. **sLon**, dorsal longitudinal sinus; **sOc**, occipital venous sinus; **sP**, parietal venous sinus; **vCD**, dorsal head vein; **vMC/sT**, middle cerebral vein and transverse venous sinus; **vTOc**, transverso-occipital vein. Not to scale.

cus: Witmer et al., 2008; *Kunbarrasaurus*: Leahey et al., 2015; *Pawpawsaurus*: Paulina-Carabajal et al., 2016). To complicate the matter further, there is a parietal sinus/vein in extant lepidosaurs (vena parietalis in Bruner [1907], parietal sinus in Porter and Witmer, [2015]), and some researchers employed the latter term to address the vessel that extends from the temporal region intracranially and connects to the transverse sinus/middle cerebral vein (Galton, 1988; Averianov et al., 2007). We have used the term "parietal sinus" to describe the anterior continuation of the dorsal head vein on the external surface of the braincase of *Bissektipelta* (sP, Figs. 6B–C, 7A, 9B–C). We face the problem that four various terms (transverso-occipital vein, dorsal head vein, caudal middle cerebral vein, parietal sinus/vein) could be interchangably applied for the two principally recognized vessels and their continuations.

Terminological issues aside, what do extant diapsid taxa inform us of the venous drainage of the temporal

and occipital regions of the skull? In extant lepidosaurs (squamates and rhynchocephalians), a short transverso-occipital vein can be found (Fig. 23A). It enters the endocranial cavity via the foramen at the parietal-supra-occipital contact and broadly communicates with the dorsal head vein/parietal sinus. The dorsal head vein of extant lepidosaurs receives small venous branches from the occipiut and drains the muscles in the occipital region (Bruner, 1907; Dendy, 1909; Porter and Witmer, 2015). The dorsal head vein extends anteriorly through the posttemporal fenestra into the temporal region (adductor cavity). Here, the dorsal head vein merges with the parietal sinus that is adjacent to the lateral wall of the temporal region and with the transverso-occipital vein (Fig. 23A). These vessels eventually communicate with the transverse sinus/middle cerebral vein endocranially (Fig. 23A; Bruner, 1907; Dendy, 1909; Porter and Witmer, 2015). Thus, in extant lepidosaurs, both the transverso-occipital and dorsal head veins are present

and connected, the dorsal head vein broadly communicates with the external parietal sinus in the temporal region, and these temporal/occipital veins eventually drain into the transverse sinus/middle cerebral vein endocranially. This is largely similar to the condition observed in *Bissektipelta* (Fig. 23B), and two stegosaur taxa — *Stegosaurus* (Leahey et al., 2015: Fig. 10F–G) and *Kentrosaurus* (Galton, 1988: Fig. 4K). Additionally, the lepidosaur vascular pattern of the temporal/occipital veins principally corresponds to the state of some theropods (*Majungasaurus*: Sampson and Witmer, 2007; *Tyrannosaurus*: Witmer and Ridgely, 2009) and sauropods (*Camarasaurus*: Witmer et al., 2008). However, the expansive parietal sinus was absent or left no deep cavity on the medial surface of the adductor cavity and was not visualized in the mentioned theropods and *Camarasaurus*. Additionally, at least in some theropods (e.g., *Tyrannosaurus*), the transverso-occipital vein is very anteroposteriorly elongated, which differs from the short, sinus-like vein found in lepidosaurs, *Bissektipelta*, and *Stegosaurus*.

In extant archosaurs (crocodylians and birds), the dorsal head vein is apparently reduced or absent, and the direct connection between the temporal and dural veins is lost (Sedlmayr, 2002; Porter and Witmer, 2016a; Porter et al., 2016; Kuzmin, pers. observ. of the open access CT data of crocodylian and bird specimens with the injected blood vessels from Porter and Witmer [2017] and Porter et al. [2017], available at Dryad). In crocodylians, there is an external occipital vein that branches off from the dorsal part of the transverse sinus/middle cerebral vein, pierces the supraoccipital, and ramifies inside the pneumatic sinus within the latter bone; however, it fails to communicate with extracranial vasculature (Sedlmayr, 2002). Likewise, the parietal sinus is also absent, and the temporoorbital vein drains the supratemporal fossa (Porter et al., 2016). Additionally, no vessels corresponding to the transverso-occipital vein have so far been confidently recognized in crocodylians. Walker (1990) summarized some positive evidence suggesting the presence of a corresponding vessel but concluded that "corroboratory evidence from the present-day crocodiles is difficult to obtain". In summary, in extant crocodylians, neither the transverso-occipital nor dorsal head vein appears to be present, and the direct connection between the dural, temporal, and occipital veins is not established. The crocodylian pattern of the head veins in the temporal and occipital regions of the skull is far divergent from that observed in *Bissektipelta* and other dinosaurs.

In birds, the dorsal head vein and the parietal sinus are absent altogether (Sedlmayr, 2002; Porter and Witmer, 2016a). However, there is the external occipital vein that in general corresponds to the transverso-occipital vein of dinosaurs. The external occipital vein of birds drains the venous blood from the encephalic veins (the rostral petrosal sinus in avian terminology) out of the braincase and into the external occipital vein and eventually — into the jugular vein (Sedlmayr, 2002). The external occipital vein leaves the endocranial cavity through the external occipital foramen at the posterodorsolateral aspect of the supraoccipital, close to the supraoccipital-otoccipital-parietal contact (Sedlmayr, 2002). A likely corresponding vein was identified on the endocasts of some birds. Witmer et al. (2008) identified a curved vein passing along the semicircular canals of *Bubo virginianus* (labeled as caudal middle cerebral vein in Witmer et al. [2008]: Fig. 6.7). Romick (2013) identified an elongated straight vein that extends posteriorly on an endocast of *Struthio camelus* (labeled as caudal middle cerebral vein in Romick [2013]: Fig. 1).

One might hypothesize that, similar to birds, dinosaurs (especially theropods like *Tyrannosaurus*) had an elongated transverso-occipital vein (= external occipital vein in extant avian nomenclature) that exited the braincase at the occipital surface of the skull and connected the dural veins with the occipital sinuses and the jugular vein. At the same time, the stapedial/orbitotemporal vein drained the adductor cavity and received the dorsal head vein. This vascular pattern would be consistent with the avian condition in all but one important detail: in birds (as also in crocodylians), the direct connection of the stapedial/temporoorbital vein with the encephalic veins has so far never been described (Sedlmayr, 2002; Porter and Witmer, 2016a). This hypothetical venous pattern would be untestable in terms of the EPB approach, as neither extant diapsid lineage exhibits such condition.

Based on the available osteological correlates and the comparison with extant taxa, we infer the presence of the parietal sinus and the dorsal head vein that drained into the transverse sinus/middle cerebral vein in *Bissektipelta* (Fig. 23B). In *Bissektipelta*, the dorsal head vein was broadly confluent with the transverso-occipital vein medially. Probably, there was a complete circumoccipital anastomotic loop between these veins (anastv, Fig. 9C) as was restored in *Majungasaurus* by Sampson and Witmer (2007). This pattern of head veins is absent in both extant outgroups of Dinosauria, but is present in extant lepidosaurs and it left clear osteological correlates. It thus corresponds to the level 3 inference of the EPB approach (Witmer, 1995). Consequentially, we may hypothesize that the whole system of external cephalic veins of *Bissektipelta* corresponds more to the basal diapsid condition. However, that would be only the level 3´ inference, as there are no obvious osteological correlates for the orbital sinus and the lateral head vein in *Bissektipelta*. Previously, the lateral head vein was restored for *Majungasaurus* (Sampson and Witmer, 2007). Porter (2015) assessed the presence of the lateral head vein and lepidosaur-like venous drainage of the head in

dinosaurs as an alternative hypothesis of the level 2 inference. Our study of the vasculature in *Bissektipelta* adds new support to the hypothesis of the basal diapsid, lepidosaur-like condition of the cephalic veins in non-avian dinosaurs.

It appears that the dorsal head vein is consistently present in various distantly related dinosaurs and represents a plesiomorphic diapsid character state. We hypothesize that the extant archosaur lineages independently lost this vein and, consequently, direct communication between the temporo-occipital and encephalic vessels. Unless the direct connections of the stapedial/temporoorbital vein with the occipital and, most importantly, dural veins are not shown in extant archosaurs, we must admit that several distantly related dinosaur taxa from the three main lineages (Ornithischia, Theropoda, Sauropoda) exhibit the pattern of cephalic veins that is principally different from that present in extant proximal outgroups. Non-avian dinosaurs may have had the cephalic venous system that corresponds more to the basal diapsid condition, or a mixed pattern of head veins around the braincase, intermediate between the basal diapsid and the derived archosaur conditions. No doubt, this statement needs to be verified on a larger sample than discussed in the present study. Nevertheless, restorations of dinosaurian cranial vasculature should not be based solely on the state of extant crocodylians and birds.

Paleobiological implications

During the last three decades, there has been a major increase in sampling and analysis of endocranial data of ankylosaurs. Latex-made or digital endocasts were gathered for an array of basal ankylosaurs (*Kunbarrasaurus*, Leahey et al., 2015), nodosaurids (*Struthiosaurus*, Pereda-Suberbiola and Galton, 1994; Hokkaido nodosaurid, Hawakaya et al., 2005; *Panoplosaurus*, Witmer and Ridgely, 2008; *Hungarosaurus*, Ösi et al., 2014; *Pawpawsaurus*, Paulina-Carabajal et al., 2016), "polacanthines" (cf. *Polacanthus*, Norman and Faiers, 1996; *Gastoniai*, Kinneer et al., 2016), and ankylosaurids (*Euoplocephalus*, Coombs, 1978b; Miyashita et al., 2011; *Cedarpelta*, Carpenter et al., 2001; *Talarurus* and *Tarchia*, Paulina-Carabajal et al., 2018; *Bissektipelta*, Alifanov and Saveliev, 2019; present study). Among taxa undoubtedly referable to Ankylosaurinae, complete endocranial casts of only the derived members are known, such as *Euoplocephalus* (Coombs, 1978b; Miyashita et al., 2011; Leahey et al., 2015) and *Talarurus* and *Tarchia* (Paulina-Carabajal et al., 2018). As a relatively basal ankylosaurine, *Bissektipelta* fills the existing gap in the sampling of endocasts and makes it possible to comment on the species' paleobiology and to assess evolutionary tendencies within the clade. Furthermore, we discuss those paleobiological implications for which the study of the specimens of *Bissektipelta* contributed new relevant data.

Olfaction. The inference of keenly developed olfaction in ankylosaurs is not new. Maryańska (1977) assumed a connection between olfactory capabilities of ankylosaurs and the "relative sluggishness of these animals". Miyashita et al. (2011) suggested that olfaction was an important sense for *Euoplocephalus* based upon the large volume occupied by the olfactory cavity and the relatively enlarged olfactory bulbs. Recently, Alifanov and Saveliev (2019) discussed the primary role of olfaction in ankylosaurs based on the investigation of the detailed synthetic endocast of *Bissektipelta*.

Paulina-Carabajal et al. (2016) presented the first quantitative data (olfactory ratios) of the size of olfactory bulbs in ankylosaurs (46.2 % for *Pawpawsaurus*, 44 % for *Panoplosaurus*, 52 % for *Euoplocephalus*). The olfactory ratio was initially proposed by Zelenitsky et al. (2009) as the ratio of the greatest diameter of the olfactory bulb to the greatest diameter of the cerebral hemisphere. We calculated the olfactory ratio value of 63–69 % for *Bissektipelta*. Our recalculation of the olfactory ratios for other ankylosaurs revealed slightly larger values than were reported previously — roughly 57–63 % for *Pawpawsaurus*, 55–58 % for *Panoplosaurus*, 54–59 % for *Euoplocephalus*, and 58 % for *Kunbarrasaurus* (based on figures from Witmer and Ridgely [2008], Miyashita et al. [2011], Paulina-Carabajal et al. [2016], Leahey et al. [2015]). These rates for ankylosaurs are similar to those olfactory ratio values calculated for allosauroid and tyrannosauroid theropods and extant *Alligator mississippiensis* presented by Zelenitsky et al. (2009). However, the latter authors claimed that "olfactory ratios should not be used to directly compare olfactory acuity among theropods without consideration of body size (Zelenitsky et al., 2009). A larger sample size and correlation with body size are needed to perform a rigorous statistical analysis of the olfactory acuity for ankylosaurs. Nevertheless, the olfactory ratios of ankylosaurs appear to be not only surprisingly high but are also relatively similar in distantly related taxa with disparate body sizes. We thus infer that olfaction was indeed a critically important sense in most known ankylosaurs based on the size of their olfactory bulbs.

Hearing. The endosseous labyrinth has proven to be a highly informative structure regarding aspects of hearing, mode of locomotion, and alert head posture for extant and extinct reptiles (Gleich et al., 2005; Witmer et al., 2008; Walsh et al., 2009). It has been shown that the dimensions of the basilar papilla (basilar membrane) situated in the cochlear duct correlate with certain properties of hearing (e.g., optimal frequency, upper limit of high-frequency hearing) and thus characterize the hearing range of amniotes (Manley, 1971; Gleich et al., 2005). The general conclusions are: 1. the longer and narrower the basilar papilla, the higher the frequencies it responds to; 2. the frequency of best hearing is correlated with the

limit of high-frequency hearing (the lower the optimal frequency of hearing, the lower the value of the upper limit for high-frequency hearing). An important correlation was found in a sample of extant archosaurs (birds plus *Caiman*): species with longer basilar papillae have more sensitive hearing at lower frequencies than do species with shorter basilar papillae (Gleich et al., 2005). These data indicate that in birds, with the exception of the highly-specialized barn owl, elongation of the basilar membrane was not an evolutionary response for extension of the range of high-frequency hearing. Best hearing frequencies for a number of bird species range from 1.8 to 4 kHz (Manley, 1971), with hearing in the larger-bodied paleognaths likely most sensitive to slightly lower frequencies, around 1.5 kHz (Gleich et al., 2005). We are not aware of comparative data on the length of basilar papilla for various crocodylian species; the known value for *Caiman* equals 4–5 mm and is comparable to that of large-bodied paleognaths (Manley, 1971; Gleich and Manley, 2000). Crocodylians are well known to have a keen sense of hearing, with best sensitivity ranging from 100 to 3000 Hz and a notable peak at 800–1000 Hz (Manley, 1971; Wever, 1971; Higgs et al., 2002). In addition, the discussed hearing capabilities, as well as vocalization frequencies, are correlated with body mass (Gleich et al., 2005; Thiagavel et al., 2017). It appears that larger animals tend to vocalize and are more sensitive to lower frequencies and vice versa (Bowling et al., 2017). The structure of the inner ear is well documented in the fossil record, and the length of the endosseous cochlear duct is a reliable proxy for assessing hearing capabilities of extinct species (Gleich et al., 2005; Walsh et al., 2009). These general conclusions from published sources have important implications for paleobiological inferences regarding and evolutionary tendencies of hearing in ankylosaurs.

In ZIN PH 1/16, the mean length of the endosseous cochlear duct equals 10.45 mm in a more conservative approach (when a straighter line with lesser curve was measured) and 12.75 mm in an extended approach (when a strongly ventromedially curved line was measured) (Table 3). In ZIN 281/16, the cochlear duct has a less pronounced ventromedial curve and is straighter overall, thus a single measurement of its maximal length was made for each labyrinth. The mean length of the endosseous cochlear duct for ZIN PH 281/16 equals 13.75 mm. We estimate the length of the basilar papilla as two thirds of the endosseous duct length, with the rest being occupied by the lagenar macula and perilymphatic spaces (Gleich et al., 2005). Applying the equations from the data set of Gleich et al. (2005), we calculate the optimal frequency of hearing for ZIN PH 1/16 as 682–1002 Hz and for ZIN PH as 576 Hz. The high-frequency hearing limit for ZIN PH 1/16 is 2299–2889 Hz and for ZIN PH 281/16—2105 Hz. *Euoplocephalus* has an even longer endosseous cochlear duct of approximately 22 mm (Miyashita et al., 2011; Leahey et al., 2015: Fig. 11). The best frequency of hearing for *Euoplocephalus* is measured as 145 Hz and the high-frequency hearing limit as 1310 Hz, which are considerably lower estimates than those for *Bissektipelta* and for the nodosaurid *Pawpawsaurus* (2000–4000 Hz, Paulina-Carabajal et al., 2016). These data indicate that ankylosaurs with known endosseous labyrinths had a keen sense of hearing at a lower range of frequencies (100–3000 Hz), similar to extant crocodylians.

Previously, the elongated cochlear duct of the derived ankylosaurids such as *Euoplocephalus* (Miyashita et al., 2011) and *Tarchia* (Paulina-Carabajal et al., 2018) was hypothesized as an adaptation to a wider range of hearing frequencies (Paulina-Carabajal et al., 2016). The aforementioned data on the anatomy of the inner ear and hearing capabilities of extant archosaurs indicate that the elongation of the cochlear duct of ankylosaurids instead was probably an adaptation to the enhanced sensitivity at the lower range of frequencies. The length of the cochlear duct of *Bissektipelta* is intermediate between those for nodosaurids and primitive ankylosaurs (Leahey et al., 2015; Paulina-Carabajal et al., 2016) and derived ankylosaurids (Miyashita et al., 2011; Paulina-Carabajal et al., 2018), indicating stepwise evolutionary changes toward low-frequency hearing in ankylosaurids. A possible if still untested explanation for these evolutionary changes in the inner ear of ankylosaurids is an increase in the size of the derived members of the clade (Arbour and Mallon, 2017). Overall, ankylosaurids appear to have been heavier than nodosaurids for any given body length (Bourke et al., 2018). As was discussed above, larger animals tend to vocalize at and are more sensitive to lower frequencies, which may explain the enhanced length of the cochlear duct of derived ankylosaurids.

Physiological implications of the braincase vasculature in ankylosaurs. In the present study, we have found a complex network of intercommunicating vessels within the highly ossified braincase and skull roof of *Bissektipelta*. We propose two interrelated hypotheses concerning their biological and physiological implications. First, the elaborated vascular system likely played a role in the processes of bone remodeling and supplied bone tissue. Second, this system was most likely involved in thermoregulation of the neurosensory tissues in the braincase.

Thermoregulatory functions of the highly vascularized osteoderms have long been hypothesized for crocodylians and thyreophorans (Seidel, 1979; Farlow et al., 1976, 2010; Tumanova, 1987; Hayashi et al., 2010) and subsequently tested for extant crocodylians and squamates (Broeckhoven et al., 2017; Clarac et al., 2017, 2018). Clarac and Quilhac (2019) demonstrated that

the outer temperature of the sculptured skull roof above the braincase in crocodiles remains warmer regardless of ambient conditions and shows fewer temperature variations than other parts of the dermal skeleton. This is direct evidence of control of the temperature in the braincase of extant archosaurs. The authors suggested that shunting blood pathways are involved in maintaining optimal physiological temperatures of the neurosensory tissues in crocodylians (Clarac and Quilhac, 2019).

The significance of cephalic vasculature for proper thermoregulation of the head has been well demonstrated in extant squamates, crocodylians, and birds (Porter and Witmer, 2015, 2016a; Porter et al., 2016). Porter and Witmer (2019) recently conducted a thorough study on the thermoregulatory strategies and corresponding vascular patterns in various dinosaurs. In a re-assessment of the structure and homology of the frontoparietal and supratemporal fossae among archosaurs, Holliday et al. (2019) hypothesized the presence of a vascular network interconnecting the supratemporal, orbital, and endocranial regions. These authors demonstrated the thermoregulatory significance of the temporoorbital vessels in extant crocodylians and inferred the presence of vascular physiological devices within the supratemporal region of extinct taxa.

Recent research on the anatomy of ankylosaurian nasal passages demonstrated that, aside from other functions, the convoluted nasal passages of ankylosaurs are efficient heat exchangers suitable for warming and cooling the air, energy and moisture recovery, and overall thermoregulation of the head (Bourke et al., 2018). The study utilized the restoration of the cephalic blood vessels of *Euoplocephalus* as a model of the venous blood flow from sites of thermoregulation within the nasal passages to the neurosensory tissue within the braincase (Bourke et al., 2018). Bourke et al. (2018) suggested that the convoluted nasal passages may have been the source of the cooled venous blood that circulated into the braincase region and maintained thermal homeostasis of the brain. Furthermore, Porter and Witmer (2019) found compelling evidence that both *Euoplocephalus* and *Panoplosaurus* had a focused thermoregulatory strategy with an unbalanced pattern of blood vessels. The authors proposed that the convoluted nasal passages of these ankylosaurs were the main sites of thermal exchange and that the modified blood flow sustained redistribution of blood from these sites to relevant organs (e.g., neurosensory tissues).

Our study of the braincase vasculature of *Bissektipelta* is in line with previous research and allows detailed hypotheses of blood distribution around the brain and cephalic thermoregulation in ankylosaurs. A number of physiological mechanisms could be hypothesized. The complex network of vessels interconnects the endocranial, occipital, skull roof, and lateral vessels of the

braincase into a single system around the neurosensory tissues. First, we suppose that blood coming from the nasal cavity through the nasal and ethmoid veins could have been subsequently efficiently redistributed around the braincase. Depending on ambient conditions, either cooling or warming of inhaled air would occur within the nasal cavity. The temperature of blood involved in the process of thermal exchange would correspondingly increase or decrease. Dependent on the temperature of the blood coming from the nasal cavity, it may have flown into the endocranial cavity and affected the brain temperature directly, or the current could have been redirected (at least partially) by means of numerous small anastomotic vessels into the anterior branching plexuses and supraorbital veins and circumvented the brain.

Second, the heat exchange could have occurred on the external surface of the skull roof of ankylosaurs. Numerous small pits and grooves indicate high vascularization of the dermis above the frontoparietal region in *Bissektipelta* and other ankylosaurs (e.g., Norman and Faiers, 1996). Vasodilation and vasoconstriction could efficiently increase or decrease blood flow to the external dermis and regulate surficial heat transfer. This mechanism was discussed for the osteoderms of crocodylians (Seidel, 1979) and ankylosaurs (Tumanova, 1987). Third, the bone pierced by numerous blood vessels could simply insulate the brain tissues from the effects of solar exposure, removing excessive heat. At present, all these remain untested hypotheses. However, the vascular system of the braincase of *Bissektipelta* demonstrated in this study indicates that ankylosaurs had intricate mechanisms of temperature control of the brain and adjacent tissues.

Conclusions

1. *Bissektipelta archibaldi* from the Bissekty Formation at the Dzharakuduk locality, Uzbekistan, is confirmed as a valid ankylosaurian taxon. Two new braincases from the same locality are attributed to *B. archibaldi*, increasing the number of specimens currently referred to this taxon to three. The phylogenetic analysis found *Bissektipelta* as a relatively basal member of Ankylosaurinae.

2. A review of the braincase anatomy among Ankylosauria allowed increased sampling of characters of the braincase for a recent character-taxon matrix for ankylosaurs and discussion of their phylogenetic distribution. We have revealed diagnostic braincase features for certain clades within Ankylosauria. Our data corroborate previous assumptions that the structure of the braincase appears to be highly conservative at low taxonomic levels among ankylosaurs but is useful for higher-level taxonomy.

3. Osteological evidence from specimens herein assigned to *Bissektipelta* allowed us to reconstruct

and discuss aspects of the neurocranial vasculature in ankylosaurs in detail. In general, our observations support previous reconstructions for various ankylosaurs and match well with known vascular patterns of extant diapsids. The canal for the supraorbital vessels and complex branching plexuses of the skull roof were for the first time reconstructed in ankylosaurs. In ankylosaurids, the course of the stapedial artery may have been anterior to the fenestra ovalis and the metotic foramen, which is different from the condition in most diapsids.

4. The presence of the dorsal head vein in dinosaurs is a plesiomorphic diapsid trait, which was independently lost in extant crocodylians and birds that lack direct communication between the temporal and encephalic veins. *Bissektipelta* and several other distantly related dinosaurs (e.g., *Stegosaurus*, *Majungasaurus*, *Tyrannosaurus*) may have had the pattern of external head veins more similar to that of extant lepidosaurs than previously realized.

5. In *Bissektipelta*, numerous small vascular canals within the skull roof and lateral wall of the braincase integrated various endo- and extracranial vessels into a single complex network around the brain. This network with numerous anastomotic connections allowed for redistribution of the blood flow and various physiological mechanisms for heat exchange and was likely used to maintain optimal temperatures for the animal's brain.

6. We hypothesize that olfaction was a keenly developed and critically important sense in most known ankylosaurs based on the relatively large size of the olfactory bulbs in distantly related and variously sized taxa.

7. The length of the endosseous cochlear duct on the inner ear endocasts of ankylosaurs suggests a keen sense of hearing at lower frequencies (100–3000 Hz). We infer that the elongated cochlear ducts in derived ankylosaurines (e.g., *Euoplocephalus*, *Tarchia*) were adapted for enhanced hearing at lower frequencies. Stepwise evolution of low-frequency hearing in ankylosaurids may have been connected with a progressive increase in body size within the clade.

References

Alifanov, V. R. and Saveliev, S. V. 2019. The brain morphology and neurobiology in armored dinosaur *Bissekipelta archibaldi* (Ankylosauridae) from the Late Cretaceous of Uzbekistan. *Paleontological Journal* 53:315–321. https://doi.org/10.1134/S003103011903002X

Almeida, L. M. and Campos, R. 2010. Systematization, description and territory of the middle and rostral cerebral arteries in broad-snouted caimans (*Caiman latirostris*). *Acta Scientiae Veterinariae* 38:265–271. https://doi.org/10.22456/1679-9216.17061

Almeida, L. M. and Campos, R. 2011. Systematization, description and territory of the caudal cerebral artery of the brain in broad-snouted caiman (*Caiman latirostris*). *Pesquisa Veterinaria Brasileira* 31:817–822. https://doi.org/10.1590/S0100-736X2011000900015

Arbour, V. M. and Currie, P. J. 2013a. *Euoplocephalus tutus* and the diversity of ankylosaurid dinosaurs in the Late Cretaceous of Alberta, Canada, and Montana, USA. *PLoS ONE* 8:e62421. https://doi.org/10.1371/journal.pone.0062421

Arbour, V. M. and Currie, P. J. 2013b. The taxonomic identity of a nearly complete ankylosaurid dinosaur skeleton from the Gobi Desert of Mongolia. *Cretaceous Research* 46:24–30. https://doi.org/10.1016/j.cretres.2013.08.008

Arbour, V. M. and Currie, P. J. 2016. Systematics, phylogeny and palaeobiogeography of the ankylosaurid dinosaurs. *Journal of Systematic Palaeontology* 14:385–444. https://doi.org/10.1080/14772019.2015.1059985

Arbour, V. M. and Evans, D. C. 2017. A new ankylosaurine dinosaur from the Judith River Formation of Montana, USA, based on an exceptional skeleton with soft tissue preservation. *Royal Society Open Science* 4:161086. https://doi.org/10.1098/rsos.161086

Arbour, V. M. and Mallon, J. C. 2017. Unusual cranial and postcranial anatomy in the archetypal ankylosaur *Ankylosaurus magniventris*. *Facets* 2:764–794. https://doi.org/10.1139/facets-2017-0063

Arbour, V. M., Currie, P. J., and Badamgarav, D. 2014. The ankylosaurid dinosaurs of the Upper Cretaceous Baruungoyot and Nemegt formations of Mongolia. *Zoological Journal of the Linnean Society* 172:631–652. https://doi.org/10.1111/zoj12185

Averianov, A. O. 2002. An ankylosaurid (Ornithischia: Ankylosauria) braincase from the Upper Cretaceous Bissekty Formation of Uzbekistan. *Bulletin de l'Institut Royal des Sciences Naturelles de Belgique, Sciences de la Terre* 72:97–110.

Averianov, A. O. 2009. Ankylosaur (Ornithischia, Ankylosauridae) humerus from the Late Cretaceous of Kazakhstan; pp. 78–80 in Shishkin, M. A. and Tverdokhlebov, V. P. (eds.), Researches on paleontology and biostratigraphy of ancient continental deposits (Memories of Professor Vitalii G. Ochev). Nauchnaya Kniga, Saratov. (In Russian)

Averianov, A. O., Leshchinskiy, S. V., Kudryavtsev, V. I., and Zabelin, V. I. 2007. Braincase of a Late Jurassic stegosaurian dinosaur from Tuva, Russia (Central Asia). *Journal of Vertebrate Paleontology* 27:727–733. https://doi.org/10.1671/0272-4634(2007)27[727:BOALJS]2.0.CO;2

Baird, I. L. 1960. A survey of the periotic labyrinth in some representative recent reptiles. *The University of Kansas Science Bulletin* 41:891–981. https://doi.org/10.5962/bhl.part.15604

Balanoff, A. M. and Bever, G. S. 2017. The role of endocasts in the study of brain evolution; pp. 223–241 in Kaas, J. (ed.), Evolution of Nervous Systems. Elsevier, Oxford. https://doi.org/10.1016/B978-0-12-804042-3.00023-3

Berman, D. S. and McIntosh, J. S. 1986. Description of the lower jaw of *Stegosaurus* (Reptilia, Ornithischia). *Annals of Carnegie Museum* 55:29–40.

Blows, W. T. 2001. Dermal armor of the polacanthine dinosaurs; pp. 363– 385 in Carpenter, K. (ed.), The Armored Dinosaurs. Indiana University Press, Bloomington.

Bourke, J. M., Porter, W. R., and Witmer, L. M. 2018. Convoluted nasal passages function as efficient heat exchangers in ankylosaurs (Dinosauria: Ornithischia: Thyreophora). *PLoS ONE* 13:e0207381. https://doi.org/10.1371/journal.pone.0207381

Bowling, D. L., Garcia, M., Dunn, J. C., Ruprecht, R., Stewart, A., Frommolt, K.-H., and Fitch, W. T. 2017. Body size and vocalization in primates and carnivores. *Scientific Reports* 7:41070. https://doi.org/10.1038/srep41070

Broeckhoven, C., du Plessis, A., and Hui, C. 2017. Functional trade-off between strength and thermal capacity of dermal armor: insights from girdled lizards. *Journal of the Mechanical Behavior of Biomedical Materials* 74:189–194. https://doi.org/10.1016/j.jmbbm.2017.06.007

Brown, B. 1908. The Ankylosauridae, a new family of armored dinosaurs. *Bulletin of the American Museum of Natural History* 24:187–201.

Bruner, H. L. 1907. On the cephalic veins and sinuses of reptiles, with description of a mechanism for raising the venous blood pressure in the head. *American Journal of Anatomy* 7:1–117. https://doi.org/10.1002/aja.1000070102

Burns, M. E. 2015. Intraspecific variation in the armoured dinosaurs (Dinosauria: Ankylosauria). PhD thesis, University of Alberta, Edmonton.

Burns, M. E., Currie, P. J., Sissons, R. L., and Arbour, V. M. 2011. Juvenile specimens of *Pinacosaurus grangeri* Gilmore, 1933 (Ornithischia: Ankylosauria) from the Late Cretaceous of China, with comments on the specific taxonomy of *Pinacosaurus*. *Cretaceous Research* 32:174–186. https://doi.org/10.1016/j.cretres.2010.11.007

Carpenter, K. 2001. Phylogenetic analysis of the Ankylosauria; pp. 455–483 in Carpenter, K. (ed.), The Armored Dinosaurs. Indiana University Press, Bloomington.

Carpenter, K. 2004. Redescription of *Ankylosaurus magniventris* Brown 1908 (Ankylosauridae) from the Upper Cretaceous of the Western Interior of North America. *Canadian Journal of Earth Sciences* 41:961–986. https://doi.org/10.1139/e04-043

Carpenter, K. and Breithaupt, B. 1986. Latest Cretaceous occurrence of nodosaurid ankylosaurs (Dinosauria, Ornithischia) in Western North America and the gradual extinction of the dinosaurs. *Journal of Vertebrate Paleontology* 6:251–257. https://doi.org/10.1080/02724634.1986.10011619

Carpenter, K. and Kirkland, J. I. 1998. Review of Lower and Middle Cretaceous ankylosaurs from North America; pp. 249–270 in Lucas, S. G., Kirkland, J. I., and Estep, J. W. (eds.), Lower and Middle Cretaceous terrestrial ecosystems. New Mexico Museum of Natural History and Science Bulletin 14.

Carpenter, K. and Everhart, M. J. 2007. Skull of the ankylosaur *Niobrarasaurus coleii* (Ankylosauria: Nodosauridae) from the Smoky Hill Chalk (Coniacian) of western Kansas. *Transactions of the Kansas Academy of Science* 110:1–9. https://doi.org/10.1660/0022-8443(2007)110[1:SOTANC]2.0.CO;2

Carpenter, K., Kirkland, J. I., Burge, D., and Bird, J. 2001. Disarticulated skull of a new primitive ankylosaurid from the Lower Cretaceous of Eastern Utah; pp. 211–238 in Carpenter, K. (ed.), The Armored Dinosaurs. Indiana University Press, Bloomington.

Carpenter, K., Bartlett, J., Bird, J., and Barrick, R. 2008. Ankylosaurs from the Price River Quarries, Cedar Mountain Formation (Lower Cretaceous), east-central Utah. *Journal of Vertebrate Paleontology* 28:1089–1101. https://doi.org/10.1671/0272-4634-28.4.1089

Carpenter, K., Kobayashi, Y., Maryańska, T., Barsbold, R., Sato, K., and Obata, I. 2011. *Saichania chulsanensis* (Ornithischia, Ankylosauridae) from the Upper Cretaceous of Mongolia. *Palaeontographica, Abt. A* 294:1–61. https://doi.org/10.1127/pala/294/2011/1

Cignoni, P., Callieri, M., Corsini, M., Dellepiane, M., Ganovelli, F., and Ranzuglia, G. 2008. MeshLab: an open-source mesh processing tool. *Sixth Eurographics Italian Chapter Conference* 1:129–136.

Clarac, F. and Quilhac, A. 2019. The crocodylian skull and osteoderms: a functional exaptation to ectothermy? *Zoology* 132:31–40. https://doi.org/10.1016/j.zool.2018.12.001

Clarac, F., de Buffrénil, V., Cubo, J., and Quilhac, A. 2018. Vascularization in ornamented osteoderms: physiological implications in ectothermy and amphibious lifestyle in the crocodylomorphs? *Anatomical Record* 301:175–183. https://doi.org/10.1002/ar.23695

Clarac, F., Goussard, F., Teresi, L., de Buffrénil, V., and Sansalone, V. 2017. Do the ornamented osteoderms influence the heat conduction through the skin? A finite element analysis in Crocodylomorpha. *Journal of Thermal Biology* 69:39–53. https://doi.org/10.1016/j.jtherbio.2017.06.003

Coombs, W. P. 1978a. The families of the ornithischian dinosaur order Ankylosauria. *Palaeontology* 21:143–170.

Coombs, W. P. 1978b. An endocranial cast of *Euoplocephalus* (Reptilia, Ornithischia). *Palaeontographica, Abt. A* 161:176–182.

Coombs, W. P. and Maryańska, T. 1990. Ankylosauria; pp. 456–483 in Weishampel, D. B., Dodson, P., and Osmólska, H. (eds.), The Dinosauria. University of California Press, Berkeley.

Dendy, A. 1909. The intracranial vascular system of *Sphenodon*. *Philosophical Transactions of the Royal Society B: Biological Sciences* 200:403–426. https://doi.org/10.1098/rstb.1909.0010

Dendy, A. 1911. On the structure, development and morphological interpretation of the pineal organs and adjacent parts of the brain in the Tuatara (*Sphenodon punctatus*). *Philosophical Transactions of the Royal Society B: Biological Sciences* 201:227–331. https://doi.org/10.1098/rstb.1911.0006

Dong, Z. 1993. An ankylosaur (ornithischian dinosaur) from the Middle Jurassic of the Junggar Basin, China. *Vertebrata PalAsiatica* 31:257–266.

Eaton, T. H. 1960. A new armored dinosaur from the Cretaceous of Kansas. *The University of Kansas Paleontological Contributions: Vertebrata* 8:1–24.

Evans, D. C. 2005. New evidence on brain-endocranial cavity relationships in ornithischian dinosaurs. *Acta Palaeontologica Polonica* 50:617–622.

Evans, D. C., Ridgely, R., and Witmer, L. M. 2009. Endocranial anatomy of lambeosaurine hadrosaurids (Dinosauria: Ornithischia): a sensorineural perspective on cranial crest function. *Anatomical Record* 292:1315–1337. https://doi.org/10.1002/ar.20984

Farlow, J. O., Thompson, C. V., and Rosner, D. E. 1976. Plates of the dinosaur *Stegosaurus*: forced convection heat loss fins? *Science* 192:1123–1125. https://doi.org/10.1126/science.192.4244.1123

Farlow, J. O., Hayashi, S., and Tattersall, G. J. 2010. Internal vascularity of the dermal plates of *Stegosaurus* (Ornithis-

chia, Thyreophora). *Swiss Journal of Geosciences* 103:173–185. https://doi.org/10.1007/s00015-010-0021-5

Galton, P. M. 1988. Skull bones and endocranial casts of stegosaurian dinosaur *Kentrosaurus* Hennig, 1915 from Upper Jurassic of Tanzania, East Africa. *Geologica et Palaeontologica* 22:123–143.

Galton, P. M. 2001. Endocranial casts of the plated dinosaur *Stegosaurus* (Upper Jurassic, Western USA): a complete undistorted cast and the original specimens of Othniel Charles Marsh; pp. 103–129 in Carpenter, K. (ed.), The Armored Dinosaurs. Indiana University Press, Bloomington.

Galton, P. M. and Upchurch, P. 2004. Stegosauria; pp. 343–362 in Weishampel, B. D., Dodson, P., and Osmólska, H. (eds.), The Dinosauria. Second Edition. University of California Press, Berkeley. https://doi.org/10.1525/california/9780520242098.003.0019

Galton, P. M. and Knoll, F. 2006. A saurischian dinosaur braincase from the Middle Jurassic (Bathonian) near Oxford, England: from the theropod *Megalosaurus* or the sauropod *Cetiosaurus*? *Geological Magazine* 143:905–921. https://doi.org/10.1017/S0016756806002561

Gilmore, C. W. 1914. Osteology of the armored Dinosauria in the United States National Museum, with special reference to the genus *Stegosaurus*. *Bulletin of the United States National Museum* 89:1–136. https://doi.org/10.5962/bhl.title.63658

Gilmore, C. W. 1933. Two new dinosaurian reptiles from Mongolia with notes on some fragmentary specimens. *American Museum Novitates* 679:1–20.

Gleich, O. and Manley, G. 2000. The hearing organ of birds and Crocodilia; pp. 70–138 in Dooling, R. J., Fay, R. R., and Popper, A. N. (eds.), Springer Handbook of Auditory Research. Comparative Hearing: Birds and Reptiles. Springer, Berlin and New York. https://doi.org/10.1007/978-1-4612-1182-2_3

Gleich, O., Dooling, R. J., and Manley, G. A. 2005. Audiogram, body mass, and basilar papilla length: correlations in birds and predictions for extinct archosaurs. *Naturwissenschaften* 92:595–598. https://doi.org/10.1007/s00114-005-0050-5

Godefroit, P., Pereda Suberbiola, X., Li, H., and Dong, Z. M. 1999. A new species of the ankylosaurid dinosaur *Pinacosaurus* from the Late Cretaceous of Inner Mongolia (P. R. China). *Bulletin de l'Institut Royal des Sciences Naturelles de Belgique, Sciences de la Terre* 69:17–36.

Goloboff, P. and Catalano, S. 2016. TNT version 1.5, including a full implementation of phylogenetic morphometrics. *Cladistics* 32: 221–238. https://doi.org/10.1111/cla.12160

Gower, D. J. 2002. Braincase evolution in suchian archosaurs (Reptilia: Diapsida): evidence from the rauisuchian *Batrachotomus kupferzellensis*. *Zoological Journal of the Linnean Society* 136:49–76. https://doi.org/10.1046/j.1096-3642.2002.00025.x

Gower, D. J. and Weber, E. 1998. The braincase of *Euparkeria*, and the evolutionary relationships of birds and crocodilians. *Biological Reviews* 73:367–411. https://doi.org/10.1017/S0006323198005222

Gower, D. J. and Walker, A. D. 2002. New data on the braincase of the aetosaurian archosaur (Reptilia: Diapsida) *Stagonolepis robertsoni* Agassiz. *Zoological Journal of the Linnean Society* 136:7–23. https://doi.org/10.1046/j.1096-3642.2002.00023.x

Gower, D. J. and Nesbitt, S. J. 2006. The braincase of *Arizonasaurus babbitti* — further evidence for the non-monophyly of 'rauisuchian' archosaurs. *Journal of Vertebrate Paleontology* 26:79–87. https://doi.org/10.1671/0272-4634(2006)26[79:TBOABE]2.0.CO;2

Haubold, H. 1990. Ein neuer Dinosaurier (Ornithischia, Thyreophora) aus dem unteren Jura des nördlichen Mitteleuropas. *Revue de Paléobiologie* 9:149–177.

Hawakaya, H., Manabe, M., and Carpenter, K. 2005. Nodosaurid ankylosaur from the Cenomanian of Japan. *Journal of Vertebrate Paleontology* 25:240–245. https://doi.org/10.1671/0272-4634(2005)025[0240:NAFTCO]2.0.CO;2

Hayashi, S., Carpenter, K., Scheyer, T. M., Watabe, M., and Suzuki, D. 2010. Function and evolution of ankylosaur dermal armor. *Acta Palaeontologica Polonica* 55:213–228. https://doi.org/10.4202/app.2009.0103

Hennig, E. 1925. *Kentrurosaurus aethiopicus*, die Stegosaurier-Funde vom Tendaguru, Deutsch-Ostafrica. *Palaeontographica Supplement-Band* 7:101–254.

Higgs, D. M., Brittan-Powell, E. F., Soares, D., Souza, M. J., Carr, C. E., Dooling, R. J., and Popper, A. N. 2002. Amphibious auditory responses of the American alligator (*Alligator mississipiensis*). *Journal of Comparative Physiology A: Neuroethology, Sensory, Neural, and Behavioral Physiology* 188:217–223. https://doi.org/10.1007/s00359-002-0296-8

Hill, R. V., Witmer, L. M., and Norell, M. A. 2003. A new specimen of *Pinacosaurus grangeri* (Dinosauria: Ornithischia) from the Late Cretaceous of Mongolia: ontogeny and phylogeny of ankylosaurs. *American Museum Novitates* 3395:1–29. https://doi.org/10.1206/0003-0082(2003)395%3C0001:ANSOPG%3E2.0.CO;2

Holliday, C. M. and Witmer, L. M. 2007. Archosaur adductor chamber evolution: integration of musculoskeletal and topological criteria in jaw muscle homology. *Journal of Morphology* 268:457–484. https://doi.org/10.1002/jmor.10524

Holliday, C. M. and Witmer, L. M. 2008. Cranial kinesis in dinosaurs: intracranial joints, protractor muscles, and their significance for cranial evolution and function in diapsids. *Journal of Vertebrate Paleontology* 28:1073–1088. https://doi.org/10.1671/0272-4634-28.4.1073

Holliday, C. M. and Witmer, L. M. 2009. The epipterygoid of crocodyliforms and its significance for the evolution of the orbitotemporal region of eusuchians. *Journal of Vertebrate Paleontology* 29:715–733. https://doi.org/10.1671/039.029.0330

Holliday, C. M., Porter, W. R., Vliet, K. A., and Witmer, L. M. 2019. The frontoparietal fossa and dorsotemporal fenestra of archosaurs and their significance for interpretations of vascular and muscular anatomy in dinosaurs. *Anatomical Record* 303:1060–1074. https://doi.org/10.1002/ar.24218

Hopson, J. A. 1979. Paleoneurology; pp. 39–146 in Northcutt, R. G. and Ulinski, P. (eds.), The Biology of the Reptilia, Vol. 9, Neurology A. Academic Press, New York.

Johnston, J. B. 1913. Nervus terminalis in reptiles and mammals. *Journal of Comparative Neurology* 23:97–120. https://doi.org/10.1002/cne.900230202

Kilbourne, B. and Carpenter, K. 2005. Redescription of *Gargoyleosaurus parkpinorum*, a polacanthid ankylosaur from the Upper Jurassic of Albany County, Wyoming. *Neues Jahrbuch für Geologie und Paläontologie, Abhandlungen* 237:111–160. https://doi.org/10.1127/njgpa/237/2005/111

Kinneer, B., Carpenter, K., and Shaw, A. 2016. Redescription of *Gastonia burgei* (Dinosauria: Ankylosauria, Polacanthidae), and description of a new species. *Neues Jahrbuch für Geologie und Paläontologie, Abhandlungen* 282:37–80. https://doi.org/10.1127/njgpa/2016/0605

Kirkland, J. I., Alcalá, L., Loewen, M. A., Espílez, E., Mampel, L., and Wiersma, J. P. 2013. The basal nodosaurid ankylosaur *Europelta carbonensis* n. gen., n. sp. from the

Lower Cretaceous (lower Albian) Escucha Formation of northeastern Spain. *PLoS ONE* 8:e80405. https://doi.org/10.1371/journal.pone.0080405

Knoll, F., Witmer, L. M., Ortega, F., Ridgely, R. C., and Schwarz-Wings, D. 2012. The braincase of the basal sauropod dinosaur *Spinophorosaurus* and 3D reconstructions of the cranial endocast and inner ear. *PLoS ONE* 7:e30060. https://doi.org/10.1371/journal.pone.0030060

Kurzanov, S. M. and Tumanova, T. A. 1978. On the structure of the endocranium in some Mongolian ankylosaurs. *Paleontological Journal* 3:90–96. (In Russian)

Leahey, L. G., Molnar, R. E., Carpenter, K., Witmer, L. M., and Salisbury, S. W. 2015. Cranial osteology of the ankylosaurian dinosaur formerly known as *Minmi* sp. (Ornithischia: Thyreophora) from the Lower Cretaceous Allaru Mudstone of Richmond, Queensland, Australia. *PeerJ* 3:e1475. https://doi.org/10.7717/peerj.1475

Lee, Y.-N. 1996. A new nodosaurid ankylosaur (Dinosauria: Ornithischia) from the Paw Paw Formation (late Albian) of Texas. *Journal of Vertebrate Paleontology* 16:232–245. https://doi.org/10.1080/02724634.1996.10011311

Lü, J., Ji, Q., Gao, Y., and Li, Z. 2007. A new species of the ankylosaurid dinosaur *Crichtonsaurus* (Ankylosauridae: Ankylosauria) from the Cretaceous of Liaoning Province, China. *Acta Geologica Sinica* 81:883–897. https://doi.org/10.1111/j.1755-6724.2007.tb01010.x

Maidment, S. C. R., Wei, G., and Norman, D. B. 2006. Re-description of the postcranial skeleton of the Middle Jurassic stegosaur *Huayangosaurus taibaii*. *Journal of Vertebrate Paleontology* 26:944–956. https://doi.org/10.1671/0272-4634(2006)26[944:ROTPSO]2.0.CO;2

Maidment, S. C. R., Brassey, C., and Barrett, P. M. 2015. The postcranial skeleton of an exceptionally complete individual of the plated dinosaur *Stegosaurus stenops* (Dinosauria: Thyreophora) from the Upper Jurassic Morrison Formation of Wyoming, U. S. A. *PLoS ONE* 10:e0138352. https://doi.org/10.1371/journal.pone.0138352

Manley, G. A. 1971. Some aspects of the evolution of hearing in vertebrates. *Nature* 230:506–509. https://doi.org/10.1038/230506a0

Maryańska, T. 1971. New data on the skull of *Pinacosaurus grangeri* (Ankylosauria). *Palaeontologia Polonica* 25:45–53.

Maryańska, T. 1977. Ankylosauridae (Dinosauria) from Mongolia. *Palaeontologia Polonica* 37:85–151.

Miles, C. A. and Miles, C. J. 2009. Skull of *Minotaurasaurus ramachandrani*, a new Cretaceous ankylosaur from the Gobi Desert. *Current Science* 96:65–70.

Miyashita, T., Arbour, V. M., Witmer, L. M., and Currie, P. J. 2011. The internal cranial morphology of an armoured dinosaur *Euoplocephalus* corroborated by X-ray computed tomographic reconstruction. *Journal of Anatomy* 219:661–675. https://doi.org/10.1111/j.1469-7580.2011.01427.x

Nesbitt, S. J. 2011. The early evolution of archosaurs: relationships and the origin of major clades. *Bulletin of the American Museum of Natural History* 352:1–292. https://doi.org/10.1206/352.1

Neumeier, C. and Lametschwandtner, A. 1994. The vascularization of the pituitary gland of the chicken (*Gallus domesticus*). A scanning electron microscope study of vascular corrosion casts. *Archives of Histology and Cytology* 57:213–233. https://doi.org/10.1679/aohc.57.213

Nopcsa, F. 1915. Die Dinosaurier der siebenbürgischen Landesteile Ungarns. *Jahrbuch der Kgl. Ungarischen Geologischen Reichsanstalt* 23:1–24.

Norman, D. B. and Faiers, T. 1996. On the first partial skull of an ankylosaurian dinosaur from the Lower Cretaceous of the Isle of Wight, southern England. *Geological Magazine* 133:299–310. https://doi.org/10.1017/S0016756800009031

O'Donoghue, C. H. 1920. The blood vascular system of the tuatara, *Sphenodon punctatus*. *Philosophical Transactions of the Royal Society of London. Series B* 210:175–252. https://doi.org/10.1098/rstb.1921.0006

Oelrich, T. M. 1956. The anatomy of the head of *Ctenosaura pectinata* (Iguanidae). *Miscellaneous Publications, University of Michigan Museum of Zoology* 94:1–122. https://doi.org/10.2307/1440299

Osborn, H. F. 1923. Two Lower Cretaceous dinosaurs of Mongolia. *American Museum Novitates* 95:1–10.

Owen, R. 1842. Report on British fossil reptiles. Part II. *Report of the British Association for Advancement of Science, 11th Meeting, Plymouth 1841*:60–204

Owen, R. 1850. On the communications between the cavity of the tympanum and the palate in the Crocodilia (gavials, alligators and crocodiles). *Philosophical Transactions of the Royal Society of London* 140:521–527. https://doi.org/10.1098/rstl.1850.0028

Owen, R. 1861. A monograph of the fossil Reptilia of the Liassic formations. Part first. *Scelidosaurus Harrisonii*. Palaeontographical Society Monographs 12:1–14. https://doi.org/10.5962/bhl.title.119568

Pang, Q. and Cheng, Z. 1998. A new ankylosaur of Late Cretaceous from Tianzhen, Shanxi. *Progress in Natural Science* 8:326–334.

Parish, J. C. and Barrett, P. M. 2004. A reappraisal of the ornithischian dinosaur *Amtosaurus magnus* Kurzanov and Tumanova 1978, with comments on the status of *A. archibaldi* Averianov 2002. *Canadian Journal of Earth Sciences* 41:299–306. https://doi.org/10.1139/e03-101

Parsons, W. L. and Parsons, K. M. 2009. A new ankylosaur (Dinosauria: Ankylosauria) from the Lower Cretaceous Cloverly Formation of central Montana. *Canadian Journal of Earth Sciences* 46:721–738. https://doi.org/10.1139/E09-045

Paulina-Carabajal, A., Lee, Y. N., and Jacobs, L. L. 2016. Endocranial morphology of the primitive nodosaurid dinosaur *Pawpawsaurus campbelli* from the Early Cretaceous of North America. *PLoS ONE* 11:e0150845. https://doi.org/10.1371/journal.pone.0150845

Paulina-Carabajal, A., Lee, Y. N., Kobayashi, Y., Lee, H. J., and Currie, P. J. 2018. Neuroanatomy of the ankylosaurid dinosaurs *Tarchia teresae* and *Talarurus plicatospineus* from the Upper Cretaceous of Mongolia, with comments on endocranial variability among ankylosaurs. *Palaeogeography, Palaeoclimatology, Palaeoecology* 494:135–146. https://doi.org/10.1016/j.palaeo.2017.11.030

Penkalski, P. 2001. Variation in specimens referred to *Euoplocephalus tutus*; pp. 261–298 in Carpenter, K. (ed.), The Armored Dinosaurs. Indiana University Press, Bloomington.

Penkalski, P. 2018. Revised systematics of the armoured dinosaur *Euoplocephalus* and its allies. *Neues Jahrbuch für Geologie und Paläontologie, Abhandlungen* 287:261–306. https://doi.org/10.1127/njgpa/2018/0717

Penkalski, P. and Tumanova, T. 2017. The cranial morphology and taxonomic status of *Tarchia* (Dinosauria: Ankylosauridae) from the Upper Cretaceous of Mongolia. *Cretaceous Research* 70:117–127. https://doi.org/10.1016/j.cretres.2016.10.004

Pereda-Suberbiola, J. and Galton, P. M. 1994. A revision of the cranial features of the dinosaur *Struthiosaurus austriacus* Bunzel (Ornithischia: Ankylosauria) from the Late Cretaceous of Europe. *Neues Jahrbuch für Geologie und Paläontologie, Abhandlungen* 191:173–200.

Porro, L. B., Witmer, L. M., and Barrett, P. M. 2015. Digital preparation and osteology of the skull of *Lesothosaurus diagnosticus* (Ornithischia: Dinosauria). *PeerJ* 3:e1494. https://doi.org/10.7717/peerj.1494

Porter, W. R. 2015. Physiological implications of dinosaur cephalic vascular systems. PhD thesis. Ohio University, Athens, OH.

Porter, W. R. and Witmer, L. M. 2015. Vascular patterns in iguanas and other squamates: blood vessels and sites of thermal exchange. *PLoS ONE* 10:e0139215. https://doi.org/10.1371/journal.pone.0139215

Porter, W. R. and Witmer, L. M. 2016a. Avian cephalic vascular anatomy, sites of thermal exchange, and the rete ophthalmicum. *Anatomical Record* 299:1461–1486. https://doi.org/10.1002/ar.23375

Porter, W. R. and Witmer, L. M. 2016b. Data from: Vascular patterns in iguanas and other squamates: blood vessels and sites of thermal exchange. v2, Dryad, Dataset, https://doi.org/10.5061/dryad.27m63

Porter, W. R. and Witmer, L. M. 2017. Data from: Avian cephalic vascular anatomy, sites of thermal exchange, and the rete ophthalmicum. v2, Dryad, Dataset, https://doi.org/10.5061/dryad.61dr5

Porter, W. R., Sedlmayr, J. C., and Witmer, L. M. 2016. Vascular patterns in the heads of crocodilians: blood vessels and sites of thermal exchange. *Journal of Anatomy* 229:800–824. https://doi.org/10.1111/joa.12539

Porter, W. R., Sedlmayr, J. C., and Witmer, L. M. 2017. Data from: Vascular patterns in the heads of crocodilians: blood vessels and sites of thermal exchange. v2, Dryad, Dataset, https://doi.org/10.5061/dryad.mt64k

Porter, W. R. and Witmer, L. M. 2019. Vascular patterns in the heads of dinosaurs: evidence for blood vessels, sites of thermal exchange, and their role in physiological thermoregulatory strategies. *Anatomical Record* 303:1075–1103. https://doi.org/10.1002/ar.24234

Ralph, C. L. 1970. Structure and alleged functions of avian pineals. *American Zoologist* 10:217–235. https://doi.org/10.1093/icb/10.2.217

Rieppel, O. 1985. The recessus scalae tympani and its bearing on the classification of reptiles. *Journal of Herpetology* 19:373–384. https://doi.org/10.2307/1564265

Romick, C. A. 2013. Ontogeny of the brain endocasts of ostriches (Aves: *Struthio camelus*) with implications for interpreting extinct dinosaur endocasts. Honors thesis. Ohio University, Athens, OH.

Russell, L. S. 1940. *Edmontonia rugosidens* (Gilmore), an armoured dinosaur from the Belly River Series of Alberta. *University of Toronto Studies, Geological Series* 43:3–28.

Sampson, S. D. and Witmer, L. M. 2007. Craniofacial anatomy of *Majungasaurus crenatissimus* (Theropoda: Abelisauridae) from the Late Cretaceous of Madagascar. *Society of Vertebrate Paleontology Memoir* 27:32–102. https://doi.org/10.1671/0272-4634(2007)27[32:CAOMCT]2.0.CO;2

Sedlmayr, J. C. 2002. Anatomy, evolution, and functional significance of cephalic vasculature in Archosauria. PhD thesis. Ohio University, Athens, OH.

Seeley, H. G. 1887. On the classification of the fossil animals called Dinosauria. *Proceedings of the Royal Society of London* 43:165–171. https://doi.org/10.1098/rspl.1887.0117

Seidel, M. R. 1979. The osteoderms of the American alligator and their functional significance. *Herpetologica* 35:375–380.

Sereno, P. C. 1999. The evolution of dinosaurs. *Science* 284:2137–2147. https://doi.org/10.1126/science.284.5423.2137

Sereno, P. C. and Dong, Z. 1992. The skull of the basal stegosaur *Huayangosaurus taibaii* and a cladistic diagnosis of Stegosauria. *Journal of Vertebrate Paleontology* 12:318–343. https://doi.org/10.1080/02724634.1992.10011463

Shindo, T. 1914. Zur vergleichenden Anatomie der arteriellen Kopfgefässe der Reptilien. *Beiträge und Referate zur Anatomie und Entwickelungsgeschichte* 51:267–356. https://doi.org/10.1007/BF02273902

Sobral, G. 2014. The evolutionary origins of impedance-matching hearing in Archosauria. PhD thesis. Humboldt-Universität zu Berlin, Berlin.

Sobral, G. and Müller, J. 2016. Archosaurs and their kin: the ruling reptiles; pp. 285–326 in Clack, J. A., Fay, R. R., and Popper, A. N. (eds.), Evolution of the Vertebrate Ear. Springer International Publishing, Cham, Switzerland. https://doi.org/10.1007/978-3-319-46661-3_10

Sobral, G., Hipsley, C. A., and Müller, J. 2012. Braincase redescription of *Dysalotosaurus lettowvorbecki* (Dinosauria, Ornithopoda) based on computed tomography. *Journal of Vertebrate Paleontology* 32:1090–1102. https://doi.org/10.1080/02724634.2012.693554

Sobral, G., Sookias, R. B., Bhullar, B.-A. S., Smith, R., Butler, R. J., and Müller, J. 2016. New information on the braincase and inner ear of *Euparkeria capensis* Broom: implications for diapsid and archosaur evolution. *Royal Society Open Science* 3:160072. https://doi.org/10.1098/rsos.160072

Sues, H.-D., Averianov, A., Ridgely, R. C., and Witmer, L. M. 2015. Titanosauria (Dinosauria, Sauropoda) from the Upper Cretaceous (Turonian) Bissekty Formation of Uzbekistan. *Journal of Vertebrate Paleontology* 35:e889145. https://doi.org/10.1080/02724634.2014.889145

Sulej, T. 2010. The skull of an early Late Triassic aetosaur and the evolution of the stagonolepidid archosaurian reptiles. *Zoological Journal of the Linnean Society* 158:860–881. https://doi.org/10.1111/j.1096-3642.2009.00566.x

Tarsitano, S. F. 1985. Cranial metamorphosis and the origin of the Eusuchia. *Neues Jahrbuch für Geologie und Paläontologie, Abhandlungen* 170:27–44.

Thiagavel, J., Santana, S. E., and Ratcliffe, J. M. 2017. Body size predicts echolocation call peak frequency better than gape height in vespertilionid bats. *Scientific Reports* 7:828. https://doi.org/10.1038/s41598-017-00959-2

Thompson, R. S., Parish, J. C., Maidment, S. C. R., and Barrett, P. M. 2012. Phylogeny of the ankylosaurian dinosaurs (Ornithischia: Thyreophora). *Journal of Systematic Palaeontology* 10:301–312. https://doi.org/10.1080/14772019.2011.569091

Tumanova, T. A. 1983. The first ankylosaur from the Lower Cretaceous of Mongolia. *Transactions from the Joint Soviet–Mongolian Paleontological Expedition* 24:110–118. (In Russian)

Tumanova, T. A. 1987. The armored dinosaurs of Mongolia. *Transactions from the Joint Soviet–Mongolian Paleontological Expedition* 32:1–80. (In Russian)

Tumanova, T. A. 2012. Infraorder Ankylosauria; pp. 310–324 in Tatarinov, L. P., Vorobyeva, E. I., and Kurochkin, E. N. (eds.), Fossil vertebrates of Russia and adjacent countries. Fossil reptiles and birds. Part 2. GEOS, Moscow. (In Russian)

Vickaryous, M. K., Russell, A. P., and Currie, P. J. 2001a. Cranial ornamentation of ankylosaurs (Ornithischia: Thyreophora): reappraisal of developmental hypotheses; pp. 318–340 in Carpenter, K. (ed.), The Armored Dinosaurs. Indiana University Press, Bloomington.

Vickaryous, M. K., Russell, A. P., Currie, P. J., and Zhao, X.-J. 2001b. A new ankylosaurid (Dinosauria: Ankylosauria) from the Lower Cretaceous of China, with comments on ankylosaurian relationships. *Canadian Journal of Earth Sciences* 38:1767–1780. https://doi.org/10.1139/e01-051

Vickaryous, M. K., Maryańska, T., and Weishampel, B. D. 2004. Ankylosauria; pp. 363–392 in Weishampel, D. B., Dodson, P., and Osmólska, H. (eds.), The Dinosauria. Second Edition. University of California Press, Berkeley. https://doi.org/10.1525/california/9780520242098.003.0020

Walker, A. D. 1990. A revision of *Sphenosuchus acutus* Haughton, a crocodylomorph reptile from the Elliot Formation (late Triassic or early Jurassic) of South Africa. *Philosophical Transactions of the Royal Society of London. Series B* 330:1–120. https://doi.org/10.1098/rstb.1990.0185

Walsh, S. A., Barrett, P. M., Milner, A. C., Manley, G., and Witmer, L. M. 2009. Inner ear anatomy is a proxy for deducing auditory capability and behaviour in reptiles and birds. *Proceedings of the Royal Society B: Biological Sciences* 276:1355–1360. https://doi.org/10.1098/rspb.2008.1390

Walsh, S. A., Iwaniuk, A. N., Knoll, M. A., Bourdon, E., Barrett, P. M., Milner, A. C., Nudds, R. L., Abel, R. L., and dello Sterpaio, P. 2013. Avian cerebellar floccular fossa size is not a proxy for flying ability in birds. *PLoS ONE* 8:e67176. https://doi.org/10.1371/journal.pone.0067176

Watanabe, A., Gignac, P. M., Balanoff, A. M., Green, T. L., Kley, N. J., and Norell, M. A. 2019. Are endocasts good proxies for brain size and shape in archosaurs throughout ontogeny? *Journal of Anatomy* 234:291–305. https://doi.org/10.1111/joa.12918

Wever, E. G. 1971. Hearing in the Crocodilia. *Proceedings of the National Academy of Sciences of the United States of America* 68:1498–1500. https://doi.org/10.1073/pnas.68.7.1498

Wiersma, J. P. and Irmis, R. B. 2018. A new southern Laramidian ankylosaurid, *Akainacephalus johnsoni* gen. et sp. nov., from the upper Campanian Kaiparowits Formation of southern Utah, USA. *PeerJ* 6:e5016. https://doi.org/10.7717/peerj.5016

Willard, W. A. 1915. The cranial nerves of *Anolis carolinensis*. *Bulletin of the Museum of Comparative Zoology at Harvard College* 59:17–116.

Witmer, L. M. 1995. The extant phylogenetic bracket and the importance of reconstructing soft tissues in fossils; pp. 19–33 in Thomason, J. J. (ed.), Functional Morphology in Vertebrate Paleontology. New York: Cambridge University Press.

Witmer, L. M. 1997. Craniofacial air sinus systems; pp. 151–159 in Currie, P. J. and Padian, K. (eds.), The Encyclopedia of Dinosaurs. Academic Press, New York.

Witmer, L. M. and Ridgely, R. C. 2008. The paranasal air sinuses of predatory and armored dinosaurs (Archosauria: Theropoda and Ankylosauria) and their contribution to cephalic structure. *Anatomical Record* 291:1362–1388. https://doi.org/10.1002/ar.20794

Witmer, L. M. and Ridgely, R. C. 2009. New insights into the brain, braincase, and ear region of tyrannosaurs (Dinosauria, Theropoda), with implications for sensory organization and behavior. *Anatomical Record* 292:1266–1296. https://doi.org/10.1002/ar.20983

Witmer, L. M., Ridgely, R. C., Dufeau, D. L., and Semones, M. C. 2008. Using CT to peer into the past: 3D visualization of the brain and ear regions of birds, crocodiles, and nonavian dinosaurs; pp. 67–87 in Endo, H. and Frey, R. (eds.), Anatomical Imaging: Towards a New Morphology. Springer, Tokyo. https://doi.org/10.1007/978-4-431-76933-0_6

Xu, L., Lu, J., Zhang, X., Jia, S., Hu, W., Zhang, J., Wu, Y., and Ji, Q. 2007. A new nodosaurid dinosaur fossil from the Cretaceous period of Ruyang, Henan. *Acta Geologica Sinica* 81:433–438.

Yang, J., You, H., Xie, L., and Zhou, H. 2017. A new specimen of *Crichtonpelta benxiensis* (Dinosauria: Ankylosaurinae) from the Mid-Cretaceous of Liaoning Province, China. *Acta Geologica Sinica* 91:781–790. https://doi.org/10.1111/1755-6724.13308

Zelenitsky, D. K., Therrien, F., and Kobayashi, Y. 2009. Olfactory acuity in theropods: palaeobiological and evolutionary implications. *Proceedings of the Royal Society B: Biological Sciences* 276:667–673. https://doi.org/10.1098/rspb.2008.1075

Zheng, W., Jin, X., Azuma, Y., Wang, Q., Miyata, K., and Xu, X. 2018. The most basal ankylosaurine dinosaur from the Albian-Cenomanian of China, with implications for the evolution of the tail club. *Scientific Reports* 8:3711. https://doi.org/10.1038/s41598-018-21924-7

SUPPLEMENTS

Supplementary File 1. Newly added characters for the phylogenetic analysis

178. External foramen for the facial (VII) nerve: (0). lies closer to the fenestra ovalis, covered laterally by crista prootica; (1) lies midway between trigeminal foramen and fenestra ovalis, not covered laterally; (2) aligned with trigeminal foramen, both foramina are in a close proximity and frequently placed in a single large recess.

179. Course of the abducens (VI) nerve: (0) anterior or anteromedial, enters hypophyseal cavity; (1) anterolateral, bypasses hypophyseal cavity.

180. Foramina for the optic (II) nerve: (0) single medial foramen; (1) paired lateral foramina.

181. Subdivision of the facial (VII) nerve passages: (0) absent, CN VII leaves braincase by a single foramen; (1) present, CN VII leaves braincase by two separate foramina.

182. Number of internal foramina for CN XII (= roots of the hypoglossal nerve): (0) two or, less common, one; (1) three.

183. Floccular (auricular) fossa: (0) shallow or absent; (1) prominent and deep.

184. Basioccipital condyle: (0) semilunar or elipsoidal, with a constricted neck; (1) rounded; (2) semilunar or elipsoidal and broad, without constricted neck.

185. Endocranial floor: (0) ventrally concave; (1) nearly flat.

186. Paroccipital process, mediolateral length: (0) twice the diametar of the foramen magnum or greater; (1) less than twice the foramen magnum diameter.

187. Basipterygoid processes and basal tubera, relative position: (0) separated, the distance between the basipterygoid process and the basal tuber is greater than the length of the basipterygoid process base; (1) aligned, tthe distance between the basipterygoid process and the basal tuber is lesser than the length of the basipterygoid process base.

188. Olfactory bulbs: (0) contact each other medially; (1) separate, diverge from the midline at an acute or right angle.

189. Hypophyseal (pituitary) endocast: (0) projects strongly caudoventrally; (1) projects strongly anteroventrally; (2) projects ventrally.

Supplementary File 2. Taxon-character matrix; first topology

```
xread
'Exported from NEXUS Data Editor'
189 62
Lesothosaurus_diagnosticus
000000???0000000??0000000000000000000000000000000000?00000000000000000?0
000001?000000000000000000?0?00000000000000000?0000?000000000000000100?00001
00000000000000000000000000??0000000??
Scelidosaurus_harrisonii
000000???0?00000??00000000010?00000000000110000000000000?10000000000??100100
001?1100?00100000010110000?00?00000000?0000000?0010?000000110000??0000000001
011[12]11110????10001012120??00???????????
Huayangosaurus_taibaii
00000000000000000?00000000010??0000?110001000000000000??111000000000010010?
000111?000000011011111?000001100000?0001000000?111010000??010?0???201011002
1221????0000000000110100??????1?0???
Kentrosaurus
??0???????????????0000???????????????????0???????0000000?11010???????10?10?
0??11?????110?1001?0111000?1100?0?01000[01]100000?1101001011000010?0111[01]
0111[01]21221????00000000000110200100100020??02
Stegosaurus
00001000?0010?000??000000000010??0000?110?01000000000000?111100000??01001
000001101100111[01]0[01]0001[01]1010001110000100000[01]100000?11101001010010
0010101100011[01][01]21221????10000000000110100100100021[01]102
Ahshislepelta_minor
????????????????????????????????????????????????????????????????????????????
???????????????????????????????????001111?110????????????????0001????????????
??22121???????1?????????????????????????
Aletopelta_coombsi
????????????????????????????????????????????????????????????????????????????
???????????111???????????????0???0?0????????????????1?????0?????????????1111?
?1?2???????2????1???3?1???????????????
Animantarx_ramaljonesi
011?1???????????????????????????????11??11?0011??0?0001101?111???????10110?
?1111110????1?0????111111?1?????????10011112101?1111?01110110110??????110???
??????????????????????????????????1?????
Ankylosaurus_magniventris
11110100?11?112101?23101011110110111?210?11101212010211111111100001111110111
01111001?211111???1111111??000011311???01110010????0?????0110100???2010111??
?122?????22100??????1??12??????2?01??
Anodontosaurus_lambei
11110100?111111110?12310101111111101112101111012121102111111111100001111111111
01111001?21111?????????1110?00?11111?????????????1110011?101001?????01011112
?122??????220?????????23???????????????
Argentinian_ankylosaur
????????????????????????????????????????????????????????????????????????????
?????????????????????01111?1012?0??????????????????????????????????111110???
?1?1??????1?????????????????????????
Cedarpelta_bilbeyhallorum
11100?00?01?0?0????10000?00?100?1000?1?0??1?0????000??101?11110??0???01??111
011??1????00??????1??????1100??0?0???11????????????????????011010????10101????
????????????????????????2?100?1101?2
```

```
Chuanqilong_chaoyangensis
?1?1?????????????????????????????????????????????????101?111?????????????????
??1111?0???111????1??101??????000?1????0100001?11100011?0000100??2211?11102
??2?????0?????0????????00?????????????
Crichtonpelta_benxiensis
111101??????????1?1000000011????000?211011?01211010111110??11000?1?011111?
?????????????????110111110010?0????00101111010?11100?1?1??0000????20101110?
????????????????????????????2?01??
Denversaurus_schlessmani
01101?0??120??00???2110100??1????0???11???1?001110??0?????1?00?????????111???
???????????????????????????????????????????????????????????????????????????????
???????????????????????1?10001?0?1?
Dongyangopelta_yangyanensis
?????????????????????????????????????????????????????????????????????????????
?????????????????????11110????????????????????????????????????????1?????????
?122???????????12??2???????????????
Dyoplosaurus_acutosquameus
??1?????????????2?10????????????????11?1???0?????1021?????????????????????
???????????1???????????????0100111?1??????????????110011?101????0??2201?11112
1122???????????1111??12211???????????
Edmontonia_rugosidens
01101000?12001000??2110100111110?0???111??1?0011100100????11?1?11???01111101
?1111100?011110?111?0111111??2?1??0???????????????????????1?????????????????
?121?????3102???????????????????1?01??
Edmontonia_longiceps
11101000?12001000??2110100111110?01??11???110011100100?11?1111111????1111??
??111100?011?1???????????11?????????????????????11111?1011???11?????????1????
?111??????10???????1??????????1?0???
Euoplocephalus_tutus
1111010011111111011231010111111110111211111101212010211111111100001111110111
01111011211110??011111110000011111011011100101111001111010010010?1201011112
1122211202210?111???12?12211011210112
Europelta_carbonensis
0?101????????????2110????11?0??0???110????01111001011011??01?????101?1?
??101???10?1100??01?0101111002?100??0?0?1??????0??????1?00111?????1?11010011?
?122???????????11?03???00???????1?0???
Gargoyleosaurus_parkpinorum
0110000011100000?221011000101??001?210??1101211000012?0111100?010?0100101
01111110??000010101????1???0?0?????????????????????????0?????????211001???
?122221??2100??10202?2??????????201???
Gobisaurus_domoculus
11100110?01101010??100000000101?1000?110?1110121201001110111110000??0011?100
?1????????1??????????11???????11?????????????????0????0?0000???1?????????
????????????0?????????00??????2?01??
Hungarosaurus_tormai
0?????01?0?10000??????????????1?0??????????1?0??111?????0???101??0??????1?1?0?
?1101110??0?00?1??111111111110001000?00111012001?1?10??1010?11000??1211010???
?12???????10???11??0???00????0010?112
Hylaeosaurus_armatus
?????????????????????????????????????1?????????????????????????????????????
??????????????01??00?0????0100011100?0100000??111??0??????0??????????00?
?111???2???????????2??12?0?????????????
```

Liaoningosaurus_paradoxus
???
?????????0111?????????0?0???01010????0?0??00?111000110010000?102?00?11100
0???????????????????????????????????

Kunbarrasaurus_ieversi
111000????????0????2????????1101?10???210?11?????00???001111110???1??0100001
0?1?11?????11?0??01??????10?????0??1???????????0010???0?00?000????????????
?121????1110011102?1212??010010200100

Mymoorapelta_maysi
???
?????????????????????11010?010?10010??????????1011010?01?00010??1?????????
?122???????????122?2?2?00???????????

Niobrarasaurus_coleii
?1???????????????1000????1????0???1???????11???????????????????????????0?
?????????111????1?1???1111110000?????1???????1110??101??00011??2111010111
1112??????????010??????00?????1?????

Nodocephalosaurus_kirtlandensis
111??????????????2?21???1?1???1011?22????1012120?0??1??11???????????1?111?
?????????????????????????0???
??2222120????0???????????????????2?????

Nodosaurus_textilis
???
?????????????????????111111???000?0???????????111??1101?????????1111?1?011
?12???2??????000?0312??????????????

Panoplosaurus_mirus
01101100???0??000??21101101?1???101??110??1?00111001100?0101111111?1??01111101
?1111?101211???0111????1?11?????????10001102001?????????????1101?1?1????????1?
?121????12100?????????????11?000100112

Paw_Paw_scuteling
?????????????????????????11?????????????????????????0?0?1??????????????1??
????????????111???01?11?????????0????000?0??21???1?100?????0000?????0?1????
???????????????????????????????????

Pawpawsaurus_campbelli
01101000?02?000101?222111021100010 11?1101111011110010011001111111111011101101
01????????01???
???????????????0???????????211000100112

Peloroplites_cedrimontanus
0?101?00?111???????2?10??????????????110??1?001110000110?0101?0???????11?1??
?0???000??1000???01?10011?1012?0?????1??1112101?111000111????????0110111000?
???????????????????????????????1?0???

Pinacosaurus_grangeri
1111010011111010 1?01000200?1111011?20221011001211 01??11111111100001110110111
01111100111111 0??01?11111100?001111010011?10?0111100111101001001012010 11112
1122????02210101020?122122??00?2?11??

Pinacosaurus_mephistocephalus
11110100?????????101???0?010???11???0?1?211?1100222101??1?0?????????????????
??1?10???1111101????????11????011111????1111??0?11100????????10?10?????????
?122????022100???1????????????????

Polacanthus_foxii
??1???21 1???????????????????????????
????????0??????01?1?01?110101000?1100?11??????10100010 11????????121101011?
?122100???101?0202021??00???????????

```
Hoplitosaurus_marshi
???????????????????????????????????????????????????????????????????????????????
????????????????????????????????????1000110200???????????????10???210110?1?
?121??????????020??2??????????????????
Gastonia_burgei
01100101?11?11000??100000000011101000?110?1110121100000111001110001?01110100
01????????1000?????????1111010?0001?????11020?1?111100010010100?0???201010???
?12221121?2?0?120202?2100011000201112
Saichania_chulsanensis
111100011?1111111??22221101110111011121101110121101111111111110011110111111
111111011211110111111??11????????????1??1?110?01??????????10100101?????????
?122????0222000??10??????21100?2?01??
Sauropelta_edwardsi
011010????????????????0??????0??10???11001110111101?00011011111???11??101101
01111110?1?1101110?01101011110000010100011121010111010101101001110211101001 1
1122????13201?011301111001?100?1?01??
Sauroplites_scutiger
???????????????????????????????????????????????????????????????????????????????
???????????????????????1???????????????????????????????????????????????????????
?1?2??????????12??2??????????????????
Scolosaurus_cutleri
11110?????????1??1?23101?1111????011?211??110121110211111111110??????111111
?????????????111???????1???100?0011111011?1110??0?1110011010?001????1????11?12
1122?????22101111101122212?????????????
Shamosaurus_scutatus
11100110?011?1010??100000000101?1000?110?11101212010111010111110011?0011?11?
?1111000?11????????????????????????????????????????????????????????????????????
?1???????2210????????????????1?01??
Silvisaurus_condrayi
01101000?02000000??21101???0100?10???110?11?0011100?0001101111??1?01101101
011111????01111???111111010?1??0??????????????0???????????????????????????
?122??????3101????????????2110??1001?2
Stegopelta_landerensis
???????????????????????????????????????????????????????????????????????????????
??????????1?????00?1?1???????????????????20?1???????????????1????????????
??????????10??????13????????????????
Struthiosaurus_austriacus
0?1?1??????????????2?10???????????????11?????0?????01100?0?1???????????1?110?
0?111????0?1??????0?10?111?1???1?????????11020?0?11100?1??0????????1211010???
?121?????3101??00???????????1?0010????
Struthiosaurus_languedocensis
???????????????????????????????????????????????????????????????????????????????
???????????111??????10111111???1000?????????????111?1?1000????????????????
?121???????????10??????????????????
Struthiosaurus_transylvanicus
0?1?0??????????????2?1???????????????????1????0?????0101????????1??1????1011??
????????????????000????1????????????????11120?0????????????????????????????
??????????????????????????????????0????
Talarurus_plicatospineus
111100?????????????102?21??0???????0?1?210?1?1012??01021?1??????0??????111111
[01]??????????????????11?0111000011111011101111000?11100111101001001201011
11??12????????2?0?????0??????211011210 1?2
```

PALAEONTOLOGY

```
Taohelong_jinchengensis
????????????????????????????????????????????????????????????????????????????????
????????????????????????1????10?????????????????????1?1?1?10????????????????????
?12??????????????12??2?????????????????
Tarchia_
11110001111?1?111??222212021111?1122?221?110122211010101011110000?010110111
11111011211110??????????????????????????????????????????????????????????????????
??????????????????????????2?10112101?2
Tatankacephalus_cooneyorum
0?101???????1??????2110????0111??????11??1?101111?0?00?1??????1?01?1?0?01101
0?????????0111???????????????????????????????????????????????????????????????????
???2????????????????????1?100??001??
Texasetes_pleurohalio
????????????????????????????????????????????????????????????????????????????????
??????????111????1???????1????0????1001111210?????????????0?111???1101??01?
?????????????????????????????????????
Tsagantegia_longicranialis
11100000?11111100??221010011111010111?210?1110121?010111111111110001?001111?1
0?????????11??0??????????????????????????????????????????????????????????????????
?????????????????????????????????
Zaraapelta_nomadis
111?00?????????????02?22???2?1???1?221220?11101212110001111111111001?1??111111
1?????????????????????????????????????????????????????????????????????????????????
?????????????????????????2??????2?01??
Zhejiangosaurus_lishuiensis
????????????????????????????????????????????????????????????????????????????????
??????????????????1????1101?001?????????????????11100?111?1???????1211011?12
?????????????????????????????????
Ziapelta_sanjuanensis
1111010??11??1110??231010111111??011?211?11101???01021??????1?0?0?1???1111??
0?????????1???????????????????????????????????????????????????????????????????????
???2???????220????????????[12]?????2?01??
Zuul_cruravastator
11110100?110?1110??231010111111?1012?211111101212110211111111100001?00111111
?1111000?001000??0???1?1??0?0?011111???????????1??0011?????????????????????
?122????1?????1112??12211??????2?01??
Jinyunpelta_sinensis
111000011111??011??1000???011????000?21?0??????1?0???????????????????????????
??1?????0101??????01??1?11??????0?1?1??????1??1????100?1??0?00?1?101????1????
?????????????1????1???11???????????
Bissektipelta
??1????????????????2?1????????????????????1????????00?1???????0??0?????10111
0?????????????????????????????????????????????????????????????????????????????????
??????????????????????211010211112
;
ccode [-.;
proc/;
```

Supplementary File 3. Taxon-character matrix; second topology

```
xread
'Exported from NEXUS Data Editor'
189 62
Lesothosaurus_diagnosticus
000000???0000000??00000000000000000000000000000000000?00000000000000000?0
000001?00000000000000000000?0?000000000000000000?0000?000000000000000100?00001
000000000000000000000000000??00000000??
Scelidosaurus_harrisonii
000000???0?00000??00000000010?0000000000011000000000000000?1000000000??100100
001?1100?00100000010110000?00?00000000?0000000?0010?000000011000??0000000001
011[12]11110????1000101212 00???????????
Huayangosaurus_taibaii
000000000000000000?000000000010??0000?11001000000000000??111000000000100010?
000111?000000011010111111?000001100000?0001000000?111010000??010?0???201011002
1221?????000000000000110100??????1?0???
Kentrosaurus
??0??????????????0000????????????????0???????0000000?11010?????? ?10?10?
0??11??????110?1001?0111000?1100?0?01000[01]100000?1110100101100010?0111[01]
0111[01]21221????000000000011020010010020??02
Stegosaurus
00001000?0010?000??00000000010??0000?110?0100000000000000?1111 00000??01001
000001101100111[01]0[01]0001[01]1010001110000100000[01]100000?1110010010
0010101100011[01][01]21221????10000000000110100 10010021[01]102
Ahshislepelta_minor
???????????????????????????????????????????????????????????????????????????????
???????????????????????????????????001111?110????????????????0001?????????????
??22121???????1??????????????????????
Aletopelta_coombsi
????????????????????????????????????????????????????????????????????????????????
?????????????111????????????????0???0?0???????????????????1??????0?????????????1111?
?1?2???????2????1???3?1???????????????
Animantarx_ramaljonesi
011?1?????????????????????????????????11??11?0011??0?0001101?111???????10110?
?1111110????1?0????111111?1?????????10011112101?1111?01110110 11?????? 110???
??????????????????????????????????1?????
Ankylosaurus_magniventris
11110100?11?112101?23101011110111011?210?1110121201021111111 1100001111110111
01111001?211111???1111111??000011311???01110010????0?????0110100???20101 11??
?122?????22100??????1??12???????2?01??
Anodontosaurus_lambei
11110100?11111110?1231010111111110111210111101212110211111111 1100001111111111
01111001?21111?????????1110?00?11111???????????????1110011?101001?????01011112
?122?????220?????????23????????????
Argentinian_ankylosaur
????????????????????????????????????????????????????????????????????????????????
????????????????????01111?1012?0????????????????????????????????????????111110???
?1?1??????1??????????????????????????
Cedarpelta_bilbeyhallorum
11100?00?01?0?0?????10000?00?100?1000?1?0??1?0????000??101?11110??0???01??111
011??1????00??????1??????1100??0?0???11??????????????????011010????10101????
??????????????????????????2?100?1101?2
```

```
Chuanqilong_chaoyangensis
?1?1????????????????????????????????????????????????101?111?????????????????
??1111?0???111????1??101???????000?1????0100001?11100011?0000100??2211?11102
??2?????0?????0????????00?0??????????
Crichtonpelta_benxiensis
111101????????????1?10000000011????000?211011?01211010111110???11000?1?0111111?
????????????????110111110010?0????00101111010?11100?1?1??0000????20101110?
?????????????????????????????2?01??
Denversaurus_schlessmani
01101?0??120??00???2110100??1????0???11???1?001110??0?????1?00?????????111???
?????????????????????????????????????????????????????????????????????????????
?????????????????????????1?10001?0?1?
Dongyangopelta_yangyanensis
??????????????????????????????????????????????????????????????????????????????
?????????????????????11110??????????????????????????????????????1?????????
?122????????????12??2????????????????
Dyoplosaurus_acutosquameus
??1?????????????2?10?????????????11?1???0?????1021?????????????????????
????????????1?????????????0100111?1?????????????110011?101????0??2201?11112
1122????????????1111??12211????????????
Edmontonia_rugosidens
01101000?12001000??2110100111110?0???111??1?00111001000???11?1?11???01111101
?1111100?011110?111?0111111??2?1?0????????????????????????1?????????????????
?121?????3102???????????????????1?01??
Edmontonia_longiceps
11101000?12001000??2110100111110?01??11???1100111001000?11?1111111????11111??
??111100?011?1????????????11????????????????????11111?1011???11?????????1????
?111??????10???????1??????????1?0???
Euoplocephalus_tutus
111101001111111101123101011111111011121111110121201021111111111100001111110111
01111101121110??0111111100000111101101110010111100111101001001?1201011112
1122211202210?111???12?12211011210112
Europelta_carbonensis
0?101?????????????2110????11?0??0???110????01111001011011?1???01?????101?1?
??101???10?1100??01?0101111002?100??0?0?1??????0??????1?00111?????1?11010011?
?122???????????11?03???00???????1?0???
Gargoyleosaurus_parkpinorum
0110000011100000?221011000101??001?210??11012110000012?0111100?010?0100101
01111110??000010101????1???0?0???????????????????????????0??????????211001???
?122221??2100??10202?2?????????201???
Gobisaurus_domoculus
11100110?01101010??100000000101?1000?110?111012120100111?011110000??0011?100
?1???????1??????????11????????11??????????????????0????0?0000???1?????????
??????????????0???????????00??????2?01??
Hungarosaurus_tormai
0?????01?0?10000????????????1?0??????????1?0??111?????0???101??0?????1?1?0?
?1101110??0?00?1??11111111110001000?00111012001?1?10??1010?11000??1211010???
?12???????10???11??0???00????0010?112
Hylaeosaurus_armatus
??????????????????????????????????1???????????????????????????????????????
?????????????????01??00?0????0100011100?0100000??111?0??????0??????????00?
?111???2????????????2??12?0?????????????
```

```
Liaoningosaurus_paradoxus
????????????????????????????????????????????????????????????????????????????????
??????????0111?????????0??0???01010????0?0??00?111000110010000?102?00?11100
0???????????????????????????????????
Kunbarrasaurus_ieversi
111000????????0???2????????1101?10???210?11?????00???001111110???1??0100001
0?1?11?????11?0??01??????10?????0??1???????????0010???0?00?000????????????
?121????1110011102?1212??010010200100
Mymoorapelta_maysi
????????????????????????????????????????????????????????????????????????????????
????????????????????11010?010?10010????????????1011010?01?00010??1?????????
?122???????????122?2?2?00????????????
Niobrarasaurus_coleii
?1???????????????1000?????1????0???1????????11????????????????????????????0?
??????????111????1?1????11111?0000?????1????????1110??101??00011??2111010111
1112??????????010?????00?????1?????
Nodocephalosaurus_kirtlandensis
111??????????????2?21???1?1???1011?22????1012120?0??1??11?????????????1?111?
????????????????????????0?????????????????????????????????????????????????
??2222120????0??????????????????2?????
Nodosaurus_textilis
????????????????????????????????????????????????????????????????????????????????
?????????????????????111111???000?0????????????111??1101?????????1111?1?011
?12?????2??????000?0312??????????????
Panoplosaurus_mirus
01101100???0??000??21101101?1???101??110??1?0011100100?01011111111??01111101
?1111?101211???0111????1?11??????????10001102001????????????1101?1?1????????1?
?121????12100????????????11?000100112
Paw_Paw_scuteling
???????????????????????????11?????????????????????????0?0?1??????????????11??
????????????111???01?11?????????0???000?0??21???1?100?????0000??????0?1????
?????????????????????????????????????
Pawpawsaurus_campbelli
01101000?02?000101?222111021100010 11?11011110111100100110011111111011101101
01???????01???????????????????????????????????????????????????????????????????
?????????????0??????????211000100112
Peloroplites_cedrimontanus
0?101?00?111???????2?10??????????????110??1?001110000110?0101?0???????11?1??
?0???000??1000??01?10011?1012?0?????1??1112101?111000111???????0110111000?
????????????????????????????????1?0???
Pinacosaurus_grangeri
1111010011111010 1?01000200?1111011?2022101100121101??111111111000011101101 11
01111100111111 0??01?11111100?00111110 10011?10?0111100111101 0010010120 1011112
1122????02210101020?122122??00?2?11??
Pinacosaurus_mephistocephalus
1111010 0??????101???0?010???11???0?1?211?1100222101??1?0??????????????????
??1?10???1111101????????11????011111????1111??0?11100????????10?10?????????
?122????022100???1?????????????????
Polacanthus_foxii
??????????????????????????????????????1???21???????????????????????????????
????????0??????01??1?01?110101000?1100?11??????1010001011???????121101011?
?122100???101?0202021??00????????????
```

```
Hoplitosaurus_marshi
????????????????????????????????????????????????????????????????????????????????
?????????????????????????????????1000110200???????????????10???210110?1?
?121??????????020??2????????????????
Gastonia_burgei
01100101?11?11000??10000000011101000?110?1110121100000111001110001?01110100
01????????1000?????????1111010?0001?????11020?1?1110010010100?0???201010???
?12221121?2?0?120202?2100011000201112
Saichania_chulsanensis
1111000111111111??22221101110111011121101110121211011111111111100111101111111
111111011211110111111??11????????????1??1?110?01??????????10100101?????????
?122????0222000??10??????21100?2?01??
Sauropelta_edwardsi
011010?????????????0??????0??10???11001110111101?0001101111??11??101101
01111110?1?1101110?01101011100000101000111210101110101011010011102111010011
1122????13201?011301111001?100?1?01??
Sauroplites_scutiger
????????????????????????????????????????????????????????????????????????????
?????????????????????1???????????????????????????????????????????????????????
?1?2???????????12??2????????????????
Scolosaurus_cutleri
11110?????????1??1?23101?1111????011?211??1101212110211111111110??????111111
?????????????111???????1???100?0011111011?1110??0?1110011010?001????1????11?12
1122?????22101111101122212???????????
Shamosaurus_scutatus
11100110?011?1010??100000000101?1000?110?1110121201011101011110011?0011?11?
?1111000?11???????????????????????????????????????????????????????????????????
?1???????2210???????????????????1?01??
Silvisaurus_condrayi
01101000?02000000??21101???0100?10??110?11?0011100?0001101111111??1?01101101
011111????01111???111111010?1??0?????????????0??????????????????????????????
?122?????3101??????????????2110??1001?2
Stegopelta_landerensis
????????????????????????????????????????????????????????????????????????????
??????????1?????00?1?1????????????????????20?1??????????????????1???????????
??????????10??????13????????????????
Struthiosaurus_austriacus
0?1?1?????????????2?10?????????????11?????0?????01100?0?1???????????1?110?
0?111????0?1??????0?10?111?1???1?????????11020?0?11100?1??0????????1211010???
?121?????3101??00??????????1?0010?????
Struthiosaurus_languedocensis
?????????????????????????????????????????????????????????????????????????????
??????????111?????10111111???1000?????????????111?1?1000????????????????????
?121??????????10????????????????????
Struthiosaurus_transylvanicus
0?1?0?????????????2?1???????????????????1????0?????0101????????1??1????1011??
??????????????000????1???????????????11120?0??????????????????????????????
??????????????????????????????0????
Talarurus_plicatospineus
111100?????????102?21??0???????0?1?210?1?1012??01021?1??????0??????111111
1???????????????11?011100000111101101111000?1110011110100100101201011?
?12???????2?0?????0??????2110112101?2
```

```
Taohelong_jinchengensis
???????????????????????????????????????????????????????????????????????????????
????????????????????1????10??????????????????1?1?1?10?????????????????????
?12?????????????12??2?????????????????
Tarchia_
11110001111?1?111??222212021111?1122?221?110122211010101011110000?010110111
11111011211110?????????????????????????????????????????????????????????????????
??????????????????????????2?1011210122?
Tatankacephalus_cooneyorum
0?101???????1??????2110????0111??????11??1?101111?0?00?1??????1?01?1?0?01101
0?????????0111??????????????????????????????????????????????????????????????????
???2??????????????????????1?100??001??
Texasetes_pleurohalio
???????????????????????????????????????????????????????????????????????????????
??????????111????1???????1????0????1001111210?????????????0?111???1101??01?
??????????????????????????????????????
Tsagantegia_longicranialis
11100000?11111100??22101001111101011?210?1110121?010111111111110001?00111?1
0?????????11??0??????????????????????????????????????????????????????????????????
??????????????????????????????????
Zaraapelta_nomadis
111?00?????????????02?22???2?1???1?221220?11012121100011111111001?1??111111
1?????????????????????????????????????????????????????????????????????????????
???????????????????????2??????2?01??
Zhejiangosaurus_lishuiensis
???????????????????????????????????????????????????????????????????????????????
?????????????????????1???1101?001?????????????????11100?111?1???????1211011?12
??????????????????????????????????
Ziapelta_sanjuanensis
1111010??11??1110??231010111111??011?211?11101???01021??????1?0?0?1???1111??
0?????????1?????????????????????????????????????????????????????????????????????
???2???????220????????????[12]?????2?01??
Zuul_cruravastator
11110100?110?1110??231010111111?1012?211111101212110211111111100001?00111111
?1111000?001000??0???1?1??0?0?011111???????????1??0011?????????????????????
?122????1?????1112??12211???????2?01??
Jinyunpelta_sinensis
111000011111??011??1000???011????000?21?0??????1?0??????????????????????????
??1?????0101??????01??1?11??????0?1?1??????1??1????100?1??0?00?1?101????1????
????????????1????1???11????????????
Bissektipelta
??1?????????????????21?????????????????1????????00?1???????0??0?????10111
0????????????????????????????????????????????????????????????????????????????
??????????????????????211010211112
;
ccode [-.;
proc/;
```